Chapter 1

Chemistry On The Pyrimidine Ring

Introduction

Pyrimidines are 6-membered heterocyclic ring compounds composed of nitrogen and carbon. They are present throughout nature in various forms and are the building blocks of numerous natural compounds from antibiotics to vitamins and liposacharides. The most commonly recognized pyrimidines are the bases of RNA and DNA, the most abundant being cytosine, thymine or uracil. The origin of the term pyrimidine dates back to 1884 when Pinner coined the term from a combination of the words pyridine and amidine because of the structural similarity to those compounds (1). Since these initial investigations hundreds of pyrimidine-containing compounds have been found in biochemistry. The numerous modifications upon this scaffold and its relative importance in nature make it an interesting area of study. Here we have chosen to explore some of the general mechanisms nature has employed to create and modify pyrimidines. Mechanistically related metabolic and catabolic enzymes involved in ring opening/closure and oxidation/reduction of pyrimidines will be examined. Enzymes involved in the methylation, thiolation and amination of the pyrimidine ring will also be compared.

Biosynthetic Origin

The majority of organisms synthesize pyrimidines through a *de novo* pathway, and a minority, depend on a uracil salvage pathway (2). The *de novo* pyrimidine biosynthetic pathway starts with bicarbonate and ammonia, often derived from glutamine, to form uridine-5'-monophosphate (Figure 1.1). There are six enzymes in the *de novo* biosynthetic pathway: carbamoyl-phosphate synthetase, aspartate carbamoyltransferase, dihydroorotase, dihydroorotate dehydrogenase, orotate phosphoribosyltransferase, and orotidine-5'-phosphate decarboxylase. In most prokaryotes each of these enzymes is a separate protein, whereas in eukaryotes the first three steps of this pathway are catalyzed by a single enzyme formed from a single polypeptide chain (3). In many organisms, the last two reactions are also performed by a single polypeptide.

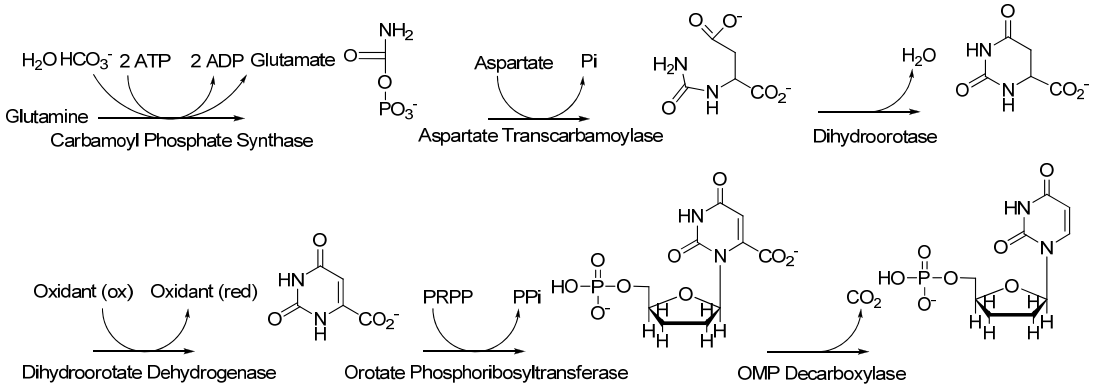

Figure 1.1: Pyrimidine Biosynthesis. The biosynthetic pathway for the formation UMP is shown. Each step in the pathway is shown indicating the substrates used and the products formed.

The first reaction in this pathway, catalyzed by carbamoyl-phosphate synthetase (CPS), is common to both the pyrimidine and arginine biosynthetic pathways, as well as being used the urea cycle in many vertebrates. In prokaryotes, there is only one CPS, while in eukaryotes there are two (4). CPS I is found in the mitochondria and uses free

ammonia for the production of carbamoyl phosphate. This enzyme controls arginine metabolism and is also used in the urea cycle. The cytosolic CPS II uses glutamine as its nitrogen source and is devoted to pyrimidine biosynthesis (5). In CPS II the first step of the reaction is the activation of bicarbonate by ATP to form carboxyphosphate. Glutamine is then hydrolyzed to give glutamate and free ammonia. The nucleophilic ammonia attacks carboxyphosphate to give carbamate. In the final step, the oxygen of carbamate attacks the gamma-phosphate of a second ATP to yield carbamoyl phosphate (6).

The next step in the *de novo* biosynthetic pathway is performed by aspartate transcarbamoylase (ATCase) (7). This is the first committed step in pyrimidine biosynthesis in prokaryotes and the enzyme is highly regulated by both the substrates and the products of nucleotide metabolism such as CTP and ATP (8). The catalytic mechanism of ATCase involves first an attack by the amino group of the substrate aspartate on the carbonyl carbon of carbamoyl-phosphate, forming a tetrahedral intermediate. The intermediate (amine of the starting aspartate) is then deprotonated by an active site lysine, yielding the product N-carbamoyl-L-aspartate (9).

The ring closure of N-carbamoyl-L-aspartate is catalyzed by the binuclear zinc metalloenzyme dihydroorotase. In the formation of dihydroorotate, the first step of the reaction is the deprotonation of the N3 nitrogen of carbamoyl aspartate by an active site aspartate residue. This nitrogen then attacks the side-chain carboxylate carbon of carbamoyl aspartate, which is polarized through a direct electrostatic interaction with the binuclear zinc center. The tetrahedral intermediate collapses by cleavage of the C-O bond, leaving a hydroxide bridging the binuclear zinc center (10).

The oxidation of dihydroorotate to form orotate is catalyzed by the flavoprotein dihydroorotate dehydrogenase (DHOD). There are three classes of DHODs. Class 1A DHODs are cytosolic homodimeric proteins that contain FMN and use fumarate as their oxidizing substrate (11). Class 1B enzymes are heterotetrameric proteins containing FMN on one polypeptide, and an FAD and an iron-sulfur cluster on another subunit, and use NAD as their physiological oxidant (12). Class 2 enzymes are membrane-bound monomers that contain FMN and use ubiquinone as their oxidizing substrate (13). Class 2 enzymes are found in almost all eukaryotes and Gram-negative bacteria, while Class 1 enzymes are generally found in Gram-positive bacteria. All of these enzymes form a carbon-carbon double bond between carbons 5 and 6 of the pyrimidine ring by a hydride-transfer from the C5 position to the N5 position of the flavin prosthetic group, along with a proton abstraction from the C6 position by an active site base forming orotate. Whether the reaction is stepwise or concerted has been investigated for both Class 1A and Class 2 enzymes, but has yet to be determined for the class 1B enzymes. Whether a stepwise iminium or enolate intermediate is formed has not been determined.

Orotate phosphoribosyltransferase (OPRTase) catalyzes the reaction between orotate and the ribose-5-monophosphate donor 5-phosphoribosyl-1-pyrophosphate (PRPP) to form orotidine-5-phosphate (OMP) and pyrophosphate. Detailed studies of this reaction have led to suggestions of a two-step, Sn1-type mechanism. An oxocarbonium-like transition state that is formed in which the N1 of orotate undergoes a nucleophilic attack on the C1 of the ribose of PRPP with inversion of stereochemistry and a final loss of pyrophosphate (14).

The final step in de novo pyrimidine biosynthesis is the decarboxylation of OMP to form UMP and CO_2, catalyzed by OMP decarboxylase (15). The mechanism of this reaction is still under investigation. Several mechanisms have been suggested, including a covalent adduct with the enzyme, ylide or carbene formation, or concerted protonation-decarboxylation, but no definitive answer has yet been reached (16).

UMP, the final product of *de novo* pyridmidine biosynthesis, is converted into dUMP by ribonucleotide reductase and then into dTMP by thymidylate synthase. Alternatively, UMP is converted into UTP, and then to CTP by CTP synthase. Finally, ribonucleotide reductase converts CTP into dCTP, the canonical pyrimidine bases of DNA and RNA. Both thymidylate synthase and CTP synthase will be explored in detail in later sections.

Catabolism

The catabolism of pyrimidines shows some striking similarities to their biosynthesis.

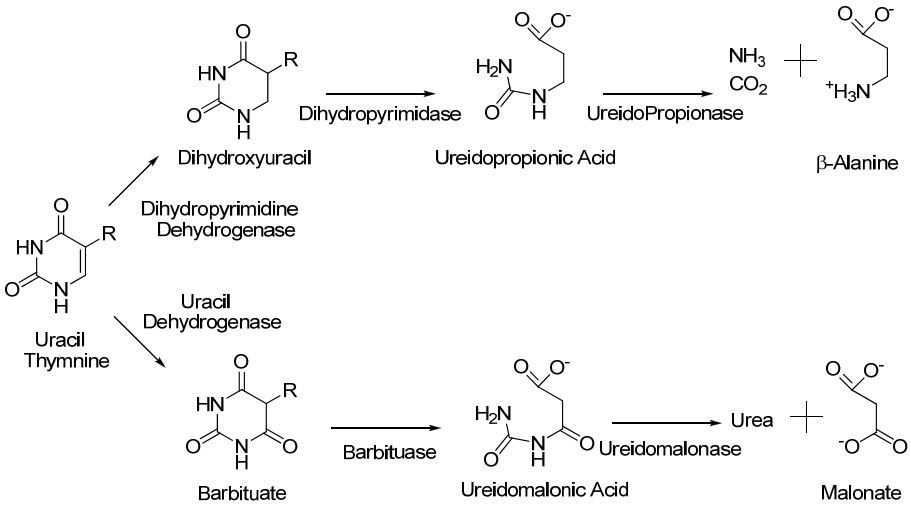

Figure 1.2: Pyrimidine Catabolism. The two main pathways of pyrimidine degradation are illustrated. The top portion shows the pathways for reductive degradation of pyrimidines while the bottom path shows the oxidative pathway for degradation.

There are three currently known pathways for pyrimidine catabolism with two of these more thoroughly explored than the third (Figure 1.2). The most explored catabolic pathway for pyrimidines is the reductive pathway, which is found in most organisms. In this pathway uracil or thymine undergoes reduction by dihydropyrimidine dehydrogenase to be converted to the dihydroxyuracil or dihydoxythymine (17). Cytosine and methylcytosine can follow this same pathway by first undergoing a deamination to uracil. These are then broken down by dihydropyrimidinase to form ureidopropionic acids, which are then converted to either beta-alanine for uracil or beta-aminoisobutyrate for thymine. These then go on to be utilized in central metabolic roles (18).

The oxidative pathway, found so far only in certain bacteria, oxidizes pyrimidines to barbituric acid via a uracil dehydrogenase (19). Barbituric acid is then broken down into ureidomalonic acid by barbiturase, and finally into urea and malonic acid by ureidomalonase. Many of the enzymes from the catabolic and metabolic pathways for pyrimidine degradation and synthesis utilize similar mechanisms.

Ring Formation and Breakdown

The chemistry for both the synthesis and the degradation of pyrimidines involves ring closure or opening. The enzymes that catalyze these reactions are called amidohydrolases, and they are part of a superfamily comprising a diverse set of enzymes that catalyze mainly hydrolysis reactions, and some isomerization reactions. They function on a variety of substrates such as sugars, nucleic acids, amino acids, and organophosphate esters. Of the known amidohydrolases, several have been shown to be

necessary for the formation or degradation of pyrimidines. This family of enzymes has a mononuclear or binuclear metal center in a $(\beta/\alpha)_8$ fold (20).

During the synthesis of dihydroorotate, the amidohydrolase dihydroorotase, catalyzes the cyclization of carbamoyl-L-aspartate. Organisms that use the reductive pathway for pyrimidine degradation utilize dihydopyrimidases to open pyrimidine rings. Organisms that utilize the oxidative pathway use barbituases (21). All of these enzymes share a seemingly common mechanism, using a metal hydroxide as an acid/base. These reactions are generally reversible. One of the best studied enzymes is dihydroorotase from *Escherichia coli* (Figure 1.3).

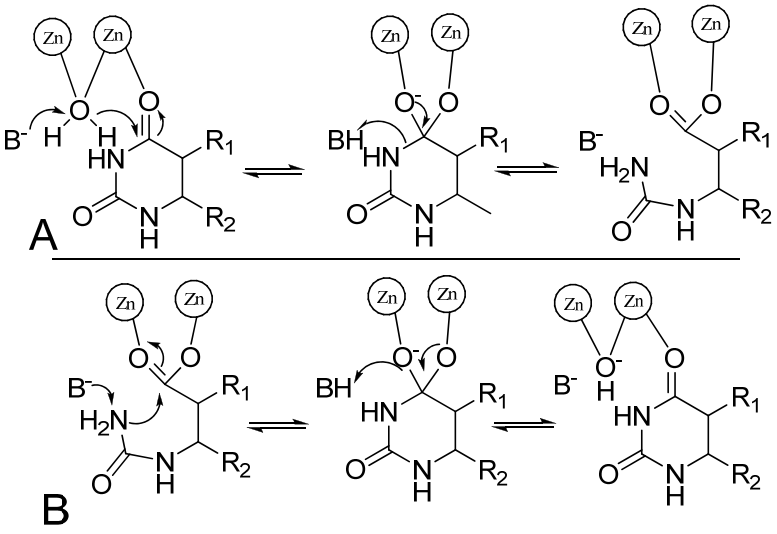

Figure 1.3: Ring Opening and Closing Reactions. The figure shows the ring opening reaction performed by dihydropyrimidases (A), and the ring closing reaction performed by dihydroorotases (B). The two reactions are essentially equivalent, but in metabolism proceed in different directions. The hydrolysis of dihydrouracil follows the same basic mechanism as that shown in A only without the aid of a metal hydroxide.

In this enzyme the cyclization of carbamoyl-L-aspartate is optimal at pH 7.0, while ring opening is favored at high pH (22). In the dihydropyrimidase from *Sacharomyeces kluyveri*, which catalyses ring opening optimally at pH 8.0, ring opening is also favored at high pH (23), with a similar pH profile to that for dihydroorotase

(Figure 1.3). The major differences between these enzymes from the anabolic and catabolic pathways are found in substrate recognition. In dihydropyrimidases, the enzymes have a wide hydrophobic pocket to accommodate modifications at the 5-position. This allows these enzymes to catalyze the ring-opening of both dihydrouracil and dihydrothymine, which has a methyl at carbon-5. These enzymes also differ from the dihydroorotases because they lack the space and hydrogen bonding contacts for the carboxyl group found in dihydroorotase. The carboxyl group of dihydroorotate and the modifaction at carbon-5 in thymine are the main differences characterizing the substrates used by these two types of enzymes (24). Beyond these changes both enzyme families show close similarities in mechanism and structure.

A less studied pyrimidine utilizing-amidohydrolase, which has recently been found, is barbiturase. This enzyme carries out a function similar to that of the dihydropyrimidases. Preliminary biochemical studies of this enzyme show that the enzyme carries out the conversion of barbiturate to uriedo malonic acid, a necessary step in the oxidative catabolism of pyrimidines (25). This enzyme show that it has relatively low homology to the dihydropyrimidases and dihydroorotases. Barbiturase has been shown to be a tetramer with 4.4 mols of zinc per enzyme, likely a mononuclear zinc aminohydrolase. This property indicates a slight difference between the mechanism of this amidohydrolase and those of dihydroorotates and dihydropyrimidases, both of which use a binuclear metal center (26). Lower metal content for dihydropyrimidase led early researchers to also conclude that it was a mononuclear zinc enzyme. This phenomenon is due to pH playing an important part in the metal binding to amidohydrolases. Both dihydroorotases and dihydropyrimidases require a posttranslational carboxylation of an

active site lysine to function properly and bind the second metal effectively. This modification and the increase in metal affinity it provides are highly dependent upon pH. Further structural studies or pH-dependent metal titrations of this enzyme should provide better insight as to whether this new amidohydrolase family does indeed use a different mechanism than that found for the dihydroorotases and dihydropyrimidases.

The ring opening of pyrimidines is also seen in nature without the aid of enzymes. At high temperatures, the pyrimidine dihydrouridine, found in modified tRNA, has been shown to undergo ring opening through hydrolysis (27). This reaction is accelerated by both heat as well as basic pH, one reason dihydrouracil is thought to be absent in the tRNA of thermophiles. The mechanism proceeds by the attack of a hydroxide at carbon-4 of dihydrouracil, which likely goes through a tetrahedral intermediate and collapses to yield the opened ring (28). Though unaided by enzymatic catalysis this ring opening reaction proceeds on a biologically relevant time scale at temperatures above 95^{o} C and utilizes a mechanism very reminiscent of that seen in the amidohydrolase enzymes.

Functional Group Conversion

Functional group interconversion occurs quite commonly in nature. Pyrimidines are no exception to this process as many positions on the ring are altered, particularly in the formation of modified nucleotides such as those found in tRNA. A few of the better understood reactions taking place on the pyrimidine ring occur at positions 2 and 4. The interconversion of these two carbonyls into amines and thiocarbonyls has been studied in considerable depth.

Though synthetic organic chemistry utilizes many types of chemistry not commonly found in nature, some of the same mechanisms and routes to natural products are similar. Given the low reactivity of the carbonyls, they must be activated before a subsequent reaction with a nucleophile can take place. The requirement for activation seems to be shared by both nature and organic synthesis.

The formation of cytidine, 2-thiouridine, 4-thiouridine, and 2-ribothymidine, in nature, all seem to follow a generalized theme (Figures 1.4, 1.5). They activate the oxygen of the ketone through formation of a phosphorylated or adenylated intermediate. A nucleophile then attacks the activated carbon releasing the phosphate or AMP.

One of the most earliest recognized pyrimidine conversions is that of uracil into cytosine. This interconversion is catalyzed by cytidine 5'-triphosphate synthases (29). These enzymes catalyze three reactions at two different active sites, the first site catalyzing the hydrolysis of glutamine to produce ammonia.

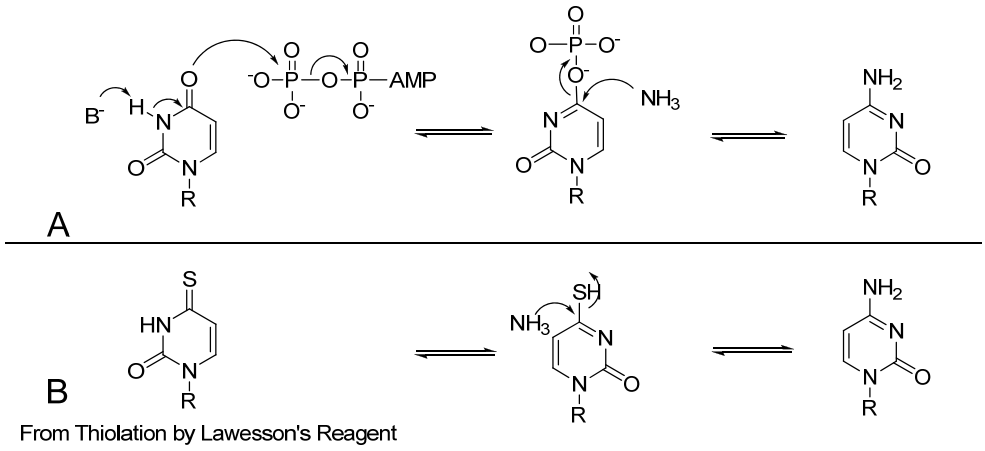

Figure 1.4: Amination of Position 2. The reaction performed by CTP synthase in shown in A and a similar organic reaction in which a thioketone is replaced by an amine is shown in B.

The ammonia is then channeled through a tunnel to the second active site. In this active site UTP is first activated by transfer of the terminal phosphate of ATP to the oxygen on carbon-4. The final reaction is the attack of ammonia on carbon-4 yielding a tetrahedral intermediate which decomposes to form CTP and free phosphate (30) (Figure 1.4).

Partially analogous to this reaction is the reaction catalyzed by the enzyme ThiI, responsible for the formation of thiolation of thiamine. This enzyme also is responsible for the conversion at the oxygen at carbon-4 of pyrimidines, by catalyzing the conversion of the carbonyl at carbon-4 into a thiocarbonyl forming 4-thiouridine (31). This same reaction occurs at position-2 in the formation of 2-thiouridine, catalyzed by MnmA (Figure 1.5A).

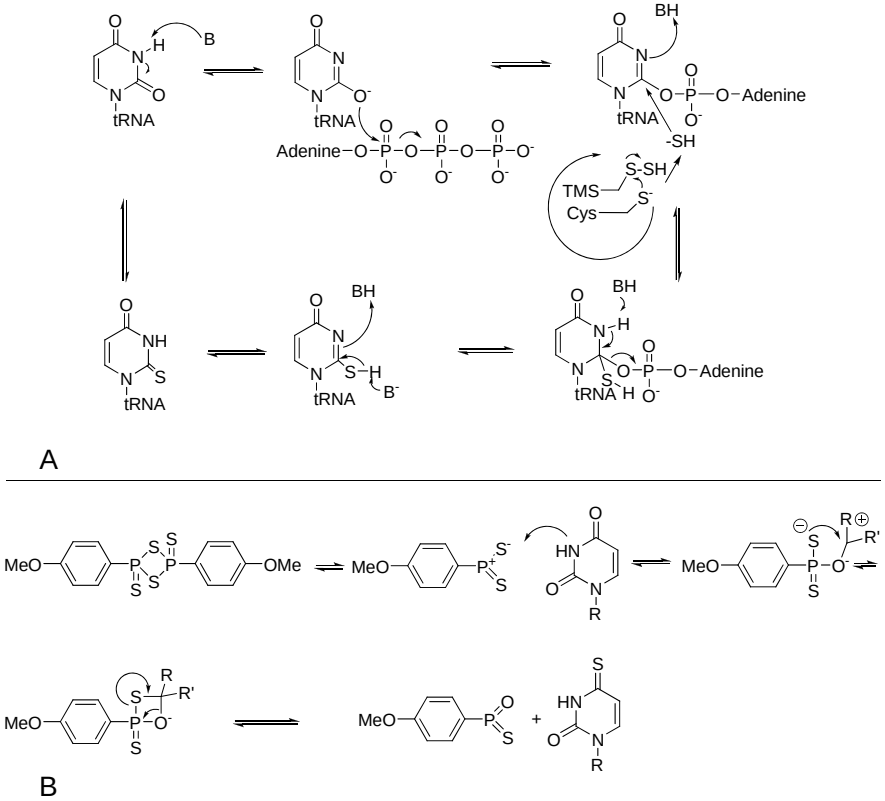

Figure 1.5: Thiolation of Positions 2 and 4. Part A shows the mechanism of MnmA forming the thioketone at the 2-position. A common synthetic route to the 4-thioketone is shown in B.

The general mechanism for both of these enzymes first involves a sulfur transfer from a donor such as IscS for ThiI, and TusE for MnmA. This yields a protein persulfide intermediate. The enzymes then bind the tRNA and activates the uridine oxygen using ATP to form an adenylated intermediate. The sulfur transfer to the tRNA occurs either through direct attack on the adenylated uridine by the persulfide or by a free bisulfide. The tetrahedral intermediate formed then decomposes to yield AMP and thiouracil (32). The mechanism of 2-thioribothymidine formation in *Thermus thermophilus* tRNA seems to also follow this general scheme (33). It requires an outside sulfur source and is ATP-dependent, though little else is known about the enzyme or its mechanism (34).

A number of synthetic chemical routes to these pyrimidines have been developed. The synthesis of 4-thiouridine or 2-thiouridine is normally done using P_4S_{10} or Lawesson's Reagent (Figure 1.5B). When Lawesson's Reagent is in solution it forms a highly reactive dithiophosphine ylide (35). This ylide reacts with the carbonyl to give a thiaoxaphosphetane intermediate. A stable P=O bond is then formed in a cycloreversion step driving the reaction to completion (36). The thiolation of pyrmidines using P_4S_{10} is very different from that seen in nature, but is commonly used in organic chemistry for thiolating ketones, esters, and amides.

In one of the earlier chemical syntheses of cytidine, the carbon-4 carbonyl of the pyrimidine is thiolated to yield a thiocarbonyl (37). This thiocarbonyl has a lower pK_a than the carbonyl and therefore makes it much more reactive (38). In this reaction the thiocarbonyl is analogous to a phosphorylated or adenylated carbonyl. The thiocarbonyl is then treated with ammonia in methanol to form cytidine, analogous to the enzymatic reaction. In the enzyme, the free ammonia is derived from hydrolysis of glutamine. Both

strategies, be it from nature or synthetic chemistry, first activate or replace the carbonyl with a more reactive group before replacing the carbonyl.

A different type of functional group interconversion is also commonly seen at position-4 of pyrimidines. This reaction is catalyzed by cytosine deaminases (Figure 1.6) and involves the metal-catalyzed hydrolysis of the amine of cytosine to form uracil, as well as in some cases, the conversion of 5-methylcytosine to thymine (39). These enzymes are found in a few different forms. The cytosine deaminase from *E. coli* is a member of the amidohydrolase family using a mononuclear zinc center (40).

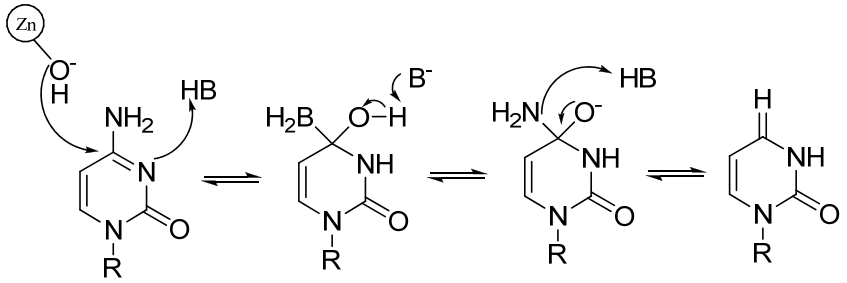

Figure 1.6: Deamination of Cytosine. Presented is the deamination of cytosine by a water activated zinc hydroxide, the mechanism used by all known cytosine deaminases. The reaction occurs uncatalyzed with water using almost the same mechanism.

The well-studied cytosine deaminase from yeast also uses a mononuclear zinc ion, but has a different structural architecture (41). Both of these enzymes are important in pyrimidine salvage pathways that modify the small molecule bases. Vertebrates utilize another more complex type of cytosine deaminase involved in somatic hyper-mutation, the activation induced cytosine deaminase (42). It induces mutations on single stranded DNA in antibody genes leading to differentiation during immune response. AID cytosine deaminases are part of a larger family of AID/APOBEC cytosine deaminases that use DNA and RNA as substrates (43).

Though all of these cytosine deaminases have very different structures and physiological functions, they all perform very similar chemical reactions. All the enzymes utilize similar chemical mechanisms in which an activated zinc serves as an acid/base catalyst to facilitate the addition of water at C4 of the pyrimidine ring, thereby forming a tetrahedral intermediate that collapses to form uracil (44). Although the binding properties and rate constants for all of these enzymes are very different, and they work on different substrates ranging from free bases to ssDNA and RNA, the overall chemistry remains the same.

The rate of deamination of cytosine without the aid of an enzyme has been measured at around 0.4 to 4 x 10^{-9} s^{-1} for mismatched cytosine pairs, and even slower in properly paired structures (45). The general reaction mechanism involves an attack by a hydroxyl at the C4 of cytosine to give a tetrahedral intermediate. Although the cytosine deaminase from *E. coli* uses the same general mechanism as the uncatalyzed reaction, there is a rate enhancement of ~10^{12} in the presence of the enzyme. In the uncatalyzed reaction, at neutral or acidic pH, deamination proceeds via an intermediate protonated at N3 (46). This same protonation occurs in the catalytic cycle of the enzymes, but protonation is brought about by an active site acid.

Oxidation and Reduction of the Pyrimidine Ring

Oxidation and reduction of pyrimidine compounds are also important parts of their anabolism and catabolism. In the synthesis, degradation and modification of pyrimidines, there are a number of different enzyme families that form and remove carbon-carbon double bonds between carbon-5 and carbon-6. During the synthesis of

UMP, dihydroorotate is oxidized to orotate by dihydroorotate dehydrogenase (47). This is the only redox step in the biosynthesis of UMP. A similar redox reaction is found in the catabolism of pyrimidines whereby dihydropyrimidine dehydrogenases reduce uracil and thymine to dihydrouracil and dihydrothymine (48). A third class of enzymes, dihydrouridine synthases, although structurally related to the above enzymes, catalyze the reduction of specific uridines found in tRNAs through a generally similar mechanism (49).

There are three classes of dihydroorotate dehydrogenases, with the most seemingly complex being the class 1B dihydroorotate dehydrogenases. These enzymes consist of four polypeptide chains with 2 FMN prosthetic groups, 2 FADs, and 2 iron-sulfur clusters (50). They oxidize dihydroorotate to orotate and reduce NADP to NADPH. Less complex enzymes are the class 1A dihydroorotate dehydrogenases (51). These enzymes consist of a homodimer with two polypeptide chains that are very similar to the central core found in the class 1B dihydroorotate dehydrogenases. They oxidize dihydroorotate to orotate and reduce fumarate to succinate (52). The third class of enzymes, which is the variety found in humans, is the class 2 dihydroorotate dehydrogenases (53). These enzymes consist of one polypeptide chain with two distinct active sites, one that catalyzes the oxidation of dihydroorotate, and the other which reduces quinones, most likely Q_{18} physiologically, and connects the enzyme to the respiratory chain. This enzyme also has a short hydrophobic domain that allows the protein to associate with the membrane.

Given the large differences in the structures, and the alternate oxidants that these enzymes use, the mechanisms of these enzymes must be somewhat different.

Interestingly, the sites of dihydrorotate binding and reduction are highly conserved amoung all three of these enzyme classes. They all use FMN, which is reduced by dihydrorotate, and all three classes have a similar active site loop that opens and closes to allow the substrate to enter and exit (54). They all also share a conserved set of asparagine residues that surround the substrate/product. They all bind to dihydroorotate with K_D values in the micromolar range and utilize an active site base to deprotonate carbon-5 and transfer a hydride from carbon-6 to the flavin prosthetic group. They differ in which residue is used as the base, either a serine or cystine, and whether protonation and hydride transfer are stepwise or concerted (55,56). Small differences in the active site architecture cause differences in the specificity of the enzymes for different inhibitors (57).

Very close relatives of the dihydroorotate dehydrogenases are the dihydropyrimidine dehydrogenases. These enzymes perform the same redox reaction as dihydroorotate dehydrogenases but in the opposite direction. They reduce the double bonds of thymine and uracil. These enzymes are generally homodimers in which each monomer contains an FMN, an FAD, and 4 iron-sulfur clusters. This architecture is most similar to the class 1 B dihydroorotate dehydrogenases. They both utilize an FMN to reduce and oxidize pyrimidines, and an FAD to reduce or oxidize NAD(P)H/NAD(P). These two sites in both enzymes are connected by an electron transfer network leading from the flavin active site to its partner redox moiety. The first obvious difference between these two classes of enzymes is in the electron transfer chain, which, though serving a similar purpose in both, is extended by three iron-sulfur clusters in the dihydropyrimidine dehydrogenases. The redox potentials for both dihydropyrimidine

dehydrogenases and the class 1B dihydroorotate dehydrogenases indicate that the FMN has a more positive redox potential than the FAD prosthetic group (58). The substrates of these reactions have potentials of around -250 mV for the pyrimidine and -320 for the NAD(P)/H couples (59). This seems surprising given that the electron flow essentially needs to be reversed in the metabolic or catabolic pathways. The potentials of the substrates indicate that the dihydropyrimidine dehydrogenase reaction is favored whereas the Class 1B dihydroorotate reaction is disfavored. The relative amounts of the substrates must affect the equilibrium of the reaction. The reaction for the Class 1B enzyme, must therefore be pushed by the proceeding or subsequent reactions in metabolism. The reactions for both of these enzymes have been shown to be reversible. It is interesting to note that all of the enzymes use an FMN prosthetic group at the immediate site of pyrimidine oxidation or reduction, and a FAD at the site of NAD(P) oxidation or reduction. Given that both of these cofactors can have similar redox potentials, there seems to be no currently understood necessity for this occurrence.

Differences at the active sites of the two types of enzymes also allow for binding to the different substrates. In the dihydroorotate dehydrogenases a series of active site asparagine residues align and bind dihydroorotate with the active site base directly above carbon-5 of this substrate. A similar set of three asparagines and a threonine are found in the active site of the dihydropyrimidine dehydrogenases (60). However, there is a more open active site pocket at carbon-5 that allows the binding of thymine; thymine cannot bind to the active site of dihydroorotate dehydrogenases. These differences are similar to those for the anabolic and catabolic amidohydrolase enzymes that utilize very similar substrates.

The most phylogenetically removed class of enzymes that oxidize and reduce pyrimidines are the dihydrouridine synthases. From sequence homology they have the closest resemblance to the class 1A dihydroorotate dehydrogenases. They utilize an FMN cofactor that is reduced by NAD(P)H and oxidized by specific uracils found in tRNA (61). The active sites of these enzymes are similar to the class 1A dihydroorotate dehydrogenases including the presence of an active site cysteine above N5 of the flavin, as well as an active site asparagine that likely binds to the uridine ring. The rest of the binding pocket is largely open and accessible to solvent. This is necessary for the enzyme to be able bind to the tRNA and allow entrance of the uracil ring. The rest of the active site cavity, and the exclusion of water from the active site, is likely influenced by the tRNA substrate.

Overall, the same chemistry is involved in all of these pyrimidine utilizing dehydrogenases, and subsequently the active site architecture and methods of catalysis have many common features. The general mechanism for double bond formation or reduction involves a hydride transfer to/from position 5 of the pyrimidine ring with protonation/deprotonation occurring at carbon 6 (Figure 1.7).

One of the methods for chemical synthesis of dihydroorotate is similar to the reaction catalyzed by the dihydropyrimidases. In this reaction orotate undergoes hydrogenation using a platinum catalyst (62). The use of metals such as Pt, Pd, Rh, or Ni to catalyze hydrogenation reactions is very common in organic syntheses. Generally there are three ways in which these metals catalyze hydrogenation: oxidative addition, hydrogenolysis, and heterolytic cleavage. The hydrogenation reaction is a surface-catalyzed reaction in which the platinum surface is coated by hydrogen. The first step of

the reaction is the complexation of the alkene, orotate, to the catalyst surface. The pi-bond interacts with the metal-H bond of the catalyst, weakening the bond and causing the transfer of a proton from the catalyst to one of the carbons of the orotate double bond. The reaction occurs a second time transferring a hydride and fully hydrogenating the alkene. The alkene is then released from the surface of the catalyst (63).

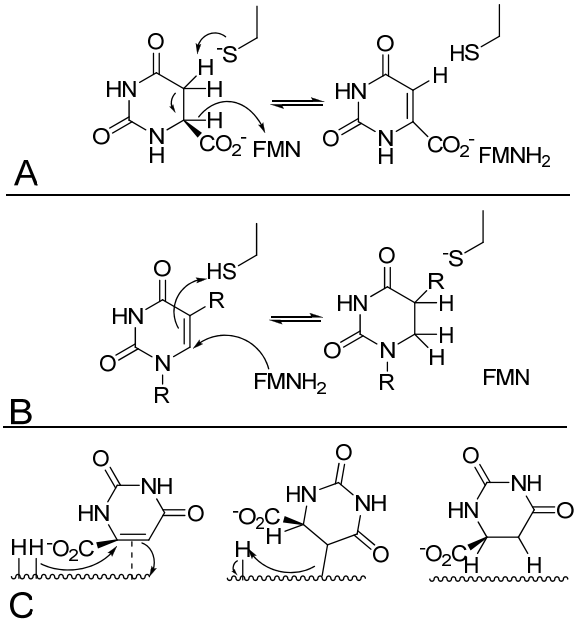

Figure 1.7: Oxidation and Reduction at Carbons 5 and 6. Part A depicts the oxidation of dihydroorotate by dihydroorotate dehydrogenases. Part B depicts the opposite by analogous reaction performed by dihydropyrimidine dehydrogenases forming a dihydropyrimidine from a pyrimidine. Part C depicts the synthetic route for this reaction via hydrogenation of the double bond on the surface of platinum.

Though somewhat dissimilar, the metal-catalyzed reaction parallels that in the dihydropyrimidine dehydrogenases in that the substrate binds, a proton is transferred to the substrate, then a second transfer occurs, and the product leaves. The transition states are likely very different because the detailed mechanisms are quite different. The reactions are similar in that both reactions are carried out through catalytic processes that involve redox-capable centers, a metal in the case of the organic synthesis method, and a flavin in the case of the enzymatic method. Hydrogenation of alkenes is commonly

performed by metal catalysts. These reactions can be driven in reverse just like the enzymatic reactions. Dehydrogenations for alkanes such as ethane tend to take place according to a 1,2-elimination mechanism on these catalysts. This would likely be the case for the dehydrogenation of dihydroorotate on these catalysts as well (64).

Activation by Attack at Carbon 6

A number of different enzymes that methylate the 5-position of the pyrimidine ring are known. Cytosine in both DNA and RNA has been found to be methylated, as well as uridine in RNA. By far the most prolific methylation occurs in the formation of thymine by thymidylate synthase. Though acting on different substrates, all these enzymes seem to share a common mechanism of activating the pyrimidine ring for subsequent methyl transfer.

The general mechanism of pyrimidine methylation occurs in four steps (Figure 1.8). First an active site cysteine nucleophilically adds to carbon-6 of the pyrimidine ring. A methyl transfer occurs from the donor S-adenosyl-L-methionine (AdoMet) or N^5,N^{10}-methylenetetrahydrofolate (mTHF) to carbon-5 of the ring to yield a methylated covalent adduct. Abstraction of a proton at carbon-5 and the beta-elimination of the nucleophile reforms the 5,6-double bond yielding the methylated pyrimidine and the free enzyme (65).

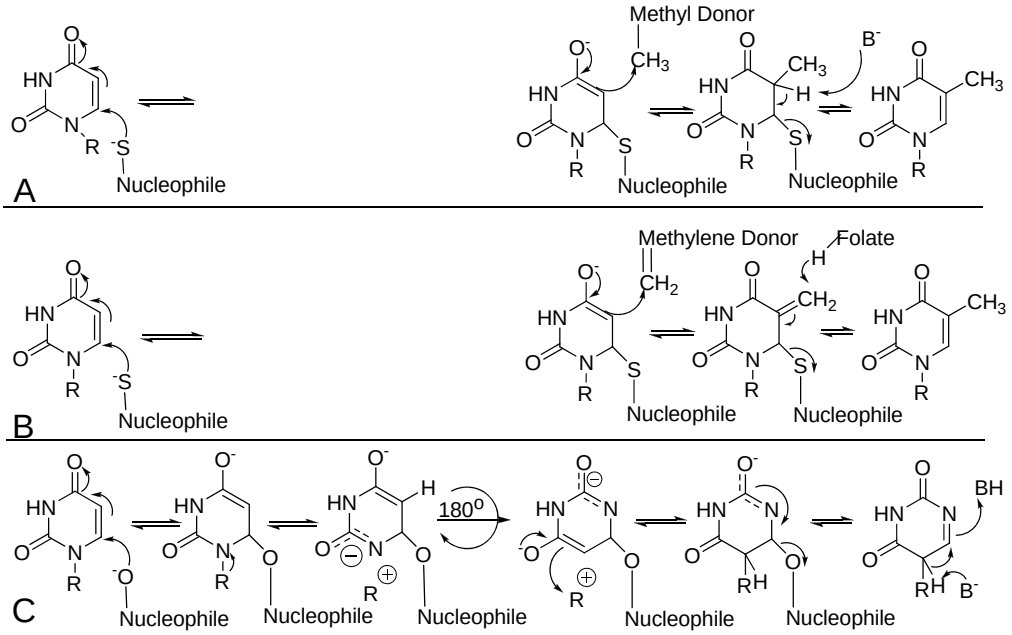

Figure 1.8: Nucleophilic Activation of Pyrimidines. Part A shows the alkylation reaction catalyzed by most cytosine and RNA methyltransferases. Part B shows the simplified mechanism for the methylation of pyrimidine by thymidylate synthase. Part C depicts the formation of pseudouridine. The analogous steps are aligned in each of these mechanisms, the attack of a nucleophile at carbon 6, an S_N2 like displacement reaction (absent in B), and the beta-elimination of the nucleophile with reformation of the double-bond.

The best-studied pyrimidine methylating enzyme is thymidylate synthase (ThyA) (66) (Figure 1.8B). Thymidylate synthase catalyzes the methylation of 2'-deoxyuridine-5'-monophosphate (dUMP) to form 2'-deoxythymidine-5'-monophosphate. This is the major pathway for the formation of thymine in DNA. The methylene donor in this reaction is the cofactor N^5,N^{10}-methylenetetrahydrofolate (mTHF). In the ThyA mechanism, the Michael addition of cysteine to the 6-position of dUMP yields an enolate, which then attacks mTHF (67). This forms a covalent bond between carbon-5 of dUMP and the one-carbon unit (C-11) of mTHF. The carbon-5 proton is abstracted, followed by elimination of H4folate to give an exocyclic methylene. Hydride transfer from non-covalently bound H4folate to the exocyclic methylene and elimination of nucleophile

yield the methylated pyrimidine and free enzyme. This reaction differs from the other pyrimidine methylases in a number of ways, but still uses the same activation by nucleophilic attack at carbon-6 to form the enolate needed to attack mTHF.

A more recently discovered class of thymidylate synthase (ThyX) uses N^5,N^{10}-mTHF as the methylene donor and $FADH_2$ as the reductant (68). Crystal structures of ThyX indicate that an active site serine is the likely nucleophile instead of cysteine, although the mechanism of these enzymes is still under investigation (69).

The enzyme tRNA(m^5U54)-methyltransferase catalyzes the methylation of Ura54 in the T-arm of tRNA using AdoMet as a methyl donor (70). This is one of the best studied RNA methyltransferases and follows essentially the same mechanism for nucleophilic activation of the ring as detailed for thymidylate synthase above (71). A recently crystallized RNA methyltransferase from *Thermotoga* has also been indicated to use mTHF as its methylene donor, showing an even closer potential connection between thymidylate synthase and some RNA methyltransfersaes (72). tRNA(m^5U54)-methyltransferase is but one example of the class I Rossmann-fold-like methyltransferases, all of which utilize an invariant cysteine residue (73). These enzymes are very similar to those of the DNA 5-methylcytosine methytransferase enzymes except that the position of the nucleophilic cysteine residue in these two groups of enzymes is located in different structural motifs (74). This difference in location of this active site cysteine is one of the definining structural differences between the m^5U and m^5C RNA methyltransferase and the m^5C DNA methyltransferases (75).

Thymine is found in DNA; with the equivalent base 5-methyluridine is found in RNA (76). 5-Methylcystosine is also found in both RNA and in DNA, with most DNA

methylation occurring in highly clustered regions called CG islands (77). The difference in the active site cysteine mentioned above sets these two families apart structurally, but mechanistically the enzymes behave similarly (78,79).

The formation of 5-methylcytosine by tRNA(m^5U54)-methyltransferase occurs through a mechanism that uses nucleophilic activation like the traditional thymidylate synthase (ThyA). In this enzyme the methyl donor is AdoMet which requires no redox reaction as a methyl is transferred rather than a methylene for ThyA. During the nucleophilic activation by this enzyme, the attack of cysteine at the 6-position of the pyrimidine ring can not form the same enolate that is seen for uracil (80,81). The tRNA(m^5U54)-methyltransferase enzyme facilitates the nucleophilic attack of the methyl donor by a transient protonation of the cytosine ring at N3, creating a cytosine 4,5-enamine that can then attack the methyl group of AdoMet (82). The reaction continues with normal abstraction of the proton from carbon-5 and beta-elimination (83,84).

Pseudouridine synthases also utilize nucleophilic attack to activate the pyrimidine ring (85) (Figure 1.8C). There are currently five known families of pseudouridine synthases and these families have little sequence similarity to one another (86). Pseudouridine synthases catalyze the post-transcriptional modifications of specific uridines in RNA to form pseudouridine (87). The reaction catalyzed by these enzymes is similar to those outlined above except the enzymes utilize an active site aspartate residue, which attacks the carbon-6 position of the uracil ring much like the attack of cysteine in the other enzymes. The N-glycosidic bond of the pyrimidine ring is then broken, allowing the ring to flip 180 degrees about the ester bond formed with aspartate (88). The glycosidic bond is then reformed and aspartate is eliminated; reprotonation at carbon-6

forms pseudouridine (89). The Michael addition and loss of the double bond between carbons 5 and 6, as well as its the subsequent reformation and elimination of the nucleophilic aspartate side chain are similar to the mechanisms of thymidylate synthase and the methyltransferases (Figure 1.8) (90,91,92).

This chapter has documented that all of these enzymes use a common chemical mechanism throughout many reactions and different enzyme families. The general principles of nucleophilic addition at C6 of the pyrimidine ring occurs in both the methylation and pseudouridilation of pyrimidines.

In examining the synthetic organic literature for methods to form thymidine, 5-methylcytidine, or pseudouridine, there are few similarities to the enzymatic reactions. The synthetic routes too many of these compounds involve multiple steps (93), particularly for pseudouridine. One of the closest synthetic reactions to those performed by methyltransferases is for the formation of thymine. This same synthetic reaction is also applicable to the formation of 5-methylcytosine. In the synthetic reaction formaldehyde acts as an electrophile adding to the pyrimidine at carbon-5. This yields a hydroxymethyl group (94). This group can be reduced by hydrogen on rhodium or platinum, as well as many other reductants to yield thymine. Though there are many synthetic routes for thymine, none seem to be similar to the enzymatic process. One interesting study has shown that cysteine alone can complex to uracil in solution and catalyze the exchange of protons at position-5 (95). This finding is intriguing given that this reaction, also used by the enzymes to activate the ring, occurs in solution without the aid of the enzyme scaffold (96,97,98). There is no alteration of the cysteine pK_a, and the

preference for addition at carbon-6 to catalyze exchange at carbon-5 is intrinsic to the pyrimidine-cysteine combination itself.

Conclusions

Through examination of the chemistry behind many of the modifications of pyrimidines we can see a number of interesting concepts develop. One of the general concepts is that many of the enzymes acting on the pyrimidine ring share common methods of activating the pyrimidine ring, such as activation of the 4-carbonyl oxygen for functional group exchange, or nucleophilic attack at position-6 to promote alkylation or psuedouridylation. Another concept that emerges along with this is that many of the enzymes involved in pyrimidine catabolism and anabolism have common though opposite functions and are perhaps derived from a common ancestor such as the dihydropyrimidases and dihydroorotases. We also see that a few of the chemical processes found in synthetic organic chemistry parallel those found in nature. Given the wide diversity of natural products based on the pyrimidine scaffold only a few enzymes were mentioned here. Nevertheless, it seems likely many of the mechanisms mentioned here are applicable to many of the as-yet uninvestigated pyrimidine modifications found in nature.

As we have just seen many pyrimidine-modifying enzymes share common modes of action and mechanisms for the reactions they perform. In the rest of this thesis we will examine some of the enzymes involved in carbon-carbon double-bond reduction and formation at carbon 5 and carbon 6.

The first chapter will examine the dihydrouridine synthase 2 from *Saccharomyces cerevisiae*. It is one of four dihydrouridine synthases found in yeast, and is involved in reducing uracil residues at positions 16 and 17 in the yeast tRNAs. The kinetics of this enzyme are examined using transient state kinetics. The results of these experiments

show that the reduction of the tRNA is the slowest step for the reaction. We also show that effiecient reduction of the tRNA by this enzyme is dependent upon a prior modification of the tRNA substrate. Site-directed-mytagenesis experiments indicate that an active site residue cystiene 117 acts as an active site acid in the reduction of the tRNA substrate. All of these experiments together show a detailed picture of how this enzyme functions to modify tRNA substrates.

The next chapter looks at the dihydrouridine synthase from the thermophilic bacterium *Thermotoga maritima*. The genome sequence of *T. maritima* shows the presence of only one dihydrouridine synthase, indicating this enzyme likely is responsible for all dihydrouridine formed in this organism. Kinetics and crystallographic studies of this enzyme were undertaken. From these studies it is shown that the enzyme can function as a dihydrouridine synthase, validating the predicted function of this gene. This enzyme is shown to have slow reactivity for both reduction by NADPH and oxidation by tRNA at 35 ^{o}C. This slow reactivity is concluded to occur due to a slow isomerization step from a comparison of reaction rates and kinetic isotope effect studies. This isomeraztion is hypothesized to occur due to blocking of the active site by a second flexible domain. Crystallization of the enzyme in the presence and absence of this domain shows that separation of this domain from the rest of the enzyme causes not major perturbations in the structure and strengthens the argument that this domain may be mobile enough to fold over the active site of the enzyme.

The last two chapters focus on the dihydroorotate dehydrogenase from the pathogenic bacterium *Enterococcus faecalis*. This enzyme is involved in the oxidation of dihydroorotate to orotate, the only redox step in pyrimidine metabolism. The kinetics of

this enzyme are examined in chapter four showing that the oxidative half-reaction with fumarate is rate limiting. The effect of pH upon the half-reactions is also studied indicating the involvement of an active site cystiene in protonation of fumarate and deprotonation of dihydroorotate, and an active site lysine is involved in binding to the carboxylates of both fumarate and dihydroorotate.

The final chapter looks at the structure and dynamics of the dihydroorotate dehydrogenase using x-ray crystallography and 3D NMR. The structure of the enzyme complexed to orotate, dihydroorotate, L-malate, 3,4-dihydroxybenzoate, and 3,5-dihydroxybenzoate are shown. Minor alterations in the enzyme are seen upon binding to different substrates, with the largest changes seen in the presence of L-malic acid. Even larger dynamic changes are seen upon binding of substrates to the enzyme in the solution structure. Partial assignment of this structure yields information about a static core of protein residues which changes little during the binding of ligands to the enzyme.

All of these chapters explore the mechanisms of the two enzyme families, dihydroorotate dehydrogenases and dihydrouridine synthases. Both enzyme families utilize an active site flavin prosthetic group in the oxidation or reduction of the pyrimidine. They also both use an active site cystiene to catalyze protonation/deprotonation of substrates. Both reactions for the oxidation/reduction of the prymidine are also shown to be reversible. Though different in many ways, both reactions show many of the same basic requirements.

The second chapter of this thesis has been submitted to the *Journal of Biological Chemistry*. The third chapter of this manuscript is in preparation for submission to *Biophysica Biochemica Acta*. The final two chapters of this thesis form the basis of a

paper examining the kinetics and structure of the dihydroorotate dehydrogenase from *E. faecalis* that is still in preparation.

References

1. Pinner A.,"Ueber die Einwirkung von Acetessigäther auf die Amidine. Pyrimidine" (1885) *Ber. Dtsch. Chem. Ges.* 18:759-763

2. Henderson, J.F, and Paterson, A.R.P., "Nucleotide Metabolism – An Introduction" Academic Press, New York (1973) 1–304.

3. Davidson, J.N., Chen, K.C., Jamison, R.S., Musmanno, L.A., Kern, C.B., "The evolutionary history of the first three enzymes in pyrimidine biosynthesis" (1993) *Bioessays* 15:157-64

4. Makoff A.J., and Radford, A.,"Genetics and biochemistry of carbamoyl phosphate biosynthesis and its utilization in the pyrimidine biosynthetic pathway" (1978) *Microbiol. Mol. Biol. Rev.* 42:307-328

5. Kothe, A., Powers-Lee, S.G., "Specificity determining residues in ammonia- and glutamine-dependent carbamoyl phosphate synthetases" (2002) *J. Biol. Chem.* 277:7231-7238

6. Rubio, V., Llorente, P., Britton, H.G., "Mechanism of carbamoyl phosphate synthetase from Escherichia coli--binding of the ATP molecules used in the reaction and sequestration by the enzyme of the ATP molecule that yields carbamoyl phosphate" (1998) *Eur. J. Biochem.* 255:262-270

7. Kantrowitz, E.R., Lipscomb, W.N., "*Escherichia coli* aspartate transcarbamylase: the relation between structure and function" (1998) *Science* 241:669-674

8. Cherfils, J., Vachette, P., Janin, J., "Modelling allosteric processes in *E. coli* aspartate transcarbamylase" (1990) *Biochimie* 72:617-624

9. Jin, L., Stec, B., Lipscomb, W.N., Kantrowitz, E.R., "Insights into the mechanisms of catalysis and heterotropic regulation of *Escherichia coli* aspartate transcarbamoylase based upon a structure of the enzyme complexed with the bisubstrate analogue N-phosphonacetyl-L-aspartate at 2.1 A" (1999) *Proteins* 37:729-742

10. Porter, T.N., Li, Y., Raushel, F.M., "Mechanism of the dihydroorotase reaction" (2004) *Biochemistry* 43:16285-16292

11. Andersen, P. S., Martinussen, J., and Hammer, K., "Sequence analysis and identification of the pyrKDbF operon from *Lactococcus lactis* including a novel gene, pyrK, involved in pyrimidine biosynthesis" (1996) *J. Bacteriol.* 178:5005–5012

12. Nielsen, F. S., Andersen, P. S., and Jensen, K. F., "The B Form of Dihydroorotate Dehydrogenase from *Lactococcus lactis* Consists of Two Different Subunits, Encoded by the *pyrDb* and *pyrK* Genes, and Contains FMN, FAD, and [FeS] Redox Centers" (1996) *J. Biol. Chem.* 271, 29359–29365

13. Liu, S., Neidhardt, E. A., Grossman, T. H., Ocain, T., and Clardy, J. "Structures of human dihydroorotate dehydrogenase in complex with antiproliferative agents" (2000) *Structure Fold. Des.* 8:25–33

14. Tao, W., Grubmeyer, C., Blanchard, T.S., "Transition state structure of *Salmonella typhimurium* orotate phosphoribosyltransferase" (1996) *Biochemistry* 35:14-21

15. Traut, T.W., Jones, M.E., "Uracil metabolism-UMP synthesis from orotic acd or uridine and conversion of uracil to beta-alanine: enzymes and cDNAs" (1996) *Prog. Nucleic Acid Res. Mol. Biol.* 53:1-78

16. Callahan, B.P., Miller, B.G., "OMP decarboxylase—An enigma persists" (2007) *Bioorg. Chem*. 35:465-469

17. Shaffer, P.M., Hsu, C., Abbott, M.T., "Metabolism of Pyrimidine Deoxyribonucleosides in *Neurospora crassa*" (1975) *J. Bact*. 121:648-655

18. Schackerz. K.D., Dobritzch, D., "Amidohydrolases of the Reductive Pyrimidie Catabolic Pathway Purification, Characterization, Structure, Reaction" (2006) *Biochem. Biophys. Acta* 67:123-130

19. Loh, D.K., Gyaneshwar, P., Papadimitriou, E.M., Fong, R., Kim, K., Parales, R., Zhou, Z., Inwood, W., Kustu, S., "A Previously Undescribed Pathway for Pyrimidine Catabolism" (2006*) Proc. Nat. Acad. Sci.* 103:5114-5119

20. Gojkovic, Z., Rislund, L., Andersen, B., Sandrini, M.P.B., Cook. P.F., Schnackerz, K.D., Piskur, J., Dihydropyrimidine amidohydrolases and dihydroorotases share the same origin and several enzymatic properties" (2003) *Nucleic Acids Res.* 31:1683-1692

21. Lohkamp, B., Andersen, B., Piskur, J., Dobritzsch, D., "The Crystal Structures of Dihydropyrimidinases Reaffirm the Close Relationship between Cyclic Amidohydrolases and Explain Their Substrate Specificity" (2006) *J. Biol. Chem.* 281:13762-13776

22. Lee, M., Chan, C.W., Guss, J.M., Christopherson, R.I., Maher, M.J., "Dihydroorotase from *Escherichia coli*: Loop Movement and Cooperativity between Subunits" (2005) *J. Mol. Biol.* 348:523-533

23. Dobritzsch, D., Andersen, B., Piskur, J., "Crystallization and X-ray diffraction analysis of dihydropyrimidinase from *Saccharomyces kluyveri*" (2005) *Acta Crys. Sect. F* 61:359-362

24. Gojkovic, Z., Rislund, L., Andersen, B., Sandrini, M.P.B., Cook, P.F., Schnackerz, K.D., Piskur, J., "Dihydropyrimidine amidohydrolases and dihydroorotases share the same origin and several enzymatic properties" (2003) *Nuc. Acids. Res.* 31:1683-1692

25. Soong, C., Ogawa, J., Sakuradan, E., Shimizu, S., "Barbiturase, a Novel Zinc-containing Amidohydrolase Involved in Oxidative Pyrimidine Metabolism" (2002) *J. Biol. Chem.* 277: 7051-7058

26. Gojkovic, Z., Jahke, K., Schnackerz, K.D., Piskur, J., "PYD2 Encodes 5,6-Dihydropyrimidine Amidohydrolase, which Participates in a Novel Fungal Catabolic Pathway" (2000) *J. Mol. Biol.* 295:1073-1087

27. Porter, T.N., Li, Y., Raushel, F.M., "Mechanism of the Dihydroorotase Reaction" (2004) *Biochemistry* 43:16285-16292

28. Thoden, J.B., Phillips, G.N., Neal, T.M., Raushel, F.M., Holden, H.M., "Molecular Structure of Dihydroorotase: A Paradigm for Catalysis through the use of a Biomolecular Metal Center" (2001) *Biochemistry* 40:6989-6997

29. MacLeod, T.J., Lunn, F.A., Bearne, S.L., "The Role of Lysine Residues 297 and 306 in Nucleoside Triphosphate Regulation of *E. coli* CTP Synthase: Inactivation by 2',3'-dialdehyde ATP and Mutational Analyses" (2006) *Biochem. Biophys. Acta* 1764:199-210

30. Endrizzi, J.A., Kim, H., Anderson, P.M., Baldwin, E.P., "Crystal Structure of *Escherichia coli* Cytidine Triphosphate Synthetase, a Nucelotide-Regulated Glutamine Amidotransferase/ATP-Dependent Amidoligase Fusion Protein and Homologue of Anticancer and Antiparisitic Drug Targets" (2004) *Structure* 43:6447-6463

31. Mueller, E.G., Palenchar, P.M., Buck, C.J., "The Role of the Cysteine Residues of ThiI in the Generation of 4-Thiouridine in tRNA" (2001) *J. Biol. Chem.* 276:33588-33595

32. Numata, T., Ikeuhi, Y., Fukai, S., Suzuki, T., Nureki, O., "Snapshots of tRNA sulphuration via adenylated intermediate" (2006) *Nature* 442:419-424

33. Waterman, D.G., Ortiz-Lombardia, M., Fogg, M.J., Koonin, E.V., Antson, A.A., "Crystal Structure of *Bacillus anthracis* ThiI, a tRNA-modifying Enzyme Containing the Predicted RNA-binding RNA-binding THUMP Domain" (2006) *J. Mol. Biol.* 356:97-110

34. Shigi, N., Suzuki, T., Terada, T., Shirouzu, M., Yokoyama, S., Watanabe, K., "Temperature-dependent Biosynthesis of 2-Thioribothymidine of *Thermus thermophilus* tRNA" (2006) *J. Biol. Chem.* 281:2104-2113

35. Fox, J.J., Praag, D.V., Wempen, I., Doerr, I.L., Cheong, L., Knoll, J.E., Eidinoff, M.L., Bendich, A., Brown, G.B., "Thiation of Nucleosides. II. Synthesis of 5-Methyl-2'-deoxycytidine and Related Pyrimidine Nucleosides" (1959) *J. Am. Chem. Soc.* 81:178-187

36. Z. Kaleta, B. T Makowski, T. Soos, R. Dembinski, "Thionation Using Fluorous Lawesson's Reagent" (2006) *Org. Lett.* 8:1625-1628

37. G. Minetto, L. F. Raveglia, A. Sega, M. Taddei, (2005) Eur. *J. Org. Chem*. 5277-5288

38. Hamed, E.A., El-Bardan, A.A., Saad, E.F., Gohar, G.A., Hassan, G.H., "Nucleophilic Substitutions at the Pyrimidine Ring. Conformational Preference of the Products and Kinetics of the Reactions of 2-chloro-3-nitro- and 2-chloro-5-nitro-pyridines with Arenethiolates" (1997) *Perkin Trans*. 2:1-10

39. Navaratnam, N., Sarwar, R., "An Overview of Cytidine Deaminases" (2006) *Int. J. Hematol*. 83:195-200

40. Sklenak, S., Yao, L., Cukier, R.I., Yan, H., "Catalytic Mechanism of Yeast Cytosine Deaminase: An ONIOM Computation Study" (2004) *Biochemistry* 126:14879-14889

41. Ko, T., Lin, J., Hu, C., Hsu, Y., Wang, A.H.J., Liaw, S., "Crystal Structure of Yeast Cytosine Deaminase" (2003) *J. Biol. Chem*. 278:19111-19117

42. Shen, M.H., Storb, U., "Activation-induced cytidine deaminase (AID) can target both DNA strands when the DNA is supercoiled" (2004) *Pro. Nat. Acad. Sci.* 101:12997-13002

43. Conticello, S.G., Thomas, C.J.F., Patersen-Mahrt, S.K., Neuberger, M., "Evolution of the AID/APOBEC Family of Polynucleotide (Deoxy)cytidine Deaminases" (2005) *Mol. Bio. And Evol*. 22:367-377

44. Ireton, G.C., Black, M.E., Stoddard, B.L., "The 1.14 Å Crystal Structure of Yeast Cytosine Deaminase Evolution of Nucleotide Salvage Enzymes and Implications for Genetic Chemotherapy" (2003) *Structure* 11:961-972

45. Frederico, L.A., Kunkel, T.A., Shaw, B.R., "Cytosine Deamination in Mismatched Base Pairs" (1993) *Biochemistry* 32:6523-6530

46. Shapiro, R., Klein, R., "The Deamination of Cytidine and Cytosine by Acidic Buffer Solutions. Mutagenic Implications" *Biochemistry* (1966) 5:2358-2362

47. Pascal, R.A., Walsh, C.T., "Mechanistic Studies with Deuterated Dihydroorotates on the Dihydroorotate Oxidase from *Crithidia fasciculate*" (1984) *Biochemistry* 23:2745-2752

48. Schanckerz, K.D., Dobritzsch, D., Lindqvist, Y., Cook, P.F., "Dihydropyrimidine Dehydrogenase: A Flavoprotein with Four Iron-Sulfur Clusters" (2004) *Biochem. Biophys. Acta* 1701:61-74

49. Xing, F., Martzen, M.R., Phizicky, E.M., "A Conserved Family of *Saccharomyces cerevisiae* Synthases Effects Dihydrouridine Modifications of tRNA" (2002) *J. Biol. Chem.* 8:370-381

50. Marcinkeviciene, J., Tinney, L.M., Wang, K.H., Rogers, M.J., Copeland, R.A., "Dihydroorotate dehydrogenate B of Enterococcus faecalis. Characterization and insights into chemical mechanism" (1999) *Biochemistry* 38:13129-13137

51. Rowland, P., Bjornberg, O., Nielsen, F.S., Jensen, K.F., Larsen, S., "The crystal structure of *Lactococcus lactis dihydroorotate dehydrogenase A complexed with the enzyme reaction product* throws light on its function" (1998) *Protein Science* 7:1269-1279

52. Norager, S., Arent, S., Bjornberg, O., Ottosen, M., Leggio, L.L., Jensen, K.F., Larsen, S., "*Lactococcus lactis* Dihydroorotate Dehydrogenase A Mutants Reveal Important Facets of the Enzymatic Function" (2003) *J. Biol. Chem.* 278:28812-28822

53. Pinheiro, M.P., Iulek, J., Nonato, M.C., "Crystal Structure of the *Trypanosoma cruzi* dihydroorotate dehydrogenase from Y strain" *Biochem. Biophys. Res. Comm.* (2008) 369: 812-817

54. Dobritzsch, D., Ricagno, S., Schneider, G., Schnackerz, K.D., Lindqvist, Y., "Crystal Structure of the Productive Ternary Complex of Dihydropyrimidine Dehydrogenase with NADPH and 5-Iodouracil" (2002) *Structure* 277:13155-13166

55. Fagan, R.L., Jensen, K.F., Björnberg, O., Palfey, B.A., "Mechanism of flavin reduction in the class 1A dihydroorotate dehydrogenase from *Lactococcus lactis*" (2007) *Biochemistry* 46:4028-4036

56. Fagan, R.L., Nelson, M.N., Pagano, P.,M., Palfey, B.A., "Mechanism of flavin reduction in class 2 dihydroorotate dehydrogenases" (2006) *Biochemistry* 45:14926-14932

57. Wolfe A.E., Thymark M., Gattis S.G., Fagan R.L., Hu Y.C., Johansson E., Arent S., Larsen S., Palfey B.A., "Interaction of benzoate pyrimidine analogues with class 1A dihydroorotate dehydrogenase from *Lactococcus lactis*" (2007) *Biochemistry* 46:5741-5753

58. Mohsen, A.A., Rigby, S.E.J., Jensen, K.F., Munro, A.W., Scrutton, N.S., "Thermodynamic Basic of Electron Transfer in Dihydroorotate Dehydrogenase B from Lactococcus lactis: Analysis by Potentiometry, EPR Spectroscopy, and ENDOR Spectroscopy" (2004) *Biochemistry* 43:6498-6510

59. Scannell, M.P, Fenick, D.J., Yeh S.R., Falvey, D.E., "Model Studies of DNA Photorepair: Reduction Potentials of Thymine and Cytosine Cyclobutane Dimers Measured by Flourescence Quenching" (1997) *J. Am. Chem. Soc.* 119:1971-1977

60. Schanckerz, K.D., Dobritzsch, D., Lindqvist, Y., Cook, P.F., "Dihydropyrimidine Dehydrogenase: A Flavoprotein with Four Iron-Sulfur Clusters" (2004) *Biochem. Biophys. Acta* 1701:61-74

61. Xing, F., Hiley, S. L., Hughes, T.R., Phizicky, E.M., "Specificities of Four Yeast Dihydrouridine Synthases for Cytoplasmic trnas" (2004) *J. Biol. Chem.* 279:17850-17860

62. Cum, G., Gallo, R., Ipsale, S., Spadaro, A., "Selective Synthesis of Alkynes by Catalytic Dehydrogenation of Alkenes over Polymer-supported Palladium Acetate in the Liquid Phase" (1985) *J. Am. Chem. Soc.* 86:1571-1577

63. Huff, M., Schmidt, L.D., "Ethylene Formation by Oxidative Dehydrogenation of Ethane over Monoliths at Very Short Contact Times" (1993) *J. Phys. Chem.* 97:11815-11822

64. Adlhart, C., Uggerud, E., "Mechanisms for the dehydrogenastion of alkanes on platinum: insights gained from the reactivity of gaseous cluster cations. Ptn+n =1-21" (2007) *Chemistry* 13:6883-6890

65. Pradhan, S., Esteve, P., "Mammalian DNA (cytosine-5) Methyltransferases and their Expression" (2003) *Clin. Imm.* 109:6-16

66. Costi, M.P., Ferrari, S., Venturelli, A., Calo, S., Tondi, D., Barlocco, D., "Thymidylate Synthase Structure, Function and Implication in Drug Discovery" (2005) *Curr. Med. Chem.* 12:2241-2258

67. Cerreras, C.W., Santi, D.V., "The Catalytic Mechanism and Structure of Thymidylate Synthase" (1995) *Science* 64:721-762

68. Myllykallio, H., Lipowski, G., Leduc, D., Filee, J., Forterre, P., Liebl, U., "An Alternative Flavin-Dependent Mechanism for Thymidylate Synthesis" (2002) *Science* 297:105-107

69. Sampathkumar, P., Turley, S., Ulmer, J.E., Rhie, H.G., Sibley, C.H., Hol, W.G., "Structure of the Mycobacterium tuberculosis flavin dependent thymidylate synthase (MtbThyX) at 2.0A resolution" (2005) *J. Mol. Biol.* 352:1091-1104

70. Cicmil, N., "Crystallization and preliminary X-ray crystallographic characterization of TrmFO, a folate-dependent tRNA methyltransferase fro *Thermotoga maritima*" (2008*) Acta Cryst. Sect. F Struct. Biol. Cryst. Commun.* 64: 193-195

71. Gu, X., Santi, D.V., "Covalent Adducts between tRNA (m5U54)-methyltransferase and RNA substrates" (1992) *Pro. Nat. Acad. Sci.* 31:10295-10302

72. Kealey, J.T., Santi, D.V., "Stereochemistry of tRNA (m5U54)-methyltransferase catalysis: 19F NMR Spectroscopy of and Enzyme-FUraRNA covalent complex" (1995) *Biochemistry* 34:2441-2446

73. Roovers, M., Oudjama, Y., Kaminska, K.H., Purta, E., Caillet, J., Droogmans, L., Bujnicki, J.M., "Sequence-structure-function Analysis of the Bifunctional Enzyme MnmC that Catalyses the Last Two Steps in the Biosynthesis of Hypermodified Nucleoside mnm^5s^2U in tRNA" (2008) *Prot. Struct. Funct. Bioinf.* In press

74. Pioszak, A.A., Murayama, K., Nakagawa, N., Ebihara, A., Kuramitsu, S., Shirouzu, M., Yokoyama, S., "Structures of a Putative RNA 5-Methyluridine Methyltransferase, *Thermus thermophilus* TTHA1280, and its Complex with S-Adenosyl-L-Homocysteine" (2005) *Structure* 61:867-874

75. Christian, T., Hou, Y.M., "Distinct Determinants of tRNA Rocognition by the TrmD and Trm5 Methyl Transferases" (2007) *J. Mol. Biol*. 373:623-632

76. Reichow, S.L., Hamma, T., Ferre-D'Amare, A.R., Varani, G., "The Structure and unction of Small Nucleolar Ribonucleoproteins" (2007) *Nucleic Acids Res.* 35:1452-1464

77. Hattman, S., "Partial Purification of the *Escherichia coli* K-12 mec^+ Deoxyribonucleic Acid-Cytosine Methylase: *In Vitro* Methylation Completely Protects Bacteriophage Lambda Deoxyribonucleic Acid Against Cleavage by R. EcoRII" (1977) *J. Bact.* 129:1330-1334

78. Motorin, Y., Grosjean, H., "Multisite-specific tRNA: m^5C-methyltransferase (Trm4) in yeast *Saccharomyces cerevisiae*: Identification of the Gene and Substrate Specificity of the Enzyme" (1999) *RNA* 5:1105-1118

79. Ferre-D'Amare, A.R., "RNA-modifying Enzymes" (2003) *Curr. Opin. Struct. Bio.* 13:49-55

80. Zhang, X., Bruice, T.C., "The Mechanism of MHhaI DNA C5 Cytosine Methyltransferase Enzyme: A Quantum Mechanics/Molecular Mechanics Approach" (2006) *Biochemistry* 103:6148-6153

81. Montfort, W.R., Weichsel, A., "Thymidylate synthase: structure, inhibition, and strained conformations during catalysis" (1997) *Pharmacol. Ther*. 76:29-43

82. Cheng, X., Blumenthal, R.M., "Mammalian DNA Methyltransferases: A Structural Perspective" (2008) *Structure* 16:341-350

83. Siedlecki, P., Zielenkiewicz, P., "Mammalian DNA Methyltransferase" (2006) *Biochem. Biophys. Acta* 53:245-256

84. Svedruzic, Z.M., "Mammalian Cystosine DNA Methyltransferase Dnmt1: Enzymatic Mechanism, Novel Mechanism-Base and RNA-directed DNA Methylation" (2008) *J. Biol. Chem.* 15:92-106

85. Ofengand, J., Malhotra, A., Remme, J., Gutgsell, N.S., Del Campo, M., Jean-Charles, S., Peil, L., Kaya, Y., "Pseudouridines and Pseudouridine Synthases of the Ribosome" (2001) *Cold Spring Harbor Quant. Biol*. 66:147-159

86. Decatur, W.A., Schnare, M.N., "Different Mechanisms for Pseudouridine Formation in Yeast 5S and 5.8S Ribosomal RNAs" (2008) *Mol. Cell Biol*. In press

87. Speraliere, C.J., Ginter, J.M., Johnston, M.V., Mueller, E.G., "The Pseudouridine Synthases: Revisiting a Mechanism That Seemed Settled" (2004) *J. Am. Chem. Soc.* 126:12758-12759

88. Hur, S., Stroud, R.M., Finer-Moore, J., "Substrate Recognition by RNA 5-Methyluridine Pseudouridine Synthases: A Structural Perspective" (2006) *J. Biol. Chem.* 281:38969-38973

89. Hamma, T., Ferre-D'Amare, A.R., "Pseudouridine Synthases" (2006) *Chemistry and Biology* 13:1125-1135

90. McCleverty, C.J., Hornsby, M., Spraggon, G., Kreusch, A., "Crystal Structure of Human Pus10 A Novel Pseudouridine Synthase" (2007) *J. Mol. Biol.* 373:1243-1254

91. Hamilton, C.S., Greco, T.M., Vizthum, C.A., Ginter, J.M., Johnston, M.V., Mueller, E.G., "Mechanistic Investigations of the Pseudouridine Synthase RluA Using RNA Containing 5-Fuorouridine" (2006) *Biochemistry* 45:12029-12038

92. Gu, X., Liu, Y., Santi, D.V., "The mechanism of pseudouridine synthase I as deduced from its interaction with 5-fluorouracil-tRNA" (1999) 96:14270-14275

93. Fox, J.J., Yung, N., Davoll, J., Brown, G.B., "Pyrimidine Nucleosides. I. A New Route for the Synthesis of Thymine Nucleosides" (1956) *Org. and Biol. Chem.* 78:2117-2122

94. Cline, R.E., Fink, R.M., Fink, K., "Synthesis of 5-Substituted Pyrimidines via Formaldehyde Addition" (1959) *J. Am. Chem. Soc.* 81:2521-2527

95. Wataya, Y., Hayatsu, H., Kawazoe, Y. "Cysteine-catalyzed hydrogen isotope effect exchange at position 5 of uridylic acid", (1957) *J. Biochem*. 1973 73: 871-877

96. Wataya, Y., Hayatsu, H., Kawazoe, Y., "Cysteine-catalyzed Hydrogen Isotope Exchange at Position 5 of Uridylic Acid" (1973) *J. Biochem*. 73:871-877

97. Wataya, Y., Hayatsu, H., "Effect of Amines on the Bisulfite-catalyzed Hydrogen Isotope Exchange at the 5 Position of Uridine" (1972) *Biochemistry* 11:3583-3588

98. Sono, M., Wataya, Y., Hayatsu, H., "Role of Bisulfite in the Deamination and the Hydrogen Isotope Exchange of Cytidylic Acid" (1973) *J. Am. Chem. Soc.* 95:4745-4749

Chapter 2

Kinetics of a Dihydrouridine Synthase from *Saccharomyces cerevisiae*

Introduction

Dihydrouridine is one of the most common modified nucleosides present in the tRNA of eubacteria, eukaryotes, and some archea (1). This modified nucleoside is formed by the reduction of the carbon-carbon double bond in uridine at specific sites in tRNA, most commonly in the D-loop. Our understanding of the physiological role of dihydrouridine is still in its infancy, but one possibility is a structural role. NMR studies have shown that dihydrouridine increases the flexibility of the RNA backbone to allow alternate conformations because its non-planar structure disrupts stacking (2). In addition, a role for dihydrouridine in conformational flexibility is also suggested by its distribution among different species. The dihydrouridine content of species adapted to cold environments (psychrophiles) is the highest found in nature, whereas thermophilic species tend to have much less or no dihydrouridine (3). It has been suggested that the chemical stability of RNA structures is enhanced by the absence of dihydrouridine, perhaps explaining why thermophilic species often lack dihydrouridine – to avoid hydrolytic ring opening at high temperatures (4).

Recent studies have hinted at further physiological roles for dihydrouridine. tRNA that lacks dihydrouridine, along with other modifications, degrades at a substantially

increased rate, approaching that seen for mRNA (5). The main function of dihydrouridine may therefore be to protect tRNA from degradation. It has long been known that dihydrouridine levels are increased in cancerous tissues (6). Recent studies have shown that the human dihydrouridine synthase 2 is responsible for the increased dihydrouridine levels formed in pulmonary carcinogenesis (7). This information suggests that dihydrouridine plays an important role in maintaining proper tRNA turnover.

The family of enzymes catalyzing the reduction of uridine in tRNA, dihydrouridine synthases (DUS), has recently been identified in *Saccharomyces cerevisiae* and *Escherichia coli*. DUSs from *S. cerevisiae* were identified by biochemical assays of pooled yeast proteins (8), while the enzymes from *E. coli* were identified by a bioinformatics approach (9). Sequencing and annotation of many microbial genomes suggests the presence of DUSs in a wide number of species. The enzymes from *S. cerevisiae* are NADPH-dependent with non-overlapping RNA specificity (10).

From recent structural and homology models, and from analogies to other flavoenzymes that act on pyrimidines, putative active site residues can be deduced. The crystal structure of the enzyme from *Thermotoga maritima* has a conserved cysteine residue positioned within a suitable distance to protonate the uracil ring as it is reduced. Although the process behind dihydrouridine formation is becoming better understood, there have been no detailed studies on the kinetics of these enzymes to date. To better understand how these enzymes function we have investigated the catalytic mechanism of DUS 2 from *S. cerevisiae* and an active-site cysteine mutant. We find that the enzyme is able to reduce tRNA and surprisingly prefers modified tRNA substrates to *in vitro*

transcribed tRNA. We also show that the active site cysteine is important for catalysis, likely acting to protonate the uracil ring.

Materials and Methods

Materials

NADP and NADPH were from Research Products International. ATP, GTP, CTP, and UTP were from Amersham Pharmacia Biotech. 1-d-Glucose was from Cambridge Isotopes Laboratories. All other chemicals were purchased from Sigma-Aldrich.

Construction of the *S. cerevisiae* C117A mutant plasmid

The C117A mutant plasmid was constructed from the pEfx-4b plasmid (donated by Eric Phyzicky) and mutated using the QuikChange site directed mutagenesis kit (Stratagene) using the following forward primer 5'-ATCAATGCAGGCGCCCCCAAA-CAGTTCT-3' and reverse primer 5'-AGAGAAGTGTTTG-GGGGCGCCTGCA-3'.

Expression and Purification of DUS

BL21 DE3 cells were transformed with the plasmid for the *S. cerevisiae* enzyme by heat shock, and plated on LB agar plates containing 0.1 g/L ampicillin and incubated overnight at 37 °C. Single colonies were used to inoculate 5 mL LB which was shaken at 400 rpm overnight in a 37 °C incubator. From these cultures 1 mL was added to 1 L of LB containing 0.1 g/L ampicillin. The cells were grown to an OD600 of 0.8 and induced using 0.1 mM IPTG (final concentration) and grown for 5-6 hrs at 37 °C.

The DUS-containing cells were pelleted by centrifugation (16,000 x g for 20 minutes) and resuspended in 100 mM HEPES pH 7.5, 100 mM NaCl, 10 mM $MgCl_2$, 10% glycerol. The cells were sonicated for 15 minutes on ice. Cell debris was removed

by centrifugation (20,000 x g for 30 minutes). The clarified supernatant was then passed over a 3.8 cm x 10 cm TALON metal affinity column (Clonetech), which had been loaded with cobalt (II) acetate and pre-equilibrated with 100 mM HEPES pH 7.5, 100 mM NaCl, 10 mM $MgCl_2$, 10% glycerol. The column was then washed with 3 column-volumes of 100 mM HEPES pH 7.5, 100 mM NaCl, 10 mM $MgCl_2$, 10% glycerol, and the protein was eluted from the column with the same buffer containing 200 mM imidazole. The eluted enzyme was then washed extensively with 100 mM HEPES pH 7.5, 100 mM NaCl, 10 mM $MgCl_2$, 10% glycerol in an Amicon ultrafiltration device (10,000 MWCO). Wild-type DUS 2 was stored at 4 °C with 1 mM DTT after elution from the metal affinity column. The DTT was removed by a PD-10 desalting column immediately prior to experiments.

The enzyme obtained by metal affinity purification showed a single band on SDS-PAGE at ~43 kDa. However, the absorbance spectrum of the enzyme purified in this way had an unusual peak at 340 nm in addition to the expected flavin absorbance. Therefore, the enzyme was purified further to remove this contaminant by applying it to a 3.8 cm x 14 cm DEAE Sepharose column at 25 °C that was pre-equilibrated in 100 mM HEPES pH 7.5, 100 mM NaCl, 10 mM $MgCl_2$, 10% glycerol. The column was washed extensively with 100 mM HEPES pH 7.5, 100 mM NaCl, 10 mM $MgCl_2$, 10% glycerol.

The yellow fractions containing protein free of the contaminating chromophore were collected. Protein which remained bound to the column was eluted with 100 mM HEPES pH 7.5, 1 M NaCl, 10 mM $MgCl_2$, 10% glycerol and showed a proportionately higher 340 nm peak. Enzyme fractions free of the chromophore were pooled,

concentrated, washed with 100 mM HEPES pH 7.5, 100 mM NaCl, 10 mM $MgCl_2$, 10% glycerol, and stored at 4 °C.

Purification of mature $tRNA^{Leu}$

Mature $tRNA^{Leu}$ was purified from a *S. cerevisiae* YNR015w knockout strain. A total of eighty liters of yeast cultured in YPD were grown to saturation by shaking at 30 °C in 1 liter flasks. The yeast was pelleted at ~5000 g for 15 minutes and frozen until use. The frozen cell pellet was resuspended in 50 mM LiCl, 10 mM EDTA, 10 mM Tris-HCl pH 6.5, 0.1% SDS and thawed to room temperature. The cells were then treated with phenol-chloroform, buffered to pH 4.7, and centrifuged (4200 x g for 30 minutes). The RNA in the supernatant was precipitated with 2 volumes of ethanol and 0.2 M LiCl. The RNA was washed with 70% ethanol, frozen, and lyophilized. The tRNA was purified further on an oligonucleotide column made by treating NHS-Sepharose (Amersham-Pharmacia) with an aminated oligonucleotide (IDT) complementary to the 3'-end of $tRNA^{Leu}$-CCA. The tRNA was heated to 50 °C in 1 M NaCl, 10 mM Tris, pH 8.5, and loaded on the column. The column was washed with 3 column volumes 1 M NaCl, 10 mM Tris, pH 8.5, heated to 50 °C, and eluted in 10 mM Tris pH 8.5.

Enzyme Concentrations

The extinction coefficient of the enzyme was determined by recording the absorbance spectrum of the enzyme, adding SDS (1% final concentration), and recording the spectrum of the FMN liberated upon protein unfolding. The extinction coefficient was calculated from the ratio of the absorbance of the free FMN (12) to that of the native

enzyme. The extinction coefficient at 457 nm was 12,800 M^{-1} cm^{-1} in 50% glycerol, 20 mM Tris, pH 8.0, 55 mM NaCl, 1 mM DTT. Enzyme concentrations were routinely determined spectrophotometrically using this extinction coefficient and are given in terms of active site concentrations.

Reaction Kinetics

Enzyme solutions for kinetics were made anaerobic in glass cuvettes or tonometers by multiple cycles of evacuation followed by equilibration with an atmosphere of purified argon. When reduced enzyme was needed, a gas-tight syringe containing a dithionite solution (~6 mM) was attached to the cuvette, and the anaerobic enzyme was titrated to complete reduction with one equivalent of dithionite, as judged by absorbance spectroscopy. Reactions were performed at 4 °C using 100 mM HEPES pH 7.5, 100 mM NaCl, 10 mM $MgCl_2$, 10% glycerol unless stated otherwise. Absorbance spectra were obtained over time using a Shimadzu UV-2501PC scanning spectrophotometer for slow oxidative half-reactions; rapid reactions were studied anaerobically using a Hi-Tech Scientific SF-61DX2 stopped-flow spectrophotometer using published techniques (13).

Binding Titrations

Binding titrations were carried out in quartz fluorescence cuvettes at 25 °C in 100 mM HEPES pH 7.5, 100 mM NaCl, 10 mM $MgCl_2$, 10% glycerol in a Shimadzu RF-5301 PC Spectrofluorophotometer. Enzyme (~20 μM) was titrated with increasing concentrations of ligands. Excitation was at 450 nm and emission was scanned from 460

to 650 nm, with a maximum fluorescence change observed at 517 nm. The change in fluorescence was plotted against the concentration of ligand and fit to Equation (1).

$$\Delta Fluorescence = \frac{\Delta F_{\max}[Ligand]}{K_D + [Ligand]} \quad (1)$$

tRNA Synthesis

tRNAs were produced in reactions containing 50 mM Tris-HCl, pH 7.5, 15 mM $MgCl_2$, 5 mM dithiothreitol, 2 mM spermidine, 20 mM of each NTP, T7 RNA polymerase, and DNA template (10 ng/μL). The templates for each reaction were synthesized by PCR using two complementary primers (Invitrogen) comprising the entire tRNA gene to be transcribed, and a T7 RNA polymerase promoter upstream. The sequence of the *S. cerevisiae* pre-$tRNA^{Leu}$ substrate and intronless variant used were GGTTGTTTGGCCGAGCGGTCTAAGGCGCCTGATTCAAGCTCAGGTATCGTAA GATGCAAGAGTTCGAATCTCTTAGCAACCA and GAAATTAATACGACTCAC-TATAGGTTGTTTGGCCGAGCGGTCTAAGGCGCCTGATTCAAGCTCAGGTATCG TAAGATGCAAGAGTTCGAATCTCTTAGCAACCA respectively. Synthetic tRNA was purified by phenol-chloroform extraction to remove RNA polymerase and the RNA was precipitated with 2 volumes of ethanol. The RNA concentration was calculated from the absorbance at 256 nm using extinction coefficients predicted from the base composition tRNA using the nearest neighbor method (14). Extinction coefficients of 1,019,100 M^{-1} cm^{-1} was used for the *S. cerevisiae* pre-$tRNA^{Leu}$ and an extinction of 764,800 M^{-1} cm^{-1} was used for the intronless and modified $tRNA^{Leu}$ purified from *S. cerevisiae*. Before use tRNA was heated to 65 degrees for 10 minutes and cooled on ice for 5 minutes to ensure proper folding of the tRNA.

Dihydrouridine Assay

Dihydrouridine produced by the reduction of tRNA was determined using a colorimetric assay (15). tRNA (125 μM in 0.3 mL) was treated with 0.03 mL 1 M KOH and incubated for 30 minutes at 37 °C, hydrolyzing the dihydrouridine ring. The sample was then acidified with 0.15 mL 1 M H_2SO_4 and 0.3 mL of a solution of 10 mM butadienone malemide and 5 mM semidine was added. The sample was heated for 5 minutes at 95° C in a heating block, cooled to 50° C for 5 minutes, 0.3 mL of 10 mM $FeCl_3$ was added, and the absorbance at 550 nm was read. Concentrations were determined by comparison with a standard curve determined from known concentrations of dihydrouracil with a linear range between 20 and 250 μM.

Preparation of [4-^{2}H]NADPH

[4*R*-^{2}H]NADPH was prepared as described by Ottolina et al. (16). A 10 mL solution of 50 mM sodium bicarbonate pH 8.5, 0.5 M 2-$_D$-isopropanol, 13 mM NADP and 20 U of *Thermoanaerobacter brockii* alcohol dehydrogenase (Sigma) was incubated at 30 °C for 4 hours. The solution was diluted to 20 mL with H_2O and chromatographed on a 2.8 cm x 40 cm DE-53 column (carbonate form). The [4*R*-^{2}H]NADPH was eluted with a sodium bicarbonate gradient (0-0.5 M, 500 mL). Fractions with a ratio of A254/A340 of 2.5 or less were pooled and lyophilized. The lyophilized product was chromatographed with water on a 2 cm x 50 cm Sephadex G-10 column to remove salt (17). Fractions containing [4*R*-^{2}H]NADPH were pooled and the product was precipitated with 70% acetone at 4 °C to concentrate, dissolved in a minimal amount of water, and lyophilized.

[4*S*-^{2}H]NADPH was prepared in a 6 mL solution of 50 mM HEPES pH 7.5, 15 mM 1-$_D$-glucose, 15 mM ATP, 15 mM NADP, 15 mM $MgCl_2$ 100 U hexokinase, and 100 U glucose-6-phosphate dehydrogenase. The reaction was incubated at 25 °C for 5 hours and the [4*S*-^{2}H]NADPH was purified as described above.

Stereochemistry

The stereochemistry of oxidation of NADPH by the enzyme was determined by incubating 1.5 mL of an aerobic solution containing 2 mM [4*R*-^{2}H]NADPH, 100 μM of DUS, 100 mM potassium phosphate pH 7.5, 100 mM NaCl, 10 mM $MgCl_2$ in D_2O at 35 °C. After [4*R*-^{2}H]NADPH was completely oxidized (no absorbance at 340 nm; ~2 hours), enzyme was removed by ultrafiltration (Amicon Ultra 10,000 MWCO) and a 300 MHz ^{1}H-NMR spectrum was recorded using the water peak as a chemical shift reference (4.2 ppm). An identical procedure was used for [4*S*-^{2}H]NADPH.

Identification of tRNAs bound to DUS

tRNA bound to the enzyme after purification by the metal affinity column was extracted with phenol-chloroform to remove the protein and precipitated with ethanol to yield the pure tRNA. Mixtures of ~3.5 μmol tRNA were incubated in a 10 mL reaction at pH 7.4 in 100 mM KPi with 0.8 mM of each amino acid, 10 mM ATP, and 2880 U aminoacyl-tRNA synthetases from *E. coli* (Sigma A3646-10KU) to ensure complete aminoacylation of the tRNAs. The reactions were incubated for 18 hours, extracted with phenol-chloroform and the tRNA was precipitated with 2 volumes ethanol. The tRNA was dissolved in 200 μL of 100 μM KPi pH 9.0 and incubated for 5 hours to hydrolyze

the aminoacyl-esters. The tRNA was separated from the amino acids by ultrafiltration with 10,000 MWCO Microcon centrifugal filtration devices (Amicon) previously washed with H_2O. The flow-through was collected and analyzed by the Protein Facility of the Iowa State University Office of Biotechnology on an automated Beckman System Gold HPLC amino acid analyzer.

Results

The catalytic cycles of flavoenzymes are frequently composed of a reductive half-reaction, in which one substrate reduces the flavin, and an oxidative half-reaction, in which another substrate oxidizes the flavin (Figure 2.1).

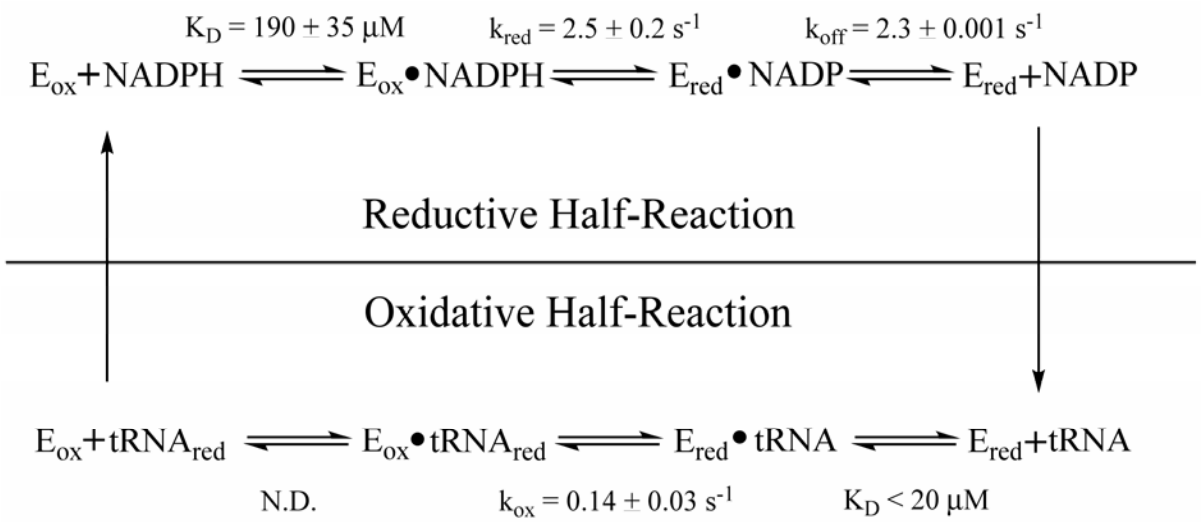

Figure 2.1: DUS2 Catalytic Cycle. Scheme for the catalytic cycle of DUS 2.

However in many flavoenzymes, the second substrate binds and reacts before the first product is released, deviating from the typical ping-pong mechanism. Transient kinetic experiments were performed in order to determine the mechanism followed by the flavoenzyme DUS 2 from *S. cerevisiae*.

Reductive Half-Reaction

NADPH has been reported to be the reducing substrate for the DUS 2 enzyme from *S. cerevisiae* (10). The reductive half-reaction of DUS 2 is proposed to start with NADPH binding to the enzyme (Figure 2.1). The NADPH then transfers a hydride to the

active site flavin prosthetic group, reducing the enzyme. Finally NADP dissociates yielding free reduced enzyme.

In attempting to further understand the mechanism of reduction, we investigated the stereofacial selectivity of NADPH oxidation. [4*R*-^{2}H]NADPH and [4*S*-^{2}H]NADPH were oxidized and the NADP produced was analyzed by ^{1}H-NMR. When [4*R*-^{2}H]NADPH was the substrate, a proton signal was observed at 8.4 ppm for the proton at the 4-position of the nicotinamide ring of NADP, the product, indicating that the *R*-deuteron was transferred (data not shown). When [4*S*-^{2}H]NADPH was used, the NADP produced lacked the signal at 8.4 ppm, indicating retention of the *S*-deuteron and transfer of the *R*-hydrogen. Therefore, DUS is specific for the *proR*-hydrogen of NADPH.

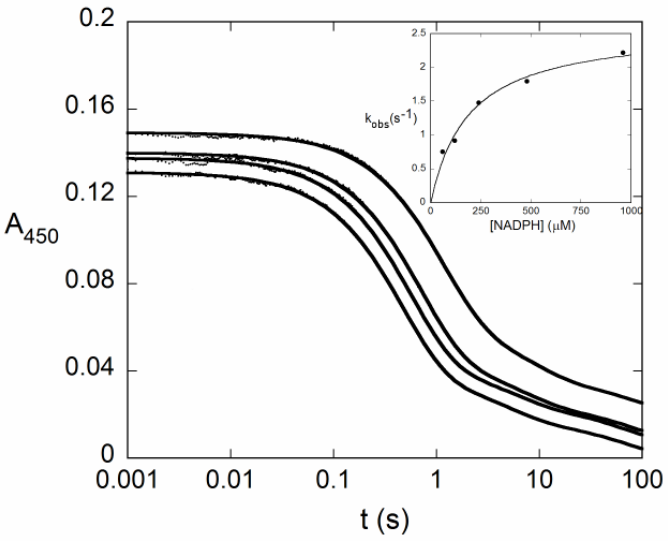

Figure 2.2: DUS2 Reduction by NADPH. Anaerobic DUS 2 (15 μM) in 100 mM HEPES pH 7.5, 100 mM NaCl, 10 mM $MgCl_2$, 10% glycerol, was mixed with anaerobic solutions of NADPH in a stopped-flow spectrophotometer at 4 °C. Reaction traces at 450 nm are shown for a series of increasing concentrations of NADPH. Note the logarithmic time scale. The inset shows the observed rate constant for the first phase of reduction obtained from fits of each trace versus concentration, giving a rate constant for reduction of 2.5 ± 0.2 s^{-1} and a K_D of 190 μM.

The kinetics of the reductive half-reaction were studied at 4 °C by mixing 15 μM anaerobic oxidized enzyme with anaerobic solutions of NADPH in a stopped-flow spectrophotometer. The absorbance of the flavin, monitored at 450 nm, decreased in three phases (Figure 2.2). The first phase, which contributed the majority of the absorbance decrease and represents flavin reduction, increased hyperbolically with NADPH concentration, giving a maximum rate constant of 2.5 ± 0.2 s^{-1} at saturating NADPH. A K_D of 190 ± 35 μM was determined from the dependence of flavin reduction on the concentration of NADPH (18). Two other decreasing exponentials, together accounting for ~30% of the absorbance change, were seen in these traces, with rate constants of 0.21 ± 0.005 s^{-1} and 0.015 ± 0.0007 s^{-1}. These did not vary with NADPH concentration and were possibly due to damaged enzyme. This damage is possibly due to the oxidation of the enzyme which occurs rapidly in the absence of the reductant DTT. A weak charge-transfer absorbance was observed at 580 nm, which corresponds to an NADP-reduced flavin charge-transfer complex seen in many NAD(P)-dependent flavoenzymes (19). A trace at 580 nm was fit to two exponentials by fixing the rate constant for the formation of the charge-transfer absorbance to 2.5 s^{-1}, the rate constant of flavin reduction. A rate constant of 2.29 ± 0.01 s^{-1} for the second phase was obtained, likely corresponding to the rate constant for NADP dissociation from the reduced enzyme. In a separate experiment, the rate constants for flavin reduction were also measured using [4*R*-^{2}H]NADPH and NADPH giving 0.42 ± .05 s^{-1} and 1.47 ± 0.3 s^{-1}, respectively. A KIE value of 3.5 ± 0.2 was calculated, indicating that hydride transfer is at least partly rate-limiting.

The reductive half-reaction of the C117A mutant of DUS 2 was studied in the same way. Traces were fit to three exponentials. A first phase (12.7 ± 2 s^{-1}) corresponded

to a small initial absorbance decrease independent of NADPH concentration. This was followed by a second phase that accounted for the majority of the absorbance decrease, giving a reduction rate constant of 5.55 ± 0.01 s^{-1} and a K_D of 53 ± 3 μM. A band was seen at 675 nm corresponding to an NADP-reduced flavin charge-transfer complex. A trace at 675 nm was fit to two exponentials by fixing the rate constant for the formation of the charge-transfer absorbance to 5.55 s^{-1}, giving the rate constant for the second phase of 7 ± 2 s^{-1}, and likely corresponds to the rate constant for NADP dissociation from the reduced enzyme.

Oxidative Half-Reaction

A general mechanism for the oxidative half-reaction is seen in Figure 2.1. The reduced enzyme first binds to tRNA. A specific uracil in the tRNA is then reduced by the enzyme to dihydrouracil. Finally the reduced tRNA leaves the enzyme, completing the oxidative half-reaction. We investigated the oxidative half-reaction of *S. cerevisiae* DUS 2 using synthetic pre-$tRNA^{Leu}$ which was reported to be a substrate (8).

The oxidative half-reaction was analyzed by mixing 60 μM reduced enzyme at 25 °C with saturating concentrations of synthetic yeast pre-$tRNA^{Leu}$ (700 μM). Surprisingly, the reaction was extremely slow. Spectra were recorded over 16 hours as the flavin was oxidized. Reaction traces at 457 nm fit to one exponential yielding a rate constant of 3.5 x 10^{-5} ± 4 x 10^{-7} s^{-1} for oxidation (Figure 2.3).

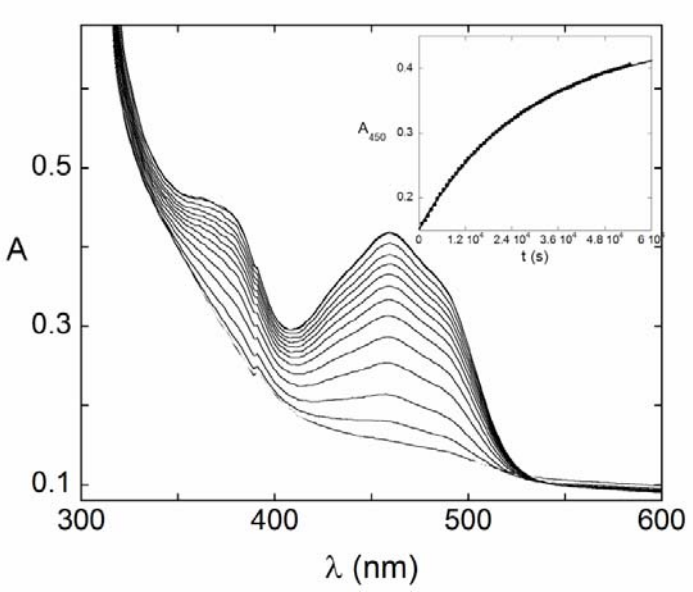

Figure 2.3: Oxidation of DUS2 by pre-tRNA^{Leu}. Anaerobic DUS 2 (35 μM) in 100 mM HEPES pH 7.5, 100 mM NaCl, 10 mM $MgCl_2$, 10% glycerol was reduced by titrating with one equivalent of dithionite. The reduced enzyme was reoxidized at 25 °C by mixing with anaerobic tRNA^{Leu}. The inset shows the time-dependence of flavin oxidation, detected at 450 nm. The trace was fit to a single exponential, giving a rate constant of 3.5 x 10^{-5} ± 3.6 x 10^{-7} s^{-1}.

Product analysis showed that 0.9 ± 0.08 moles of dihydrouridine were formed per mole of flavin oxidized. The same experiment, carried out with the C117A mutant enzyme, gave a similar rate constant for flavin oxidation, 4.8 x 10^{-5} ± 3 x 10^{-7} s^{-1}. The ratio of dihydrouridine produced per flavin molecule oxidized was 0.84 ± 0.1. The very slow reaction of the pre-tRNA^{Leu} could conceivably be caused by the intron that is excised during normal maturation. Therefore, the oxidative half-reaction was performed using synthetic tRNA^{Leu} without the intron. Reduction of the intronless RNA was faster by a factor of about 6, with a rate constant of 2.2 x 10^{-4} ± 5 x 10^{-6} s^{-1} – still a very slow reaction.

Given these slow reaction rates, as well as slow steady-state turnover numbers previously reported (8), we hypothesized there are other factors affecting the reaction of DUS 2 with tRNA. One possibility is that *in vitro* transcribed tRNA is not the native

DUS 2 substrate. During processing, there are multiple modifications of tRNA, and it has been shown that some modification enzymes are dependent upon prior post-transcriptional modifications (20). We therefore attempted to determine if one or more other modifications of the tRNA was necessary for rapid reaction. To accomplish this we purified a single $tRNA^{Leu}$ species from a DUS 2 knockout strain using an oligonucleotide affinity column. This allowed us to purify tRNA that should have have all the modifications present that are not dependent on the reduction step DUS 2 performs.

This partially matured tRNA was reduced by DUS 2 dramatically faster than synthetic tRNA. Reduced DUS 2 (20 μM) was oxidized at 4 °C by mixing with various concentrations of the modified $tRNA^{Leu}$ lacking dihydrouridine in anaerobic stopped-flow experiments. The absorbance increases at 450 nm were fit to single exponentials. The observed rate constants did not vary with tRNA concentration, indicating a K_D much lower than 20 μM, in stark contrast to synthetic tRNA (Figure 2.4). The rate constant for reaction of the modified $tRNA^{Leu}$ substrate was $0.14 \pm 0.03\ s^{-1}$, more than 600-fold faster than the reaction of the *in vitro* transcribed intronless substrate at 25 °C. These results indicate that at least one prior modification of the tRNA is very important for substrate recognition by the enzyme.

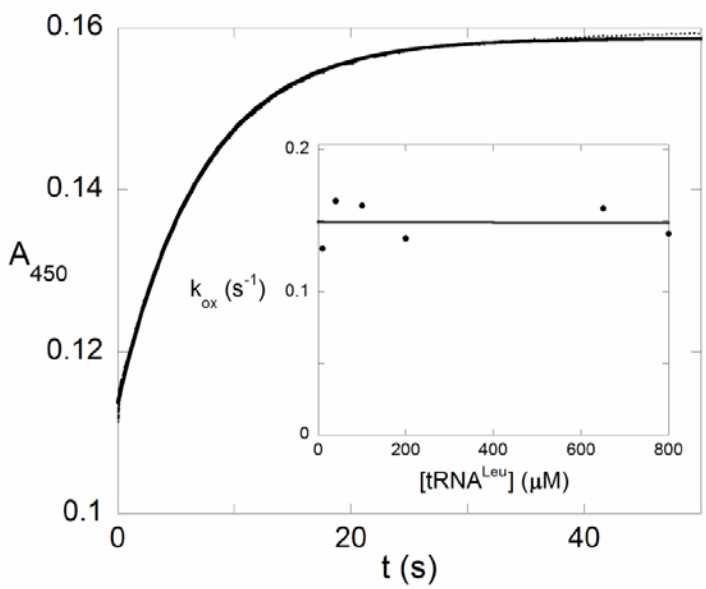

Figure 2.4: Oxidation of DUS2 by modified $tRNA^{Leu}$. Anaerobic DUS 2 (20 μM) in 100 mM HEPES pH 7.5, 100 mM NaCl, 10 mM $MgCl_2$, 10% glycerol was reduced by titrating with dithionite. The reduced enzyme was reoxidized at 4 °C by mixing with increasing amounts of $tRNA^{Leu}$, up to 800 μM, in a stopped-flow spectrophotometer. The absorbance was monitored at 450 nm and traces were fit to single exponentials. The inset shows concentration dependence for flavin oxidation by modified $tRNA^{Leu}$ yielding a rate constant of 0.14 ± 0.03 s^{-1}.

The same experiment was carried out using the C117A mutant of DUS 2. Reduced enzyme (15 μM) was mixed with 50 μM and 100 μM of partially matured tRNA in anaerobic cuvettes at 25 °C; both yielded the same rate, and this result indicated saturation. Because the reaction was very slow, spectra were taken over several hours. The increase in absorbance at 450 nm with time (Figure 2.5), was fit to an exponential, giving a rate constant of 8.7 x 10^{-5} s^{-1} ± 3 x 10^{-6} s^{-1}, 1600-fold slower than the wild-type. This indicates that Cys 117 is very important for the reduction of tRNA, consistent with its proposed role as an active site acid. Interestingly, the rate constant is only enhanced two-fold over that obtained with the *in vitro* transcribed pre-$tRNA^{Leu}$, and is about 2.5-fold slower than the intronless tRNA. This may indicate that the reason for the slow

reaction rate in the *in vitro* transcribed substrate is improper positioning of the tRNA relative to Cys 117.

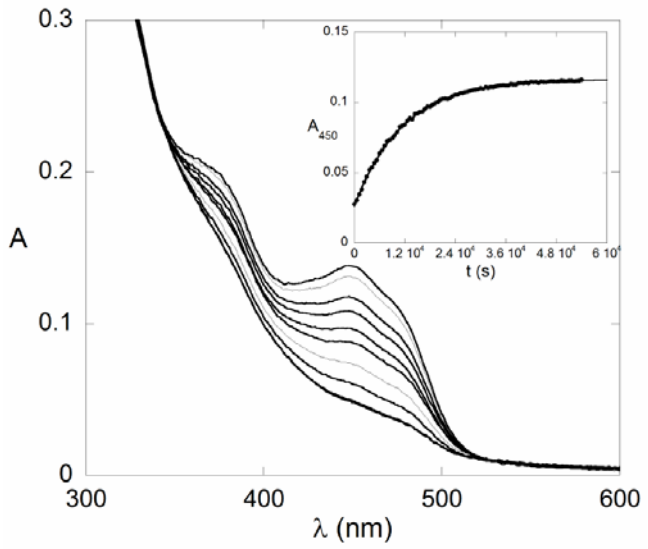

Figure 2.5: Oxidation of the C117A mutant by modified $tRNA^{Leu}$. Anaerobic enzyme (15 μM) in 100 mM HEPES pH 7.5, 100 mM NaCl, 10 mM $MgCl_2$, 10% glycerol was reduced by titrating with one equivalent of dithionite. The reduced enzyme was reoxidized by mixing with anaerobic modified $tRNA^{Leu}$. The inset shows the time-dependence of flavin oxidation, detected at 450 nm. The trace was fit to a single exponential, giving a rate constant of $8.7 \times 10^{-5} \pm 3 \times 10^{-6}$ s^{-1}.

The importance of modifications in increasing the affinity of tRNA was corroborated by an observation from the purification of DUS 2 by affinity chromatography. The enzyme expressed in *E. coli* and purified by metal affinity chromatography gave a single protein band on an SDS-PAGE. The absorbance spectrum of this preparation had peaks characteristic of a flavoenzyme at 370 nm and 450 nm, but also had a peak at 340 nm. This unusual chromophore was separated from the enzyme either by DEAE chromatography or by phenol-chloroform extraction. The compound isolated by phenol-chloroform extraction has the spectrum of a nucleic acid, with absorbance maxima at 260 nm and also at 340 nm, where 4-thiouridine absorbs. Since 4-thiouridine is a minor constituent of tRNAs, this suggested that tRNA is tightly bound to

both the wild-type and C117A mutant the enzymes when purified by metal affinity chromatography. Similar results were obtained with the dihydrouridine synthase from *Thermotoga maritima*, and a chemical analysis in that case confirmed the presence of 4-thiouridine (Chapter 3).

In order to identify which tRNA(s) were bound to wild-type DUS, tRNA isolated from the enzyme was treated with a mixture of amino acids and aminoacyl tRNA synthetases. The charged tRNA was purified, amino acids were hydrolyzed at basic pH at 25° C or 60° C, and the free amino acids were determined by amino acid analysis (Figure 2.6).

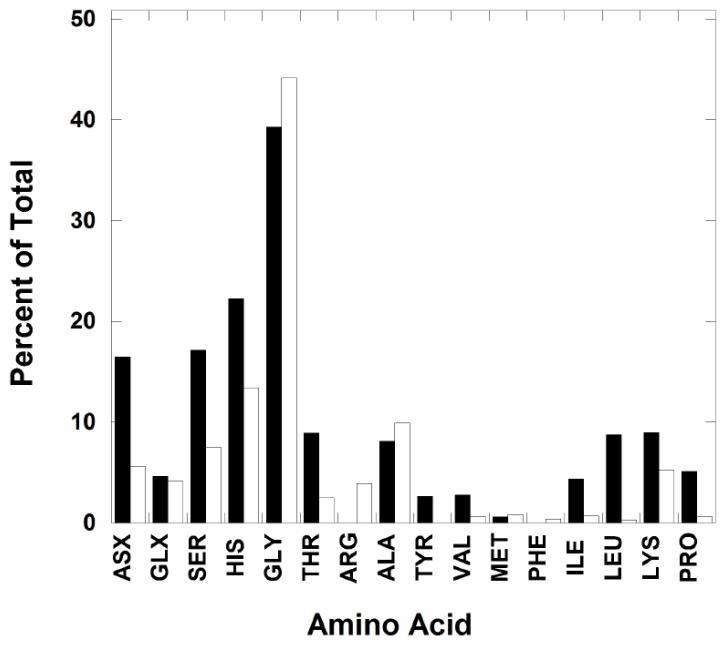

Figure 2.6: Identification of tRNAs bound to DUS2. tRNA was extracted with phenol-chloroform from the enzyme purified by metal-affinity chromatography and aminoacylated by *E. coli* tRNA synthetases. After isolating the charged tRNA from the small molecules, the amino acids were hydrolyzed from the tRNA at 25° C (white) or 65° C (black). The percentage of each was determined by amino acid analysis. The plot shows the percentage of each amino acid except for tryptophan and cysteine, which were not analyzable. Aspartate and asparagine are indistinguishable from one another by this method as are glutamine and glutamate. Almost all amino acids are present, with glycine being the major component at ~40 %.

Glycine constituted over 40% of the total. All other amino acids were detected, except for tryptophan, which is degraded by the amino acid analysis procedure. These results suggest either a strong preference for *E. coli* $tRNA^{Gly}$ over the other *E. coli* tRNAs or that there is a higher proportion of $tRNA^{Gly}$ in *E. coli* expressing DUS 2.

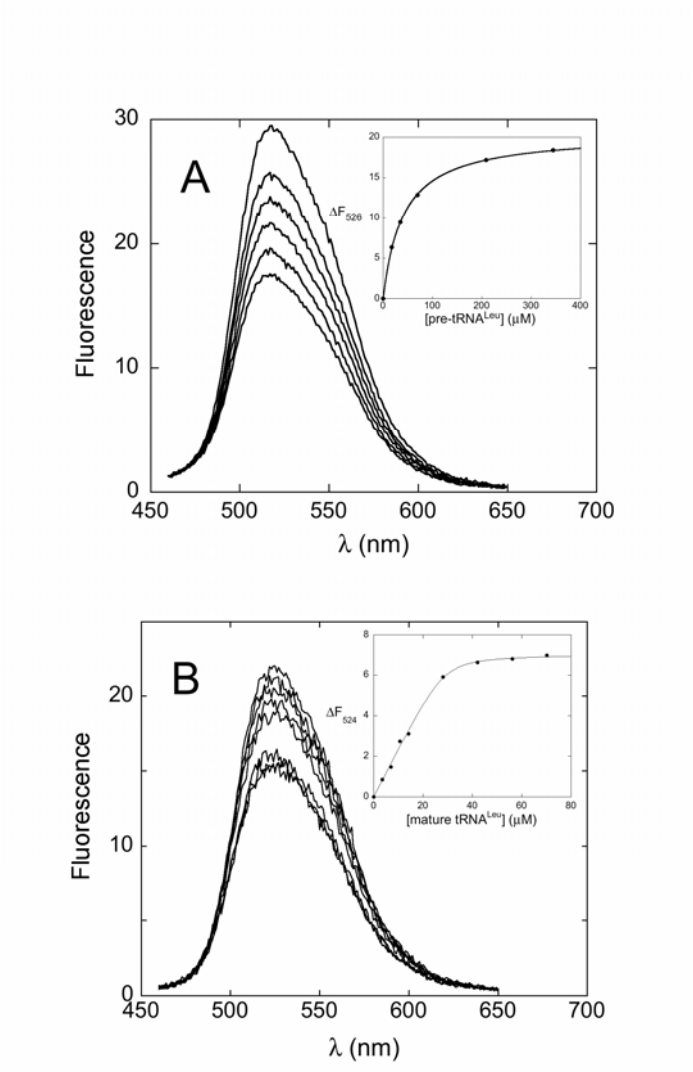

Figure 2.7: Ligand Binding to DUS2. a: Binding of pre-$tRNA^{Leu}$ to DUS 2. DUS 2 was titrated at 25 °C with increasing amounts of pre-$tRNA^{Leu}$ up to 380 μM. Upon addition of tRNA the fluorescence emission spectrum of the flavin was recorded (excitation 450 nm). The change in fluorescence versus the concentration (inset) gave a K_D of 40 ± 1 μM. b: Binding of modified $tRNA^{Leu}$ to DUS 2. DUS 2 was titrated with increasing amounts of modified $tRNA^{Leu}$ up to 68 μM. Upon addition of tRNA the fluorescence emission spectrum of the flavin was recorded (excitation at 450 nm). The change in fluorescence versus the concentration was fit to a tight binding quadratic to give an approximate K_D of 0.8 ± 0.5 μM.

The affinities of synthetic tRNAs were measured in fluorometric titrations. Binding to the oxidized enzyme caused a significant quenching of flavin fluorescence (Figure 2.7a). Pre-tRNA^{Leu} has a K_D of 40 ± 1 μM, and the intronless Pre-tRNA^{Leu} has a K_D of 160 ± 40 μM much higher than that of modified tRNA purified from *S. cerevisiae* (which was too low to be measured accurately) (Figure 2.7b), indicating that modification of tRNA is important for the binding the DUS 2.

Reverse Reaction with *E. coli* tRNA

In order to investigate whether reduction of the tRNA could be reversed, bulk *E. coli* tRNA (90 μM) was treated with 40 μM DUS 2 aerobically for 18 hours. Analysis of the tRNA showed a 78% decrease in dihydrouridine, indicating that the enzyme can oxidize dihydrouridine of tRNA to uridine, and the enzyme can be oxidized by oxygen.

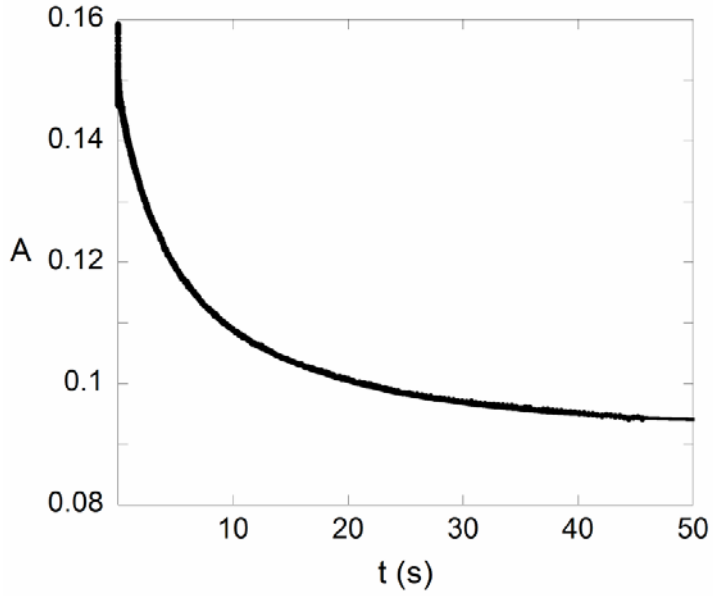

Figure 2.8: Reduction of DUS 2 with *E. coli* tRNA. Anaerobic DUS 2 (20 μM) in 100 mM HEPES pH 7.5, 100 mM NaCl, 10 mM $MgCl_2$, 10% glycerol, was mixed with anaerobic solutions of *E. coli* tRNA in a stopped-flow spectrophotometer at 4 °C. A reaction trace at 450 nm is shown. The fit gives an observed rate constant for the first phase of flavin reduction of 0.28 ± 0.03 s^{-1}, contributing to the majority of the absorbance change. The second phase shows a much smaller absorbance change and gives a rate constant of 0.05 ± 0.001 s^{-1}.

The presence of some dihydrouridine in tRNA after extended incubation with dihydrouridine synthases suggests a preference for certain tRNA substrates. *E. coli* tRNA has dihydrouridine modifications in several positions, so it is likely that the enzyme from yeast used to oxidize the tRNA mixture has a preference for only a subset of these modified positions.

The kinetics of enzyme reduction by dihydrouridine-containing tRNA from *E. coli* was studied at 4 °C, pH 7.5, with 20 μM enzyme (after mixing) in anaerobic stopped-flow experiments that recorded the flavin absorbance decrease at 450 nm (Figure 2.8). Traces were fit with two exponentials. The first phase, which contributed the major absorbance decrease, had an observed rate constant that increased hyperbolically to a maximum rate constant for flavin reduction of $0.28 \pm 0.03\ s^{-1}$. The second phase, which contributed a small absorbance change, gave a rate constant of $0.05 \pm 0.001\ s^{-1}$. These data indicate reducing uracil on tRNA to dihydrouracil is reversible; i.e., the redox potential of the bulk *E. coli* tRNA is close to or lower than that of the enzyme.

Oxidation of DUS 2 by molecular oxygen

Oxidation of the enzyme by molecular oxygen was studied in stopped-flow experiments at 4 °C by mixing reduced enzyme with buffer bubbled with various concentrations of oxygen (0-100%). Flavin oxidation was followed at 450 nm, and traces were fit to three exponentials. The second phase constituted the majority of the absorbance change and is attributed to oxidation, while the other rate constants had much smaller amplitudes. These are attributed to damaged enzyme or free FMN. The observed

rate constant of the large phase showed a linear dependence on oxygen concentration, indicating a simple bimolecular reaction having a rate constant of 14 M^{-1} s^{-1}.

Discussion

Dihydrouridine, a modified nucleoside found in most forms of life, is synthesized by dihydrouridine synthases. These flavin-dependent enzymes use NADPH to reduce specific uracils in tRNA and are homologous to dihydroorotate dehydrogenases and dihydropyrimidine dehydrogenases (9). All of these enzymes use a flavin prosthetic group to transfer a hydride when either reducing the enone of the pyrimidine or oxidizing the dihydropyrimidine to the enone, and have either a cysteine or a serine as an active site acid/base. Dihydroorotate dehydrogenases oxidize the dihydrouracil ring of dihydroorotate using FMN and either cysteine or serine as a base; their FMNs are oxidized by fumarate, quinones, or an iron-sulfur protein. Dihydropyrimidine dehydrogenases reduce uracil using FMN as the hydride donor and an active site cysteine as an acid after the FMN is first reduced by an iron-sulfur cluster. In both cases, the chemistry of the half-reaction involving the pyrimidine is similar, and these enzymes use TIM-barrel scaffolds and similar active site architectures to accomplish the chemistry.

There is significant sequence similarity between DHODs, DHPDHs, and known DUSs (9). Furthermore, the structure of an FMN-binding TIM barrel from *T. maritima* having significant similarity to DHODs and DHPDHs was determined (11). This protein was identified by sequence homology as a DUS, and we have shown that it performs this function (unpublished data). Its structure reinforces the analogy to the other, more thoroughly characterized pyrimidine-metabolizing flavoproteins. Therefore, it seemed likely that DUSs would use a similar mechanism for catalysis, involving two half-reactions. In the reductive half-reaction, NADPH would bind to the oxidized enzyme, a

hydride would be transferred to N5 of FMN, and NADP would then dissociate (Figure 2.1). In the oxidative half-reaction, tRNA would bind to the reduced enzyme and the hydride from FMN would reduce C6 of the uracil ring accompanied by a proton transfer from an active site acid to C5. Our results show that DUS 2 from *S. cerevisiae* conformed to this template for the catalytic cycle.

In the reductive half reaction, the enzyme was reduced by the *pro-R* hydrogen of NADPH with a rate constant of 2.5 s^{-1}, which is fast enough to be physiologically relevant. The KIE of 3.5 on flavin reduction indicates that the chemistry for this step is at least partially rate-limiting and is similar to the reductive half-reactions of many NADP-utilizing flavoenzymes.

In the oxidative half-reaction, tRNA oxidizes the reduced flavin, accomplishing the presumed physiological role of the enzyme. Synthetic tRNA, used in most studies of tRNA-modifying enzymes, is a poor substrate for this enzyme. The K_D value was higher than found for many tRNA-modifying enzymes, and even at saturation, the reaction was extremely slow. Interestingly, tRNA co-purifies with the enzyme, which would require a very low K_D value, strongly suggesting that modifications of the tRNA strengthen binding

An estimate of the minimum rate DUS 2 must have to sustain normal cellular dihydrouridine levels can be made from published data. *S. cerevisiae* has at least ~1.5 x 10^6 tRNA molecules per cell (21). This number of tRNA molecules must be made each generation (neglecting turnover). Yeast has a doubling time of 1.5-2 hours. This means 1.5 x 10^6 tRNAs would need to be modified every 120 minutes, or ~200 per second. In *S. cerevisiae in vivo* DUS 2 specificity studies show DUS 2 should modify all the tRNAs in

the cell once. DUS 2 has a copy number of about 2,650 proteins per cell (22) which means it must modify ~0.080 tRNA molecules per second, giving a lower threshold for how fast the overall catalytic cycle, and each of its steps, must be. The reductive half-reaction of *S. cerevisiae* DUS 2 easily meets this physiological requirement at 2.5 ± 0.2 s^{-1}. However, the rate of the oxidative half-reaction ($3.5 \times 10^{-5} \pm 3.6 \times 10^{-7}$ s^{-1}) with an *in vitro* transcribed tRNA, was not fast enough to meet our estimated physiological requirement. Interestingly, a specific activity was reported for DUS 1 from *S. cerevisiae* with *in vitro* transcribed tRNA (10). When this number (22,200 Units/mg) is converted to a turnover number, a very low value - ~10^{-7} s^{-1} - is obtained.

All available data, therefore, indicate that purified DUSs reduce synthetic tRNA too slowly to accomplish their demonstrated physiological roles. However, modified tRNA reacts much more rapidly, with a rate constant of 0.14 ± 0.03 s^{-1}, ~600 times faster (although determined at a temperature 21° lower) than the corresponding *in vitro* transcribed tRNA. This is much faster than our estimate for the minimum value necessary to support physiology. The large difference between synthetic and processed tRNA indicates there is a critical need for one or more modifications in order for it to be recognized as a substrate and is consistent with the observation that tRNA is tightly bound when the enzyme is purified from *E. coli*. Co-purification requires a very low K_D, yet *in vitro* transcribed tRNAs have dissociation constants of tens of micromolar or higher. The identity of the necessary modification is not yet known, but the data allow us to narrow down the possibilities. Firstly the enzyme shows high affinity for both *S. cerevisiae* tRNA and *E. coli* tRNA. Secondly we know that the partially mature pre-$tRNA^{Leu}$ carries the modification necessary for rapid reactivity. From these data and the

known modifications of these tRNAs (1) we can narrow the list of potential modifications down to 7. They are N4-acetylcytidine, 5-methylcytidine, 1-methylguanosine, 2'-O-methylguanosine, pseudouridine, and ribothymidine. The best potential candidate for this critical tRNA modification is the Gm18 2'-O-methylguanosine modification. Knockouts of the Trm3 enzyme lack not only methylated guanosine eighteen, but also lack dihydrouridine at position 20 (24). In contrast, the approximately 6-fold increase in RNA reduction in the absence of the intron in synthetic substrates suggests that the intron plays a small role in substrate recognition.

It is also possible that DUSs might act *in vivo* in a complex with one or more protein partners. The recent findings that the human DUS 2 interacts with a multifunctional glutamyl-prolyl-tRNA-synthetase complex (7) supports this hypothesis. However, no protein partners for the *E. coli* or *S. cerevisiae* DUSs have yet been identified and our data present no reason to invoke such a complex.

All DUSs have a conserved cysteine. Sequence and structural similarities to dihydroorotate dehydrogenases and dihydropyrimidine dehydrogenases imply that this cysteine will act as the acid during the reduction of the uracil ring. The importance of this cysteine was demonstrated for the *E. coli* DUS ybjN (20) by transforming a knockout strain with the C117A mutant, causing a clear loss in dihydrouridine content in tRNA isolated from this strain. However, the oxidation of the C117A DUS 2 mutant with synthetic tRNA gave rates similar to those for the wild-type enzyme, indicating that the active site cysteine is not important in this half-reaction when reducing synthetic substrates. In contrast, when using modified tRNA from *S. cerevisiae*, a dramatic difference (~1600x) in the rate constants for reaction with the wild-type and C117A

mutants is seen. These reactions were carried out at different temperatures, with the reactions for the C117A mutant being 19^{o} C higher than those used for the wild-type enzyme. It is likely that the reaction rate for tRNA reduction with the C117A mutant enzyme would be even slower at a lower temperature. These data are therefore consistent with C 117 protonating the uracil ring during reduction of the tRNA (Scheme 1). Interestingly, our results indicate that C 117 cannot act as a general acid unless tRNA has at least one critical modification, suggesting that the modification is needed to properly orient the reactive uracil in the active site.

Conclusions

DUS 2 from *S. cerevisiae* is reduced by NADPH in a *pro-R* specific fashion. It then uses C117 as a general acid in the reduction of tRNA along with donation of the hydride from the reduced flavin. Unlike most tRNA modifying enzymes thus studied, rapid reaction requires at least one prior modification of the tRNA substrate. This necessity for modification indicates and ordered mechanism for tRNA maturation in which certain modifications must come before others, and also indicates that dihydrouridine formation may be one of the later steps in this process. Further studies with the dihdroduridine synthase from *T. maritima* in the next chapter also strengthen the argument that many of the characteristics of this enzyme, such as stereospecificity, are common to this family of enzymes.

References

1. Sprinzl, M., Steegborn, C., Hübel, F. and Steinberg, S., "Compilation of transfer RNA sequencing and sequences of transfer RNA genes" (1996) *Nucleic Acids Res.*, 24:68-72

2. Dalluge, J J, Hashizume, T., Sopchik, A. E., McCloskey, J. A., Davis, D. R., "Conformational flexibility in RNA: the role of dihydrouridine" (1996) *Nucleic Acids Res.*, 24:1073-1079

3. Noon, K. R., Guymon, R., Crain, P. F., McCloskey, J. A., Thomm, M. Lim, J., Cavicchiolo, R.,, "Influence of Temperature on tRNA Modification in Archaea: Methanococcoides burtonii (Optimum Growth Temperature [Topt], 23^{o} C) and Stetteria hydrogenophila (Topt, 95^{o} C)" (2003) *J. Bacteriol*., 185:5483-5490

4. House, C. H., Miller, S. L., "Hydrolysis of dihydrouridine and related compounds" (1996) *Biochemistry*, 35:315-320

5. Alexandrov, A., Chernyakov, I., Gu, W., Hiley, S. L., Hughes, T. R., Grayhack, E. J., Phizicky, E. M., (2006) "Rapid tRNA decay can result from lack of nonessential modifications" (2006) *Mol. Cell*, 21:87-96

6. Kuchino, Y, Borek, E. (1978), "Tumour-specific phenylalanine tRNA contains two supernumerary methylated bases" (1978) *Nature*, 271:126–129

7. Kato, T., Daigo, Y., Hayama, S., Nobuhisa, I., Yamabuki, T., Ito, T., Miyamoto, M., Kondo, S., Nakamura, Y., (2005) "A novel human tRNA-dihydrouridine synthase involved in pulmonary carcinogenesis" (2005) *Cancer Res.,* 65:5638-5646

8. Xing, F., Hiley, S. L., Hughes, T. R., Phizicky, E. M., (2004) "The specificities of four yeast dihydrouridine synthases for cytoplasmic tRNAs" (2004) *J. Biol. Chem*., 279:17850-17860

9. Bishop, A. C., Xu J., Johnson, R. C., Schimmel, P., de Crécy-Lagard V., (2002) "Identification of the tRNA-dihydrouridine synthase family" (2002) *J. Biol. Chem.*, 277:25090-25095

10. Xing, F., Martzen, M. R., Phizicky, E. M., (2002) "A conserved family of *Saccharomyces cerevisiae* synthases effects dihydrouridine modification of tRNA" (2002) *RNA*, 8:370-381

11. Park, F., Gajiwala, K., Noland, B., Wu, L., He, D., Molinari, J., Loomis, K., Pagarigan, B., Kearins, P., Christoper, J., Peat, J., Badger, J., Hendle, J., Lin, J., Buchanan, S., (2004) "The 1.59 angstrom resolution crystal structure of TM0096 a flavin mononucleotide binding protein from *T. maritima*" Proteins, 55, 772-774
12. Whitby, G. (1953) "A new method for preparing flavin-adenine dinucleotide" (2004) *Biochem. J.* 54:437-442

13. Palfey, B.A. "Time resolved spectral analysis", (2003) Ch. 9 in Kinetic Analysis of Macromolecules: A practical Approach (Johnson, K. A., ed.), Oxford University Press, pp. 203-228

14. Kallansrud, G., and Ward, B., "A comparison of measured and calculated single- and double-stranded oligodeoxynucleotide extinction coefficients" (1996) *Anal. Biochem.* 236:134-138

15. Hunninghake, D. and Grisolia, S., "A sensitive and convenient micromethod for estimation of urea, citrulline, and carbamyl derivatives" (1966) *Anal. Biochem.*, 16:200-205

16. Ottolina, G., Riva, S., Carrea, G., Danieli, B., Buckmann, A.F., "Enzymatic synthesis of [4*R*-^{2}H]NAD(P)H and [4*S*-^{2}H]NAD(P)H and determination of the stereospecificity of 7 alpha- and 12 alpha hydroxysteroid dehydrogenase" (1989) *Biochim. Biophys. Acta*., 998:173-178

17. Engel, P C., "Problems in the application of gel filtration to the desalting of organic compounds: retardation of aromatic and heteroaromatic anions by commonly used salts" (1977) *Anal. Biochem*., 82:512-552

18. Strickland, S., Palmer, G., Massey, V., "Determination of dissociation constants and specific rate constants of enzyme-substrate (or protein ligand) interactions from rapid reaction kinetic data." (1975) *J. Biol. Chem*. 250:4048-4052

19. Palfey, B. A. and Massey, V. "Flavin-Dependent Enzymes", (1998) Ch. 29 in Comprehensive Biological Catalysis, volume III/Radical Reactions and Oxidation/Reduction (Sinnott, M., ed.), Academic Press, pp. 83-154

20. Shigi, N., Suzuki, T., Terada, T., Shirouzu, M., Yokoyama, S., Watanabe, K., "Temperature-dependent biosynthesis of 2-thioribothymidine of *Thermus thermophilus* tRNA" (2006) *J. Biol. Chem*., 281:2104-2113

21. Savage, D F., de Crécy-Lagard, V., and Bishop, A. C., "Molecular determinants of dihydrouridine synthase activity" (2006) *FEBS Letters*, 580: 5198-5202

22. Warner, J. R.,"The economics of ribosome biosynthesis in yeast" (1999) *TIBS*, 24: 437-440

23. Ghaemmaghami, S., Huh, W.-K., Bower, K., Howson, R.W., Belle, A., Dephoure, N., O'Shea, E.K., Weissman, J.S., "Global analysis of protein expression in yeast" (2003) *Nature* 425:737-741

24. Cavaille, J. Chetouani, F. Bachellerie, J.P., "The yeast *Saccharomyces cerevisiae* YDL112w ORF encodes the putative 2'-O-ribose methyltransferase catalyzing the formation of Gm18 tRNAs" (1999) *RNA* 5:66-81

Chapter 3

Kinetics of the Dihydrouridine Synthase from *Thermotoga maritima*

Introduction

The maturation of transfer RNA is a complex and important process. During the maturation of tRNA a number of post-transcriptional modifications of the tRNA occur (1). One of the most abundant of these modifications is the formation of dihydrouridine. Dihydrouridine is found in most forms of life with the majority of exceptions being hyperthermophiles (2). This lack of dihydrouridine in hyperthermophiles has been attributed to the increased likelihood of dihydrouridine undergoing ring opening at high temperatures (3). Dihydrouridine is formed by reduction of the double bond of uridine. The enzymes carrying out this reaction, dihydrouridine synthases (DUS)s, have been identified in *Saccharomyces cerevisea*, *Escherichia coli*, and *Aquifex aeolicus* (4,5,6,7).

A number of outstanding questions remain for these enzymes, such as how they regulate substrate specificity and what is the mechanism of tRNA reduction. An important step in answering these questions is the dissection of structural and functional features of these enzymes *in vitro*. Because of the importance of structures, we decided to investigate a recently crystallized putative DUS from *Thermotoga maritima* (8). Crystallographic studies of this protein showed that it had a TIM-barrel domain that binds FMN and a second domain of unknown function. This protein shares homology with the newly verified DUS proteins as well as with the dihydroorotate dehydrogenases. Previous

studies have shown that *T. maritima* forms dihydrouridine in its tRNA (9) and searches of the *T. maritima* genome suggest that this is the only putative DUS, obviating the question of substrate specificity. Previous studies have mentioned a lack of stability for DUS (7). The expected increased stability of this thermophilic protein, and need for information about DUSs from thermophilic species made the putative DUS from *T. maritima* a good candidate for study. Here we present a characterization of this enzyme.

Materials and Methods

Materials

NADP and NADPH were from Research Products International. ATP, GTP, CTP, and UTP were from Amersham Pharmacia Biotech. 1-$_D$-Glucose was from Cambridge Isotopes Laboratories. All other chemicals were purchased from Sigma-Aldrich.

Construction of pET151-TMA plasmid

Forward and reverse primers GATTACTATATTATCTCATC and GTCATGATAGCTCAGTCAGCTA were used to amplify the gene from *T. maritima* genomic DNA from the ATCC (43589D-5) by PCR. The PCR product was then cloned in-frame into the pET151/D-TOPO plasmid with an N-terminal His 6x tag and a TEV protease cleavage site using the PET151/D-TOPO topoisomerase-mediated cloning system (Invitrogen).

Expression and Purification of DUS

BL21 DE3 cells were transformed with the plasmid for the *T. maritima* enzyme by heat shock, and plated on LB agar containing 0.1 g/L ampicillin and incubated overnight at 37^o C. Single colonies were used to inoculate 5 mL LB, which was shaken at 400 rpm overnight in a 37^o C incubator. From these cultures, 1 mL was added to 1 L of LB containing 0.1 g/L ampicillin. The cells were grown to an OD_{600} of 0.8 and induced using 0.1 mM IPTG (final concentration) and grown for 5-6 hrs at 37^o C.

The DUS-containing cells were pelleted by centrifugation (16,000 x g for 20 minutes) and resuspended in 100 mM HEPES pH 7.5, 100 mM NaCl, 10 mM $MgCl_2$,

10% glycerol. The cells were sonicated for 15 minutes on ice. Cell debris was removed by centrifugation (20,000 x g for 30 minutes). The clarified supernatant was then passed over a 3.8 cm x 10 cm TALON metal affinity column (Clonetech), which had been loaded with cobalt (II) acetate and pre-equilibrated with 100 mM HEPES pH 7.5, 100 mM NaCl, 10 mM $MgCl_2$, 10% glycerol. The column was then washed with 3 column-volumes of 100 mM HEPES pH 7.5, 100 mM NaCl, 10 mM $MgCl_2$, 10% glycerol, and the protein was eluted from the column with the same buffer containing 200 mM imidazole. The eluted enzyme was then washed extensively with 100 mM HEPES pH 7.5, 100 mM NaCl, 10 mM $MgCl_2$, 10% glycerol in an Amicon ultrafiltration device (10,000 MWCO).

A major band of approximately ~38 kDa was seen on a 12% SDS PAGE gel using Coomassie Blue staining, indicating that the enzyme was greater than 90% pure. However, the absorbance spectra of the enzyme purified in this way had an unusual peak at 340 nm in addition to the expected flavin absorbance. Therefore, the enzyme was purified further to remove this contaminant by applying it to a 3.8 cm x 14 cm DEAE Sepharose column at 25^{o} C which was pre-equilibrated in 100 mM HEPES pH 7.5, 100 mM NaCl, 10 mM $MgCl_2$, 10 % glycerol. The column was washed extensively with 100 mM HEPES pH 7.5, 100 mM NaCl, 10 mM $MgCl_2$, 10% glycerol. The yellow fractions containing protein free of the contaminating chromophore were collected. Protein that remained bound to the column was eluted with 100 mM HEPES pH 7.5, 1 M NaCl, 10 mM $MgCl_2$, 10% glycerol and showed a proportionately higher 340 nm peak. Enzyme fractions free of the chromophore were pooled, concentrated, washed with 100 mM

HEPES pH 7.5, 100 mM NaCl, 10 mM $MgCl_2$, 10% glycerol, 10% glycerol and stored at 4^o C.

Enzyme Concentration

The extinction coefficient of the enzyme was determined by recording the absorbance spectrum of the enzyme, adding SDS (1% final concentration), and recording the spectrum of the FMN liberated upon protein unfolding. The extinction coefficient was calculated from the ratio of the absorbance of the free FMN (10) to that of the native enzyme. The extinction coefficient at 452 nm of the enzyme was 13,200 M^{-1} cm^{-1} in 100 mM HEPES pH 7.5, 100 mM NaCl, 10 mM $MgCl_2$, 10% glycerol. Enzyme concentrations were routinely determined spectrophotometrically using this extinction coefficient and are given in terms of active site concentrations.

Reaction Kinetics

Enzyme solutions for kinetics were made anaerobic in glass cuvettes by multiple cycles of evacuation followed by equilibration with an atmosphere of purified argon. When reduced enzyme was needed, a gas-tight syringe containing a dithionite solution was attached to the cuvette, and the anaerobic enzyme was titrated to complete reduction with one equivalent of dithionite, as judged by absorbance spectroscopy. All studies were performed using 100 mM HEPES, pH 7.5, 100 mM NaCl, 10 mM $MgCl_2$, 10% glycerol at 35^o C unless otherwise indicated. Absorbance spectra were obtained over time using a Shimadzu UV-2501PC scanning spectrophotometer.

Binding Titrations

Binding titrations were carried out in quartz fluorescence cuvettes at 35° C in 100 mM HEPES, 100 mM NaCl, 10 mM $MgCl_2$, 10% glycerol in a Shimadzu RF-5301 PC Spectrofluorophotometer. Enzyme (~20 μM) was titrated with increasing concentrations of ligands. Excitation was at 450 nm and emission was scanned from 460 to 650 nm, with a maximum fluorescence change observed at 517 nm. The change in fluorescence was plotted against the concentration of ligand and fit to equation (1).

$$\Delta F = \frac{\Delta F_{max}[Ligand]}{K_D + [Ligand]} \qquad (1)$$

Redox Potential

The reduction potential of the enzyme was determined at pH 7.0 at 25° C in a solution containing 100 mM HEPES, 10% glycerol, 10 mM $MgCl_2$, 0.1 μM methyl viologen, 35 mM xanthine, by the coupled xanthine/xanthine oxidase method of Massey (11). Phenosfranin (E_{m7} = -252 mV) was used as the redox indicator dye. The reduction of the dye was followed at 525 nm, where the flavin does not absorb. The reduction of the flavin was monitored at 407 nm, an isosbestic point of the dye. The intercept from the fit to the linear portion of the plot of $\ln[Dye_{ox}]/[Dye_{red}]$ vs. $\ln[Flavin_{ox}]/[Flavin_{red}]$ was used to determine the redox potential according to the Nernst equation.

tRNA Synthesis

tRNAs were produced in reactions containing 50 mM Tris-HCl, pH 7.5, 15 mM $MgCl_2$, 5 mM dithiothreitol, 2 mM spermidine, 20 mM of each NTP, T7 RNA polymerase, and DNA template (10 ng/μL). The templates for each reaction were synthesized by PCR using two complementary primers (Invitrogen) comprising the entire tRNA gene to be transcribed, and a T7 RNA polymerase promoter upstream. Synthetic tRNA was purified by phenol-chloroform extraction to remove RNA polymerase, and the RNA was precipitated with 2 volumes of ethanol. The RNA concentration was calculated from the absorbance at 256 nm using extinction coefficients predicted from the base composition of each tRNA using the nearest neighbor method (12). The extinction coefficients used were 695,100 M^{-1} cm^{-1} for *T. maritima* $tRNA^{Ala}$-CGC ; 800,700 $M^{-1}cm^{-1}$ for *T. maritima* $tRNA^{Tyr}$-GTA; 697,700 M^{-1} cm^{-1} for *T. maritima* $tRNA^{Phe}$-GAA; 682,900 M^{-1} cm^{-1} for *T. martitima* $tRNA^{Gly}$-CCC; 677,400 M^{-1} cm^{-1} for *T. martitima* $tRNA^{Gly}$-GCC; and 681,100 M^{-1} cm^{-1} for *T. martitima* $tRNA^{Gly}$-TCC.

Dihydrouridine Assay

Dihydrouridine produced by the reduction of tRNA was determined using a colorimetric assay (13). tRNA (125 μM in 0.3 mL) was treated with 0.03 mL 1 M KOH and incubated for 30 minutes at 37° C, hydrolyzing the dihydrouridine ring. The sample was then acidified with 0.15 mL 1 M H_2SO_4, and 0.3 mL of a solution of 10 mM butadienone malemide and 5 mM semidine was added. The sample was heated for 5 minutes at 95° C in a heating block, cooled to 50° C for 5 minutes, 0.3 mL of 10 mM $FeCl_3$ was added, and the absorbance at 550 nm was read.

Preparation of [4*R*-^{2}H]NADPH and [4*S*-^{2}H]NADPH

[4*R*-^{2}H]NADPH was prepared as described by Ottolina et al. (14). A 10 mL solution of 50 mM sodium bicarbonate pH 8.5, 0.5 M 2-d-isopropanol, 13 mM NADP and 20 U of *Thermoanaerobacter brockii* alcohol dehydrogenase (Sigma) was incubated at 30^o C for 4 hours. The solution was diluted to 20 mL with H_2O and chromatographed on a 2.8 cm x 40 cm DE-53 column (carbonate form). The [4*R*-^{2}H]NADPH was eluted with a sodium bicarbonate gradient (0-0.5 M, 500 mL). Fractions with a ratio of A_{254}/A_{340} of 2.5 or less were pooled and lyophilized. The lyophilized product was chromatographed with water on a 2 cm x 50 cm Sephadex G-10 column to remove salt (15). Fractions containing [4*R*-^{2}H]NADPH were pooled and the product was precipitated with 70% acetone at 4^o C to concentrate, dissolved in a minimal amount of water, and lyophilized.

[4*S*-^{2}H]NADPH was prepared in a 6 mL solution of 50 mM HEPES pH 7.5, 15 mM 1-d-glucose, 15 mM NADP, 15 mM $MgCl_2$ 100 U hexokinase, and 100 U glucose-6-phosphate dehydrogenase. The reaction was incubated at 25^o C for 5 hours and the [4*S*-^{2}H]NADPH was purified as described above.

Stereochemistry

The stereochemistry of oxidation of NADPH by the enzyme was determined by incubating 1.5 mL of an aerobic solution containing 2 mM [4*R*-^{2}H]NADPH, 100 μM of DUS, 100 mM potassium phosphate pH 7.5, 100 mM NaCl, 10 mM $MgCl_2$ in D_2O at 35^o C. After [4*R*-^{2}H]NADPH was completely oxidized (no absorbance at 340 nm; ~6 hours), enzyme was removed by ultrafiltration (Amicon Ultra 10,000 MWCO) and a 300 MHz ^{1}H-NMR spectrum was recorded using the water peak as a chemical shift reference (4.2 ppm). An identical procedure was used for [4*S*-^{2}H]NADPH.

Thiouridine Assay

The presence of thiouridine was demonstrated in tRNA obtained by phenol-chloroform extraction of enzyme purified with the TALON metal affinity column but not the subsequent DEAE ion exchange column. 40 μM tRNA in 1.5 mL was irradiated with a Bio-Rad UV transilluminator for 30 minutes in 150 mM sodium cacodylate buffer, pH 7.0, at 25^{o} C. The irradiated tRNA was then treated with 4 mg of sodium borohydride. The fluorescence emission spectrum of the product was obtained while exciting at 396 nm (16).

Identification of tRNAs bound to *T. maritima* DUS

tRNA bound to the *T. maritima* enzyme purified by the metal affinity column only was extracted with phenol-chloroform to remove the protein and ethanol-precipitated to yield the pure tRNA. Mixtures of ~3.5 μmol tRNA was incubated in a 10 mL reaction at pH 7.4 in 100 mM KPi with 0.8 mM of each amino acid, 10 mM ATP, and 2880 U aminoacyl-tRNA synthetases from *E. coli* (Sigma A3646-10KU) to ensure complete aminoacylation of the tRNAs. The reactions were extracted with phenol-chloroform and the tRNA was precipitated with 2 volumes ethanol. The tRNA was dissolved in 200 μL of 100 μM KPi pH 9.0 and incubated for 5 hours to hydrolyze the aminoacyl-esters. The tRNA was separated from the amino acids by ultrafiltration with 10,000 MWCO Microcon centrifugal filtration devices (Amicon) previously washed with H_2O. The flow-through was collected and analyzed by Iowa State University Office of Biotechnology on an automated Beckman System Gold HPLC amino acid analyzer.

Temperature Stability of *T. maritima* DUS

The temperature stability of 40 μM *T. maritima* DUS enzyme was tested in 100 mM HEPES, 100 mM NaCl, 10 mM $MgCl_2$, 10% glycerol. The enzyme was allowed to equilibrate for 5 minutes at 10^{o} C. At each temperature, a spectrum was recorded, the temperature was raised 5 degrees, and the process was repeated up to 50^{o} C.

Hydrogen Peroxide Assay

Formation of hydrogen peroxide by the enzymes upon reaction with *E.coli* tRNA and O_2 was followed using a coupled assay with horseradish peroxidase and o-dianisidine. Reactions were performed using 385 μM o-dianisidine, 0.19 mg/mL horseradish peroxidase, 40-80 μM *E. coli* tRNAs in 100 mM HEPES, 100 mM NaCl, 10 mM $MgCl_2$, 10% glycerol at 25^{o} C. The reactions were started by addition of *T. maritima* (6 μM) enzyme and monitored at 460 nm to observe hydrogen peroxide formation.

Superoxide Assays

Formation of superoxide was assayed in 1 mL turnover reactions using 0.1 mg/mL acetylated ferri-cytochrome c in 100 mM HEPES pH 7.5, 100 mM NaCl, 10 mM $MgCl_2$, 10% glycerol, 200 μM *E.coli* tRNA with 6 μM *T. maritima* enzyme. Superoxide dismutase (0.02 mg/mL) was added as a control to obtain the background rate of cytochrome c reduction by tRNA and enzyme.

Crystallization

Crystals were obtained with protein purified by metal affinity chromatography, with tRNA still present. Enzyme (5 mg/ml) in 10 mM HEPES pH 7.5, 150 mM NaCl, 1 mM ß-mercaptoethanol, 10 mM methionine, and 10% glycerol was mixed with an equal volume of reservoir consisting of 100 mM bicine pH 9.0, 2% v/v 1,4-dioxane, 10 % w/v PEG 20,000. Crystals grew within 3 weeks and were flash-frozen in liquid nitrogen. Data were collected at the APS LS-CAT beam line and processed and reduced with HKL200. The model was determined by molecular replacement using the 1VHN (PDB) as a reference structure with the program Phaser. Refinement was performed with iterative cycles of manual building with Coot and Refmac.

Results

Reductive Half-Reaction

The reductive half-reaction of DUS starts with NADPH binding to the enzyme. The NADPH then transfers a hydride to the active site flavin, reducing the enzyme. Finally, NADP leaves the enzyme, yielding free reduced enzyme. We first looked at the thermodynamics of the system by determining the redox potential of the *T. maritima* enzyme. Clean two-electron reduction with no semiquinone was observed when the enzyme was reduced with xanthine oxidase. The two-electron reduction potential was -252 mV, well above the NADP/NADPH couple (-340 mV). Therefore, the reductive half-reaction is very favorable thermodynamically, consistent with reduction of the flavin by NADPH being a step in catalysis.

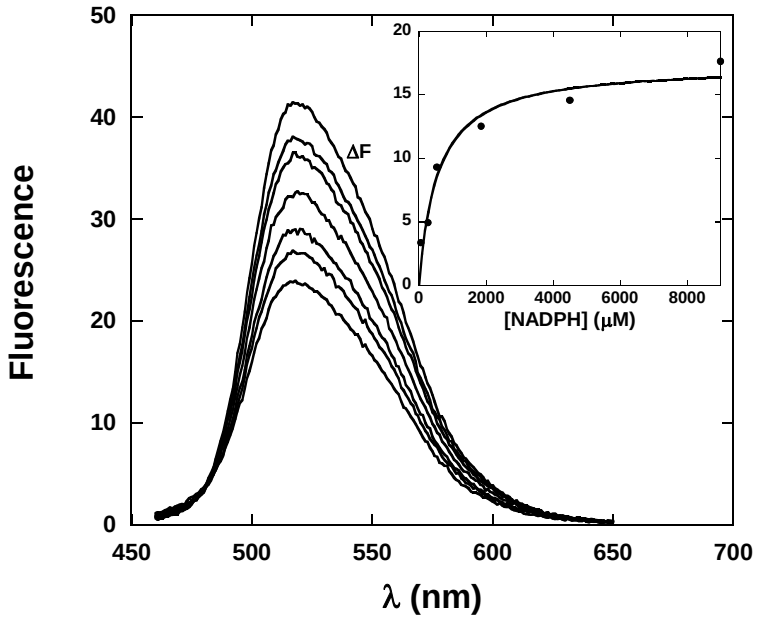

Figure 3.1: NADPH Binding to Oxidized *T. maritima* DUS. Enzyme (20 μM) in 100 mM HEPES pH 7.5, 100 mM NaCl, 10 mM $MgCl_2$, 10% glycerol, was titrated with NADPH up to 2 mM. Flavin fluorescence emission spectra were recorded after each addition (excitation 456 nm). The inset shows the fluorescence change at 517 nm versus the concentration of NADPH used, giving a K_D of 550 μM.

The binding of NADPH to the enzyme was determined in fluorometric titrations. This was possible because NADPH is oxidized by the enzyme extremely slowly (see below), so that the extent of reaction occurring over the time-scale of titrations was negligible. Binding of NADPH to the oxidized enzyme quenched the fluorescence of the flavin. The dependence of quenching on NADPH concentration gave a K_D of 550 ± 60 μM (Figure 3.1). Binding of NADP to the oxidized enzyme was studied in the same manner, giving a K_D for NADP of 37 ± 7 mM. Given the large difference in the K_D values of NADPH and NADP, product inhibition is unlikely in the reductive half-reaction.

The stereofacial selectivity of NADPH oxidation was investigated by oxidizing [4*R*-^{2}H]NADPH and [4*S*-^{2}H]NADPH with the enzyme and analyzing the NADP produced by ^{1}H-NMR. When the [4*R*-^{2}H]NADPH was the substrate, a proton signal was observed at 8.4 ppm for the proton at the 4-position of the nicotinamide ring of NADP, indicating that the *R*-deuteron was transferred (data not shown). When [4*S*-^{2}H]NADPH was used, the NADP produced lacked the signal at 8.4 ppm, indicating retention of the *S*-deuteron and transfer of the *R*-hydrogen. Therefore, DUS is specific for the *proR*-hydrogen of NADPH.

The kinetics of enzyme reduction by NADPH was studied anaerobically at 35^o C by mixing 40 μM enzyme and 10 mM NADPH (more than ten times the K_D) in an anaerobic cuvette. Spectra were recorded over several hours. Flavin reduction was followed by the loss in absorbance at 452 nm over time. A fit to an exponential decay gave a rate constant of $2.5 \times 10^{-4} \pm 4 \times 10^{-6}$ s^{-1} (Figure 3.2). Charge-transfer bands at long

wavelength are frequently seen in pyrimidine nucleotide-utilizing flavoenzymes (17), but none were seen during the reduction of the *T. maritima* enzyme.

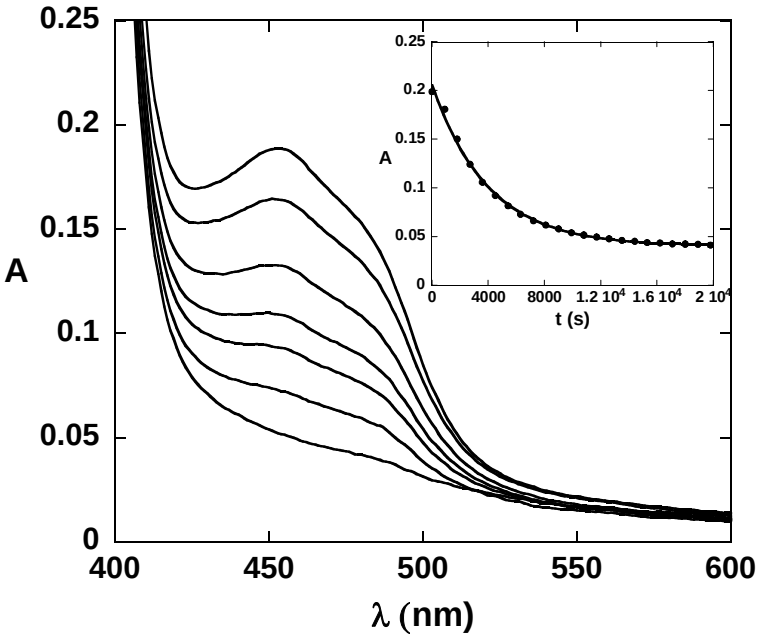

Figure 3.2: Reduction with NADPH. Anaerobic enzyme in 100 mM HEPES pH 7.5, 100 mM NaCl, 10 mM $MgCl_2$, 10% glycerol, was mixed with 10 mM NADPH and spectra (not all shown) were taken over several hours. The inset shows a fit to a single exponential, giving a rate constant of 2.5 x 10^{-4} ± 4 x 10^{-6} s^{-1}.

Isotope effects on flavin reduction were measured, giving rate constants of 2.2 x 10^{-4} ± 3 x 10^{-6} s^{-1}, 2.3 x 10^{-4} ± 1 x 10^{-5} s^{-1} and 2.5 x 10^{-4} ± 4 x 10^{-6} s^{-1} for [4*R*-^{2}H]NADPH, [4*S*-^{2}H]NADPH, and NADPH respectively. KIE values of 1.2 ± 0.1 and 1.1 ± 0.2 were calculated. Thus, no significant isotope effect was observed in the reduction of the enzyme. The lack of a KIE means that hydride transfer is not the rate-determining step for the reductive-half reaction, suggesting that a slow conformational change could be rate-determining. The optimum growth temperature of *T. maritima* is 45^o C higher than the temperatures used here. At 35^o C, the enzyme might be trapped in an inactive conformation whose isomerization to the reactive form may be rate-determining.

The stability of the *T. martima* enzyme was investigated to determine if the reduction rate could be increased. The temperature stability of the *T. maritima* DUS enzyme was tested from 10^{o} C to 50^{o} C. An increase in turbidity caused by enzyme precipitation and aggregation was observed at 600 nm as the enzyme was heated above 40^{o} C, showing that the enzyme is not stable at high temperatures.

We also investigated whether the slow rate of reduction was due to pH. The rate constant for reduction with NADPH did not change from pH 6.5 to pH 11 (data not shown), indicating that no ionizable groups with pK_a values within this range altered the rate-determining step. The K_D for NADPH, determined by fluorometric titrations, decreased slightly at higher pH values, varying from 550 μM at pH 7.5 to 250 μM at pH 11.

RNA Binding and the Oxidative Half-Reaction

When the enzyme was expressed in *E. coli* and purified by affinity chromatography, it gave a single band of 38 kDa on SDS PAGE. The absorbance spectrum of the enzyme had peaks characteristic of a flavoenzyme at 370 nm and 450 nm (Figure 3.3). However, an uncharacteristic peak in the absorbance spectrum at 340 nm was also seen. This same chromophore was also found bound to the *S. cerevisiae* enzyme (chapter 2). This unexpected chromophore could be separated from the protein by DEAE chromatography or by phenol-chloroform extraction. The final compound isolated by phenol-chloroform extraction has the spectrum of a nucleic acid (Figure 3.3), with absorbance maxima at 260 nm and also at 340 nm, where 4-thiouridine absorbs.

Electrophoresis on 20% polyacrylamide gels containing 8 M urea resolved a series of bands that stained with ethidium bromide.

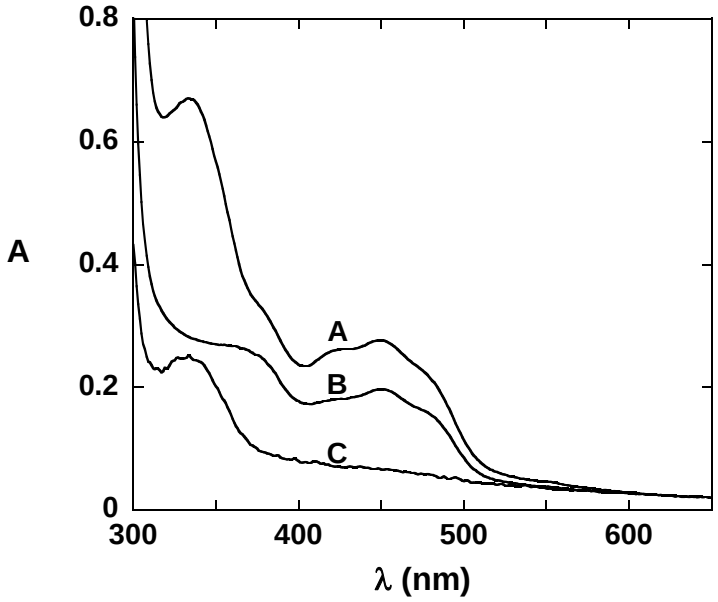

Figure 3.3: tRNA co-purifies with *T. maritima* DUS. All spectra were taken at 25° C in 100 mM HEPES pH 7.5, 100 mM NaCl, 10 mM $MgCl_2$, 10% glycerol. Curve (A) shows the enzyme spectrum as purified with a metal affinity column. Bound tRNA contributes a peak at 340 nm due to thiouridine. Curve (B) shows the enzyme spectrum after removal of tRNA by DEAE anion exchange chromatography, with normal flavoprotein peaks at 450 nm and 370 nm. Curve (C) shows the spectrum of phenol-chloroform extracted tRNA showing a thiouridine peak at 340 nm.

These bands were similar in size to purchased *E. coli* tRNA. Treatment with RNase A prior to electrophoresis caused these bands to disappear. UV irradiation of the RNA followed by treatment with sodium borohydride formed a fluorescent adduct with an emission at 421 nm when excited at 396 nm (Figure 3.4). The absorbance at 340 nm and the fluorescent adduct generated by irradiation and reduction strongly suggest the presence of 4-thiouridine (16).

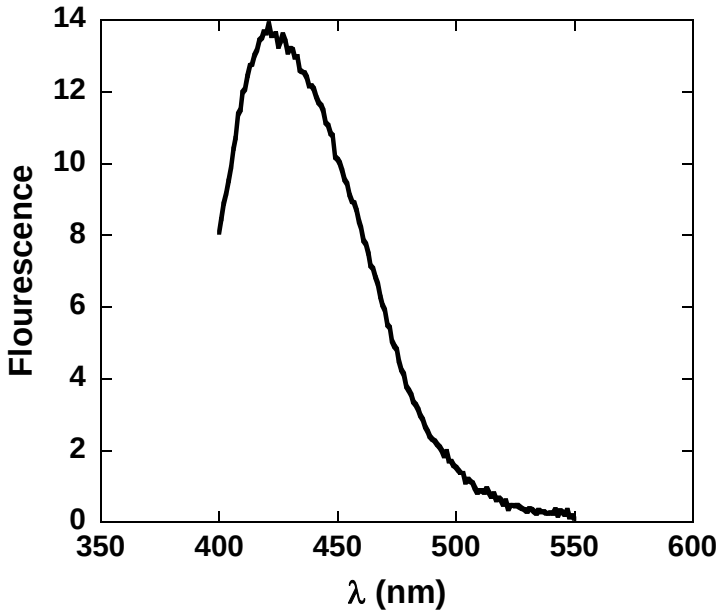

3.4: Identifying 4-thiouridine in tRNA. tRNA (40 μM) in 150 mM sodium cacodylate buffer was irradiated with UV light for 30 minutes and treated with sodium borohydride. The emission spectrum has a peak at 421 nm (excitation 396 nm) indicating a thiouridine-cytidine adduct.

In order to identify which tRNA(s) were bound to the enzyme, tRNA was isolated from the enzyme and treated with a mixture of amino acids and aminoacyl tRNA synthetases. The charged tRNA was purified, amino acids were hydrolyzed by base at 25^{o} C and 65^{o} C, and the free amino acids were determined by amino acid analysis (Figure 3.5). A large percentage of the amino acids were glycine (50%), when hydrolyzed at 25^{o} C and 65^{o} C. All other amino acids were detected, except for tryptophan which is degraded by the amino acid analysis procedure. These results suggest a preference for many tRNAs.

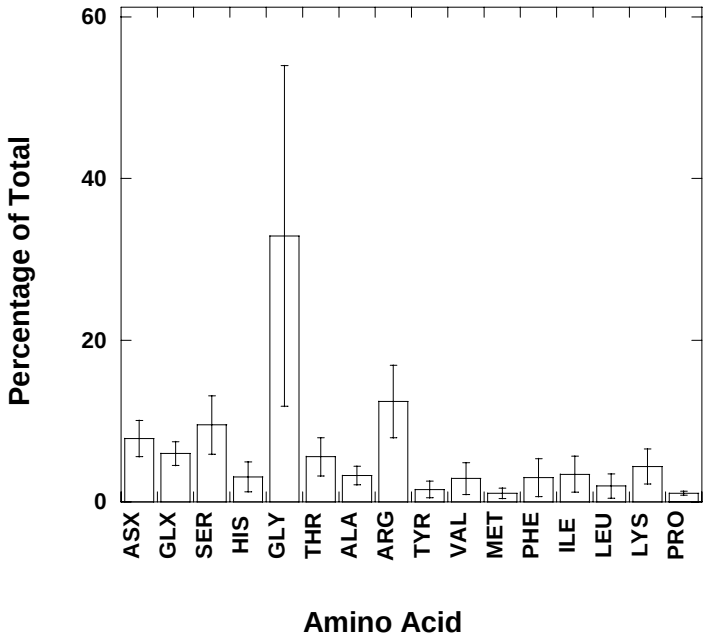

Figure 3.5: Identification of tRNAs bound to *T. maritima* DUS. tRNA was extracted from the enzyme with phenol-chloroform and aminoacylated by *E. coli* tRNA synthetases. After isolating the charged tRNA from the small molecules, the amino acids were hydrolyzed from the tRNA and analyzed to determine the percentage of each. The plot shows the percentage of each amino acid except for tryptophan, which was not analyzable. The error bars indicate one SD from the mean. Aspartate and asparagine are indistinguishable from one another by this method, as are glutamine and glutamate.

Table 3.1: A Summary of Dissociation Constants and Rate Constants

Ligand	K_D (μM)	Rate Constant (s^{-1})	Temperature
$tRNA^{Tyr}$-GTA	128 ± 14		25° C
$tRNA^{Ala}$-CGC	130 ± 10		25° C
$tRNA^{Phe}$-GAA	72 ± 7		25° C
$tRNA^{Phe}$-GAA	33 ± 2		35° C
$tRNA^{Tyr}$-GTA	9 ± 3	$4.1 \times 10^{-5} \pm 3 \times 10^{-7}$	35° C
$tRNA^{Gly}$-CCC	21 ± 3	$2.6 \times 10^{-4} \pm 5 \times 10^{-6}$	35° C
$tRNA^{Gly}$-GCC	43 ± 5	$1.3 \times 10^{-4} \pm 4 \times 10^{-7}$	35° C
$tRNA^{Gly}$-TCC	36 ± 7	$1.9 \times 10^{-4} \pm 3 \times 10^{-6}$	35° C
NADP	37 ± 7 mM		35° C
NADPH	550 ± 60	$2.5 \times 10^{-4} \pm 4 \times 10^{-6}$	35° C

Binding of synthetic tRNAs to the oxidized enzyme caused significant quenching of flavin flouresence (Figure 3.6). Binding was the same within an order of magnitude for all of the tRNAs, as shown by their K_D values (Table 3.1). Though not all tRNAs have been tested, this group represents a diverse set of tRNA structures. Only one DUS is annotated in the genome of *T. maritima*, so it is probably responsible for the reduction of all tRNAs in that organism. The similar dissociation constants of the synthetic tRNAs tested and the presence of only one DUS in *T. maritima* suggests that this enzyme binds to a common tRNA structural feature. These results also indicate that the *in vivo* processed tRNA has a much high affinity that the *in vitro* transcribed tRNA. The results also show a temperature dependence upon tRNA binding, with tRNA binding more tightly at higher temperatures.

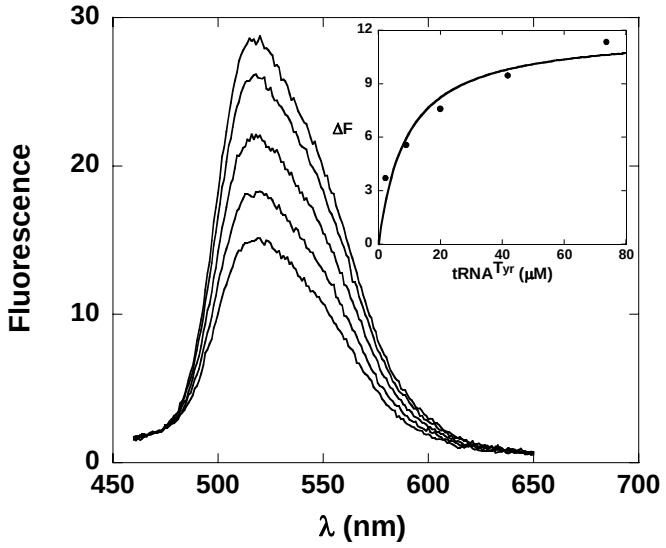

Figure 3.6: Binding of $tRNA^{Tyr}$ to *T. maritima* DUS. Enzyme (20 μM) in 100 mM HEPES pH 7.5, 100 mM NaCl, 10 mM $MgCl_2$, 10% glycerol, was titrated with $tRNA^{Tyr}$ up to 80 μM, causing the flavin fluorescence to be quenched. The inset shows the change in fluorescence at 517 nm (excitation at 456 nm) plotted versus $tRNA^{Tyr}$ concentration, giving a K_D of 9 ± 3 μM.

We investigated the oxidative half-reaction of the *T. maritima* enzyme by mixing ~40 μM reduced enzyme at 35° C pH 7.5, with a saturating concentration of synthetic

tRNA: 410 μM for $tRNA^{Tyr}$, 477 μM for $tRNA^{Gly}$-TCC, 226 μM for $tRNA^{Gly}$-CCC, 216 μM for $tRNA^{Gly}$-GCC. Spectra were recorded over several hours as the flavin was oxidized. Reaction traces at 452 nm were fit to a single increasing exponential (Figure 3.7). The observed rate constants for the reactions with synthetic $tRNA^{Tyr}$, $tRNA^{Gly}$-TCC, $tRNA^{Gly}$-CCC, and $tRNA^{Gly}$-GCC were $4.1 \times 10^{-5} \pm 3 \times 10^{-7}\ s^{-1}$, $2.6 \times 10^{-4} \pm 5 \times 10^{-6}\ s^{-1}$, $1.3 \times 10^{-4} \pm 4 \times 10^{-7}\ s^{-1}$, and $1.9 \times 10^{-4} \pm 3 \times 10^{-6}\ s^{-1}$ respectively (Table 3.1). The reduction of uracil in the tRNA was confirmed by quantifying dihydrouridine using a colorimetric assay (13). The reaction using 47 μM enzyme and 410 μM $tRNA^{Gly}$-GCC gave 56 ± 14 μM dihydrouridine, a ratio of 1.2 ± 0.3 dihydrouridines produced per flavin oxidized. This reaction was also slow, perhaps due to a slow isomerization step in the enzyme.

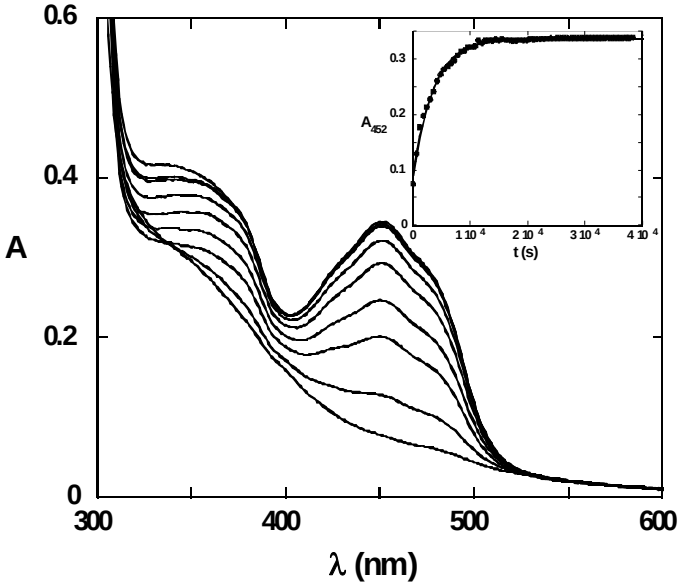

Figure 3.7: Oxidation of *T. maritima* DUS by $tRNA^{Tyr}$. Anaerobic *T. maritima* DUS (40 μM) in 100 mM HEPES pH 7.5, 100 mM NaCl, 10 mM MgCl2, 10% glycerol was reduced by titrating with one equivalent of dithionite. The reduced enzyme was reoxidized by mixing with $tRNA^{Tyr}$ (410μM). The inset shows time dependence of flavin oxidation, detected at 452 nm. The trace was fit to a single exponential, giving a rate constant of $4.1 \times 10^{-5} \pm 3 \times 10^{-7}\ s^{-1}$.

Oxidation of *E.coli* tRNA with DUS

In order to investigate whether reduction of tRNA was reversible, bulk *E. coli* tRNA (90 μM) was treated aerobically with 40 μM *T. maritima* enzyme for 18 hours at 25^{o} C. Analysis of the tRNA showed a 58% decrease in dihydrouridine, indicating that the enzyme catalyzes the oxidation of dihydrouridine to uridine. The presence of some dihydrouridine in tRNA after extended incubation with dihydrouridine synthases suggests a preference for certain tRNA substrates. *E .coli* tRNA has dihydrouridine modifications in several positions, so it is likely that the enzyme has a preference for only a subset of these modified positions. It is also possible that the enzyme was unable to complete the reaction in this amount of time, but given the rate constant for reduction of the enzyme, discussed below, the reaction should have gone to completion in this time frame.

The kinetics of enzyme reduction by dihydrouridine-containing *E. coli* tRNA was studied anaerobically at 35^{o} C by mixing 40 μM enzyme and 4 mM bulk *E. coli* tRNAs. Flavin reduction was followed by the loss in absorbance at 452 nm over time. A fit to an exponential decay gave a rate constant of $1.8 \times 10^{-4} \pm 4 \times 10^{-6}$ s^{-1} (Figure 3.8). The rate of the reverse reaction is comparable to that of the forward reaction using synthetic *T. maritima* tRNA.

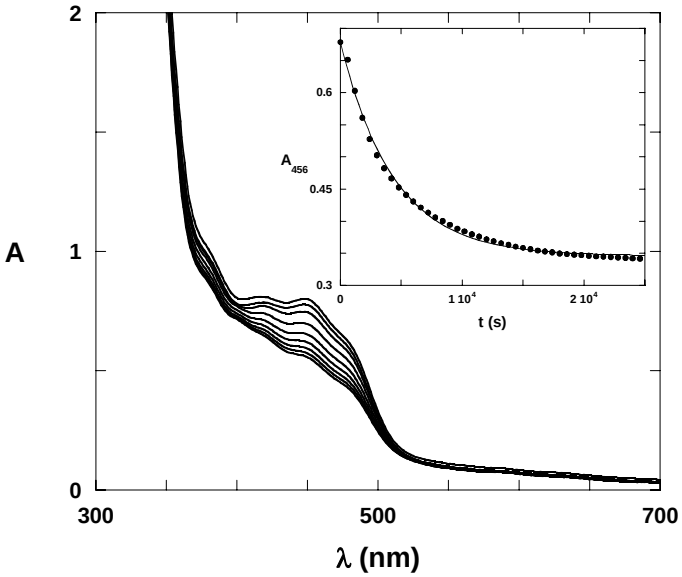

Figure 3.8: Reduction of *T. maritima* DUS with *E. coli* tRNA. Anaerobic enzyme in 100 mM HEPES pH 7.5, 100 mM NaCl, 10 mM $MgCl_2$, 10% glycerol, was mixed with 4 mM *E. coli* tRNA and spectra were taken over several hours. The inset shows a fit to a single exponential, giving a rate constant of $1.8 \times 10^{-4} \pm 4 \times 10^{-6}$ s^{-1}.

These data show that the reaction catalyzed by this enzyme, the formation of dihydrouridine from uridine, is reversible and that mature tRNA is capable of reducing the flavin under anaerobic conditions, indicating a redox potential for tRNA close to or lower than that of the enzyme.

Oxidation of DUS by molecular oxygen

Oxidation of the enzyme by molecular oxygen was carried out in stopped-flow experiments at 4^{o} C pH 7.5, by mixing dithionite-reduced enzyme with buffer bubbled with various concentrations of oxygen (0-100%). Flavin oxidation was followed by the increase in absorbance at 450 nm and traces were fit to three exponentials. The second phase constituted the majority of the absorbance change and is attributed to the rate constant for flavin oxidation, while the other phases showed much smaller amplitude

changes, and are attributed to damaged enzyme or free FMN. The observed rate constant of the second phase had a linear dependence on oxygen concentration, indicating a simple bimolecular reaction. The second order rate constant was 79 $M^{-1}s^{-1}$.

The final product of the reaction of the enzyme with molecular oxygen is hydrogen peroxide. The rates of hydrogen peroxide formation using 40-80 μM *E. coli* tRNA and air saturated buffer (255 μM oxygen) were measured using a horseradish peroxidase coupled assay, yielding a rate of $2.6 \times 10^{-9} \pm 4 \times 10^{-10}$ M s^{-1}. There was no change in rate over the tRNA concentrations, used indicating the K_m for the tRNA is much lower than 40 μM. Dividing by the enzyme concentration used (6 μM) gives a k_{cat} of 4.4×10^{-4} s^{-1}. The rate for hydrogen peroxide formation for the *T. maritima* enzyme is therefore close to the rate of reduction by tRNA. Reactions were analyzed for superoxide by oxidizing tRNA aerobically in the presence of acetylated ferri-cytochrome *c*. A slight increase in absorbance at 550 nm was observed, but the reaction rate did not change upon addition of superoxide dismutase. Ferri-cytochrome *c* was also reduced slowly under anaerobic conditions, indicating that this is simply the background rate of acetylated ferri-cytochrome *c* reduction by the enzyme. Therefore, the enzyme reduces molecular oxygen directly to hydrogen peroxide.

Crystal Structure Model

Protein, purified only by affinity chromatography, was crystallized along with the co-purifying tRNA. The crystal structure of the protein was determined to a resolution of 1.51 Å with an R-factor of 0.196 and an R_{free} of 0.231. The resolved structure contains only the FMN binding domain. The C-terminal domain was likely lost due to proteolysis.

This structure has the crystallization buffer bicine bound to the active site. The sulfate bound in the 1VHN structure is replaced by the carboxylate of bicine and the majority of the molecule over the FMN prosthetic group (Figure 3.9).

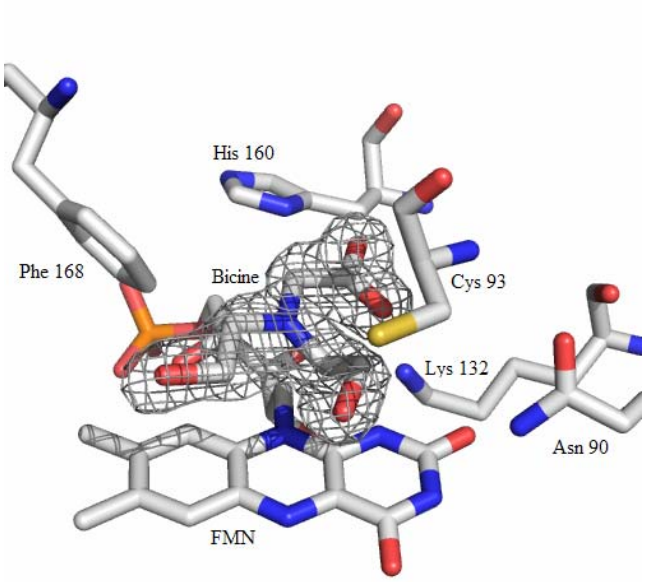

Figure 3.9: *T. maritima* Dihydrouridine Synthase Active Site with Bound Bicine. Shown is the active site of the FMN binding domain crystallized with bicine. Bicine, shown with its electron density map is located between the FMN prosthetic group and the potential active site acid Cys 93.

Even though the C-terminal domain was lost, the overall structure of the FMN-binding domain hardly changes. The two largest changes occur in the positions of the side-chains of Arg 219 and Tyr 15 near the interface between the missing C-terminal helix-bundle and the FMN-binding domain (Figure 3.10). These residues play a role in the interaction between these two domains with Arg 219 forming a salt bridge with Lys 276 and Tyr 15 hydrogen bonding to Lys 269.

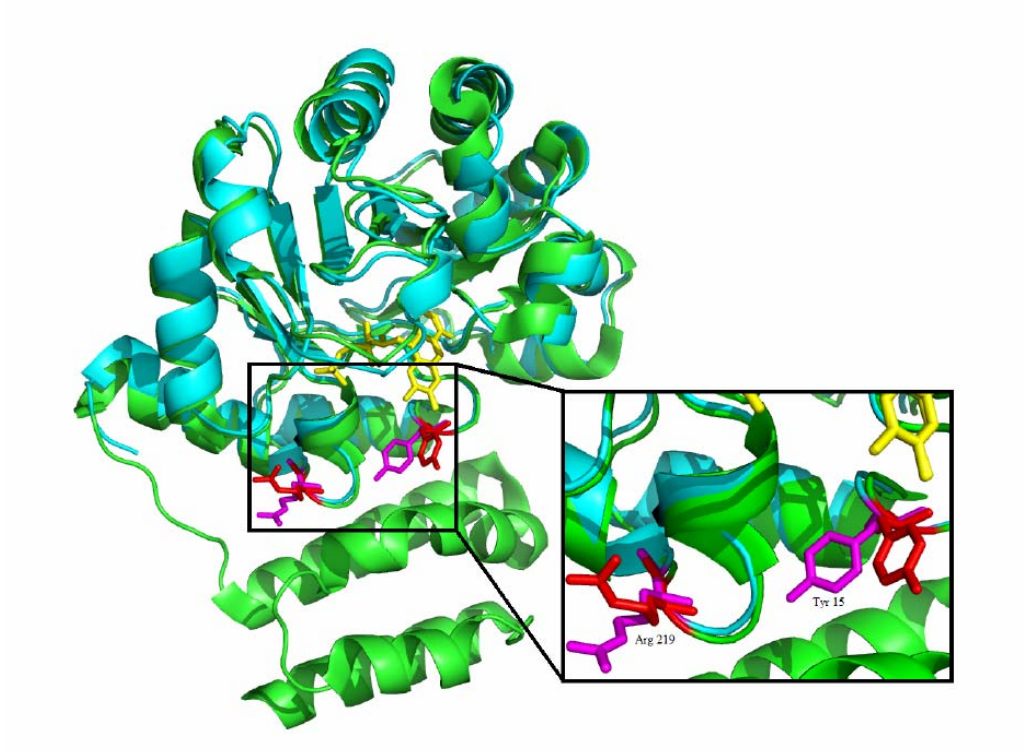

Figure 3.10: Domain Interface Residues in the *T. maritima* Proteolyzed Structure. The figure shows a superimposition of the 1VHN structure (green) and proteolyzed structure (cyan) indicating a similar structure without the C-terminus. The Residues Arg 219 and Tyr 15 highlighted in red (proteolyzed structure) and magenta (1VHN structure) show the largest rmsd difference between the structures.

Discussion

Dihydrouridine synthases are flavin-dependent enzymes that use NADPH to reduce specific uracils in tRNA. Recent structural genomics efforts determined a potential member of this family from *T. maritima* (8). The structure of this FMN-binding TIM-barrel protein has significant similarity to dihydroorotate dehydrogenases (DHODs) and dihydropyrimidine dehydrogenases (DHPDHs) and shows high sequence homology to known DUSs from *E. coli* and *S. cerevisiae* (7). Given the similarity of DUS to DHODs and DHPDHs, it seems likely that DUSs would use a similar mechanism for catalysis, involving two half-reactions. In the reductive half-reaction, NADPH binds to oxidized enzyme, a hydride equivalent is transferred to N5 of FMN, and NADP dissociates. In the oxidative half-reaction, tRNA binds to the reduced enzyme and the hydride from FMN reduces the uracil ring accompanied by a proton transfer from an active site acid. Using this template for the catalytic cycle, we investigated the enzyme from *T. maritima.*

The redox potential of FMN bound to the enzyme is high enough so that it should be readily reduced by NADPH. NADPH binds to the enzyme, though with a rather high K_D. Enzyme was reduced specifically by the *pro-R* hydride of NADPH, which would be unlikely in a non-specific reaction. The reduction of the enzyme, though thermodynamically favorable, occurs with a rate constant of only 2.2×10^{-4} s^{-1}, quite slow compared to most enzymes. A number of reasons were considered for this impaired reduction. The slow reaction was not caused by being far from the pH optimum because there was no sizable effect of pH on the reduction rate constant and there was only a slight change in the K_D for NADPH. There was no KIE on the reductive-half reaction,

suggesting that a conformational change, rather than chemistry, is rate-limiting. The low temperature of our experiments (35^{o} C) is approximately 45^{o} C below the optimum growth temperature of *T. maritima*. It is conceivable that at this low temperature, the enzyme is trapped in a non-reactive conformation. Unfortunately we were unable to examine the reductive-half reaction at a higher temperature because the enzyme was unstable above 40^{o} C.

The oxidative half-reaction did not indicate a substrate preference for the enzyme. Interestingly, tRNA from *E. coli* co-purified with the enzyme, indicating very low K_D values. By determining the tRNAs which co-purified with the enzyme we gained some insight into the potential binding preference of the enzyme. These data indicated that the enzyme binds to many of the *E. coli* tRNAs, with a preference for glycine tRNA. The K_Ds for most *in vitro* transcribed substrates were in the high micromolar range, higher than expected given the co-purification of *E. coli* tRNAs with the enzyme. We also saw that increasing the temperature lowered the K_D values, suggesting that weak binding may be due to the low temperature. The reactions of these substrates were always slow. The $tRNA^{Gly}$-CCC substrate had the highest oxidative rate constant ($1.9 \times 10^{-4} \pm 3 \times 10^{-6}$ s^{-1}). Product analysis detected stoichiometric dihydrouridine formation, showing that these substrates were reduced.

The slow reactions seen for reduction by NADPH, oxidation by tRNA, and reduction by dihydrouridine-containing tRNA all had rate constants of approximately 2×10^{-4} s^{-1}. This, and the lack of an isotope effect on reduction suggest that the rate-limiting step in each of these reactions is a slow isomerization step from an inactive to an active

conformation. Most likely, the inactive conformation is favored because of the much higher temperature optimum of the enzyme.

The crystal structure of the FMN domain of the enzyme suggests that the two domains of the enzyme are capable of moving in relation to one another. Little change in the N-terminal FMN binding domain of the enzyme is seen upon loss of the C-terminal domain, which indicates the two domains may act independently. The position of bicine in this structure over FMN is likely to be close to where NADPH and uridine bind to the active site. The conformation of the two domains in the 1VHN structure shows no obvious hindrance to approaching the flavin. The domain architecture seen in the 1VHN structure, and the location of the likely substrate binding site, and the seperability of the domains implied by the structure of the FMN-binding domain suggest that the C-terminal domain could act as a lid, protecting FMN from solvent. If this is the case, the putative isomerization step controlling the kinetics of the reactions in our experiments may be due to the C-terminal domain uncovering the active site in solution, a state not yet seen in crystals.

Alternatively, it is possible, that DUSs might act *in vivo* in a complex with one or more protein partners. The recent findings that the human DUS 2 interacts with a multifunctional glutamyl-prolyl-tRNA-synthetase complex (18) support this hypothesis, but there is no evidence that this happens with the enzyme from *T. maritima*.

Conclusions

As seen for the dihydrouridine synthase in the previous chapter, this enzyme is also reduced by NADPH in a *proR* specific fashion. We also see that this enzyme binds to *E.coli* tRNA with a much tighter affinity than for *in vitro* transcribed tRNA substrates. The active site cystiene seen in the cystal structures of this enzyme also bolster conclusions of the mutagenic studies of cysiene 117 performed for the *S. cerevisea* enzyme, indicating that this residue is in close proximity to the flavin. The structure determined with bicine in the active site shows that binding to this active site allows for the binding of substrates directly between the cysteine thiol and N5 of the flavin. The slow reactivity of this enzyme makes further comparisons to the *S. cerevisea* enzyme difficult, but those characteristics which we can compare show that both of these enzymes do share important features of their reaction mechanisms.

Appendix

tRNA substrates used

T. maritima $tRNA^{Phe}$-GAA
GGCCAGGTAGCTCAGTTGGTAGAGCACTGGACTGAAAATCCAGGTGTCGGCG
GTTCGATTCCGCCCCTGGCCACCA

T. maritima $tRNA^{Ala}$-CGC
GGGGCCGTAGCTCAGCTGGGAGAGCGCTACCTTCGCACGGTAGAGGTCGTGG
GTTCAAGTCCCATCGGCTCCACCA

T. maritima $tRNA^{Tyr}$-GTA
GGTGGGGTGCCCGAGTGGCCAAAGGGGGCGGACTGTAAATCCGCTGGCAGA
ATGCCTTCGGAGGTTCAAATCCTCCCCCCACCACCA

T. maritima $tRNA^{Gly}$-TCC
GCGGGTGTAGCTCAACTGGTAGAGCATCGGCCTTCCAAGCCGAGGGTTGCGG
GTTCGAGTCCCGTCGCCCGCTCCA

T. maritima $tRNA^{Gly}$-GCC
GCGGGTGTAGCTCAGTGGTAGAGCACCAGCTTGCCAAGCTGGGGGTCGCGGG
TTCGAATCCCGTCGCCCGCTCCA

T. maritima $tRNA^{Gly}$-CCC
GCGGGTGTAGCTCAGCTGGTAGAGCACCAGCTTCCCAAGCTGGGGGTCGCGG
GTTCGAATCCCGTCGCCCGCTCCA

References

1. Sprinzl, M., Steegborn, C., Hübel, F. and Steinberg, S., "Compilation of transfer RNA sequencing and sequences of transfer RNA genes" (1996) *Nucleic Acids Res*., 24:68-72

2. Noon, K. R., Guymon, R., Crain, P. F., McCloskey, J. A., Thomm, M. Lim, J., Cavicchiolo, R., "Influence of Temperature on tRNA Modification in Archaea: *Methanococcoides burtonii* (Optimum Growth Temperature [T_{opt}], 23^{o} C) and *Stetteria hydrogenophila* (T_{opt}, 95^{o} C)" (2003) *J. Bacteriol.*, 185:5483-5490

3. House, C. H., Miller, S. L., "Hydrolysis of dihydrouridine and related compounds" (1996) *Biochemistry*, 35, 315-320

4. Xing, F., Martzen, M. R., Phizicky, E. M., "A conserved family of *Sacchromyces cerevisiae* synthases effects dihydrouridine modification of tRNA" (2002) *RNA*, 8, 370-381

5. Bishop, A. C., Xu J., Johnson, R. C., Schimmel, P., de Crécy-Lagard V., "Identification of the tRNA-Dihydrouridine Synthase Family" (2002) *J. Biol. Chem*., 277:25090-25095

6. Xing, F., Hiley, S. L., Hughes, T. R., Phizicky, E. M., "The Specificities of Four Yeast Dihydrouridine Synthases for Cytoplasmic tRNAs" (2004) *J. Biol. Chem*., 279:17850-17860

7. Savage, D F., de Crécy-Lagard, V., and Bishop, A. C., "Molecular determinants of dihydrouridine synthase activity" (2006) *FEBS Letters*, 580:5198-5202

8. Park, F., Gajiwala, K., Noland, B., Wu, L., He, D., Molinari, J., Loomis, K., Pagarigan, B., Kearins, P., Christoper, J., Peat, J., Badger, J., Hendle, J., Lin, J., Buchanan, S., "The 1.59 angstrom Resolution Crystal Structure of TM0096 a Flavin Mononucleotide Binding Protein from *T. maritima*" (2004) *Proteins*, 55: 772-774

9. Edmonds, C.G., Crain, P.F., Gupta R., Hashizume, T., Hocart, C.H., Kowalak, J.A., Pomerantz, S.C., Stetter, K.O., McCloskey, J.A., "Posttranscriptional modification of tRNA in thermophilic archaea (Archaebacteria)" (1991) *J. Bacter.* 173: 3138-3148

10. Whitby, G. (1953) "A New Method for Preparing Flavin-adenine Dinucleotide" (1953) *Biochem. J.* 54:437-442

11. Massey, V., "A Simple Method for the Determination of Redox Potentials." (1991) In: Flavins and Flavoproteins, edited by Curti B., Ronichi S., and Zanetti G., Berlin: Walter de Gruyter, pp. 59-66

12. Kallansrud, G., and Ward, B., "A comparison of measured and calculated single- and double-stranded oligodeoxynucleotide extinction coefficients" (1996) *Anal. Biochem.* 236:134-138

13. Hunninghake, D., Grisolia, S., "A sensitive and convenient micromethod for estimation of urea, citrulline, and carbamyl derivatives" (1966) *Anal. Biochem.*, 16:200-205

14. Ottolina, G., Riva, S., Carrea, G., Danieli, B., Buckmann, A.F., "Enzymatic synthesis of [4*R*-^{2}H]NAD(P)H and [4*S*-^{2}H]NAD(P)H and determination of the stereospecificity of 7 alpha- and 12 alpha hydroxysteroid dehydrogenase" (1989) *Biochim. Biophys. Acta.,* 998:173-178

15. Engel, P C., "Problems in the Application of Gel Filtration to the Desalting of Organic Compounds: Retardation of Aromatic and Heteroaromatic Anions by Commonly Used Salts" (1977) *Anal. Biochem.*, 82:512-552

16. Favre, A., Fourrey, J.L., "Intramolecular cross-linking of single-stranded copolymers of 4-thiouridine and cytidine" (1974) *Biochem. Biophys. Res. Commun*. 58:507-515

17. Palfey, B. A. and Massey, V. "Flavin-Dependent Enzymes", (1998) Ch. 29 in Comprehensive Biological Catalysis, volume III/Radical Reactions and Oxidation/Reduction (Sinnott, M., ed.), Academic Press, pp. 83-154

18. Kato, T., Daigo, Y., Hayama, S., Nobuhisa, I., Yamabuki, T., Ito, T., Miyamoto, M., Kondo, S., Nakamura, Y., "A Novel Human tRNA-Dihydrouridine Synthase Involved in Pulmonary Carcinogenesis" (2005) *Cancer Res.*, 65:5638-5646

Chapter 4

Kinetics of the Dihydroorotate Dehydrogenase from *Enterococcus faecalis*

Introduction

Dihydroorotate dehydrogenases (DHODs) are flavoproteins that catalyze the oxidation of dihydroorotate to orotate, one of the critical reactions in the de novo biosynthesis of pyrimidines. There are two classes of DHODs with one farther broken down into two subclasses. Class 1A dihydroorotate dehydrogenases are cytosolic homodimeric proteins that contain only FMN and use fumarate as their oxidizing substrate. Class 1B enzymes are heterotetrameric proteins composed of two FMN containing polypeptides, and two polypeptides each containing an FAD and an two-iron two-sulfur cluster. Class 1B DHODs use NAD as their physiological oxidant. Class 2 enzymes are membrane-bound monomers that contain FMN and use ubiquinone as their oxidizing substrate. The class 1 DHODs are found mostly in prokaryotes, and Class 2 enzymes found primarily in eukaryotes and Gram-negative bacteria.

Due to the differences between these forms of DHODs and their important role in pyrimidine metabolism for many bacteria, DHODs might be useful antimicrobial targets. Many recent studies have investigated DHODs from other pathogenic organisms through both structural studies and steady-state kinetics (1,2,3). Previous studies have led to considerable insight into the mechanism and structure of the Class 1A *Lactococcus lactis* enzyme (4,5,6), but less is known about Class 1A DHODs from pathogenic species.

The Class 1 DHOD from *Enterococcus faecalis* is 68% identical to that from *L. lactis*. *E. faecalis* is a pathogenic Gram-positive bacterium that is resistant to a number of different antibiotics. The health risk that this bacterium presents makes finding alternate compounds inhibiting this organism important. DHOD, one of the necessary enzymes in cellular metabolism, provides a potentially useful target for antimicrobial agents. Previously, the Class 1A DHOD from *E. faecalis* was examined by steady-state kinetics with menadione as an oxidant of the enzyme. In this study, we report detailed transient and steady-state kinetics of the DHOD from *E. faecalis*. We show that the oxidative half-reaction of this enzyme is rate-limiting and give rate constants for both the reduction and oxidation of the enzyme by substrates. We also show the effect of pH upon the reaction rate constants and ligand binding constants. The pH dependence of reaction rate constants for reduction and oxidation indicates an ionizable group affects catalysis, likely the thiol of an active site cysteine. The pH dependence for ligand binding shows another pK_a profile indicating the likely interaction of an active site lysine in substrate binding.

Materials and Methods

Cloning of *E. faecalis* DHOD

The gene for the Class 1A DHOD from *E. faecalis* was cloned from genomic DNA purchased from ATCC (Strain 700802D). A PCR product for this gene was amplified using the following forward and reverse primers: 5'-GTGAAGGTGGTAAGC-ATATGAGTAAAACAA-3' and 5'-GAGATGTAACAAAGGATCCGTCAAGAAATT-TTC-3', respectively. The PCR fragment was ran on a 1% agarose gel and gel purified using a (QIAGEN) gel extraction kit. The product was cloned into the pCR-Blunt II-TOPO vector using the Zero Blunt TOPO Cloning Kit (Invitrogen). Plasmid DNA was used to transform DH5α cells and plated on 100 μg/μL kanamycin LB plates and grown overnight. DNA, extracted and purified by alkaline lysis, phenol chloroform extractions, and ethanol precipitations from single colonies was sequenced by the University of Michigan DNA Sequencing Core.

Expression and Purification of *E. faecalis* DHOD

BL21 DE3 cells were transformed by heat shock with the *E. faecalis* DHOD expression plasmid and plated on kanamycin overnight at 37^{o} C. Single colonies were picked and grown overnight in 5 mL LB, and 1 mL of this culture was added to 1 L of LB. The cells were gown to an OD of 0.6 at 600 nm and induced using 1 mM IPTG (final concentration) and grown for 24 hrs at 37^{o} C.

The DHOD-containing cells were pelleted by centrifugation (16,000 x g for 20 minutes) and resuspended in 100 mM Bis-Tris, pH 6.5. The cells were then sonicated for 15 minutes on ice, and cell debris was removed by centrifugation (20,000 x g for 20

minutes). Solid ammonium sulfate was added to 50% saturation, and the precipitated proteins were removed by centrifugation at (16,000 x g for 20 minutes). The supernatant was dialyzed against 2 L of 100 mM Bis-Tris pH 6.5 at 4^{o} C. The dialyzed protein was then applied to a DEAE Sepharose column 25^{o} C (70 mL volume equilibrated in 100 mM Bis-Tris, pH 6.5). The column was washed extensively with 100 mM Bis-Tris, pH 6.5, containing 100 mM NaCl. The protein was then eluted with 100 mM Bis-Tris, pH 6.5, containing 250 mM NaCl and fractions were collected. Fractions containing the protein were identified by their yellow color, pooled, concentrated, and dialyzed against 100 mM Bis-Tris, pH 6.5; the protein was precipitated with 0.472 g/mL ammonium sulfate and stored at 4^{o} C. A single band of approximately 35 kDa, seen on an SDS PAGE (12%) using Coomassie Blue staining, indicated that the enzyme was greater than 95% pure.

Enzyme Concentrations

The extinction coefficient of the enzyme was determined from in 100 mM Tris Buffer, pH 8.5, 25^{o} C. The absorbance of the enzyme was measure before and after treatment with 1% SDS. Upon treatment with SDS FMN was liberated due to protein unfolding. The extinction coefficient at 456 nm of (11,800 $M^{-1}cm^{-1}$) was calculated from the ratio of the absorbances of the free FMN and the FMN containing native enzyme. Enzyme concentrations were routinely determined spectrophotometrically using this extinction coefficient and are given in terms of active site concentrations.

Absorbance spectra were obtained using a Shimadzu UV-2501PC scanning spectrophotometer. Enzyme solutions for steady-state kinetics and rapid reaction kinetics

were made anaerobic in glass tonometers by multiple cycles of evacuation and equilibration with an atmosphere of purified argon. When reduced enzyme was needed, a gas-tight syringe containing a dithionite solution was attached to a tonometer that had a sidearm cuvette. Anaerobic enzyme was then titrated to complete reduction with an equivalent of dithionite as judged by absorbance spectroscopy. Stopped-flow and steady-state kinetic studies were performed at 4^{o} C using a Hi-Tech SF-61 DX2 stopped-flow spectrophotometer. All studies were performed using 100 mM TAPS pH 8.5, with the ionic strength held at 50 mM by adding an appropriate amount of KCl, unless otherwise indicated.

Results

Redox Potential

The reduction potential of the enzyme-bound flavin was determined spectrophotomectrically at 25^{o} C in 100 mM Tris, pH 7.0, by the coupled xanthine/xanthine oxidase method of Massey (7). Phenosafranin (E_{m7} = -252 mV) was used as the redox indicator dye. A phenosafranin and enzyme mixture was slowly reduced using xanthine oxidase in the presence of a small amount of methyl viologen that acted catalytically to transfer electrons to the protein. A redox potential of -262 mV was determined. This compares to the redox potential of -243 mV found for the closely related *L. lactis* Class 1A DHOD (3).

Ligand Binding

Orotate binding to the oxidized enzyme

The K_D for orotate binding to the oxidized enzyme was determined from the red shift in the flavin spectrum (maximal at 510 nm), which occurs when orotate binds (Figure 4.1). The K_D, determined using equation (1) was 151 ± 32 μM at pH 8.0, 25° C, similar to the K_D previously reported for this enzyme (3).

$$\Delta A = \frac{\Delta A_{max}[L]}{K_D + [L]} \qquad (1)$$

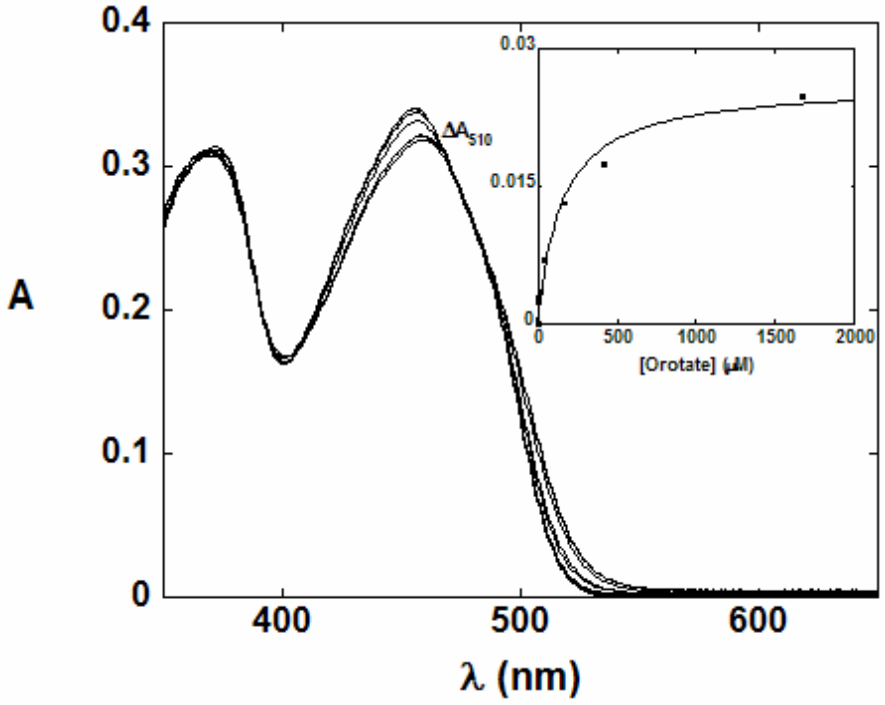

Figure 4.1: Binding to Orotate. Oxidized DHOD (30 μM enzyme) was titrated with increasing amounts of orotate from 0.25 μM to 4.2 mM, causing a red shift in the flavin peak. The inset shows the plot of the change in absorbance at 510 nm versus orotate concentration, yielding a K_D of 151 ± 32 μM.

Orotate Binding Stoichiometry

The stoichiometry of orotate binding to the oxidized enzyme was determined by titrating 1.51 mM enzyme with orotate and monitoring the change in absorbance at 511 nm in a 1 mm cell. The stoichiometry of orotate binding to the enzyme was determined to be 1 orotate molecule per dimer, suggesting that only half of the enzyme active sites bind (Figure 4.2). This is similar to the behavior reported from the Class 1A enzyme for *L. lactis* (6). The stoichiometry of orotate binding to enzyme treated with hydrogen peroxide was also measured giving a similar 2:1 ratio, indicating that oxidation of the enzyme is unlikely to be the reason for the half-sites binding of orotate.

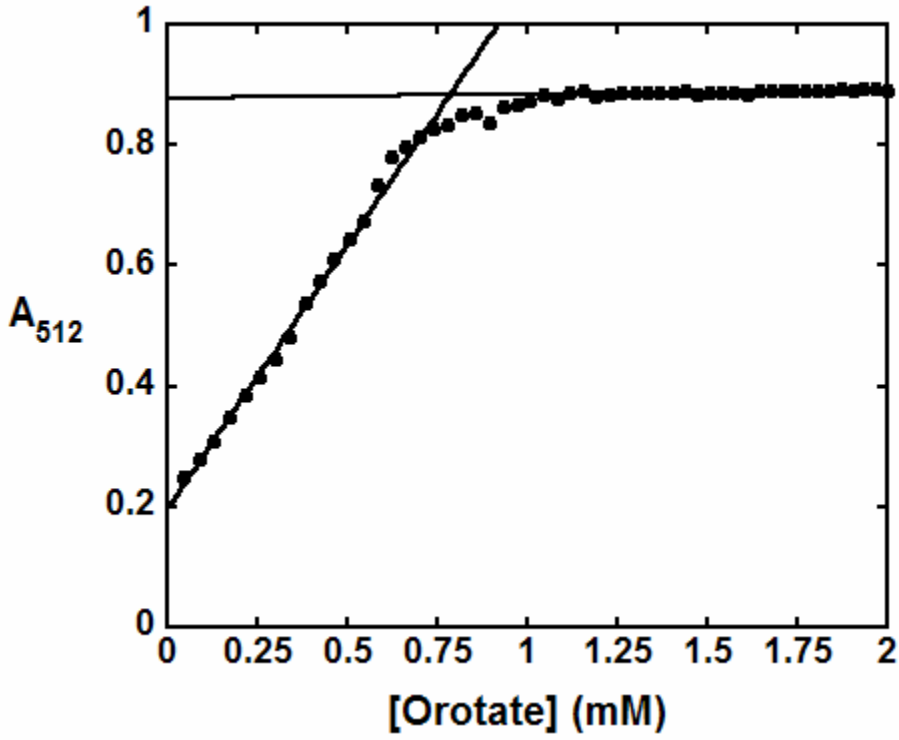

Figure 4.2: Stoichiometry of Orotate Binding. Oxidized enzyme (1.51 mM), at a concentration far above the K_D for orotate, was titrated with orotate in a 0.1 cm pathlength cuvette. The absorbance plotted versus orotate concentration yields two straight lines giving 0.74 mM orotate bound, showing roughly 1 orotate bound per dimer of enzyme.

pH Dependence of Orotate Binding

The K_D for orotate binding to the oxidized enzyme was measured over the pH range of 6.5 to pH 11 at 25^o C (Figure 4.3). The binding of orotate to the enzyme was monitored by spectral changes at 511 nm. The K_D values increased with increasing pH. No plateau was observed indicating the pK_a is likely above 11. The most likely residue a pK_a in this range would indicate would be a lysine residue which binds to the substrate.

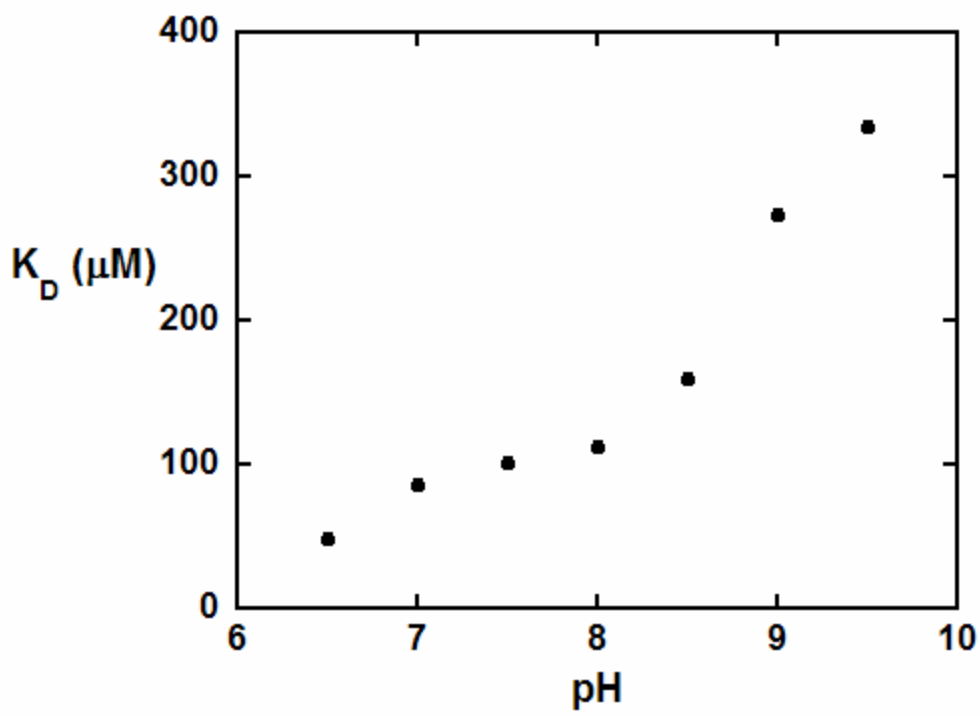

Figure 4.3: Dependence of Orotate Binding on pH. The dissociation constant for orotate to oxidized enzyme was measured as a function of pH from 6.5 to 9.5.

DHO Binding to Reduced Enzyme

The K_D for the binding of DHO to the reduced enzyme was determined in 100 mM Tris, pH 8.5, at 25 ^oC. Reduced anaerobic enzyme was mixed with increasing concentrations of anaerobic DHO in a stopped-flow spectrophotometer (Figure 4.4). Binding was monitored by an increase in absorbance in the reduced flavin spectrum at 425 nm, giving a K_D of 4.1 ± 0.5 mM.

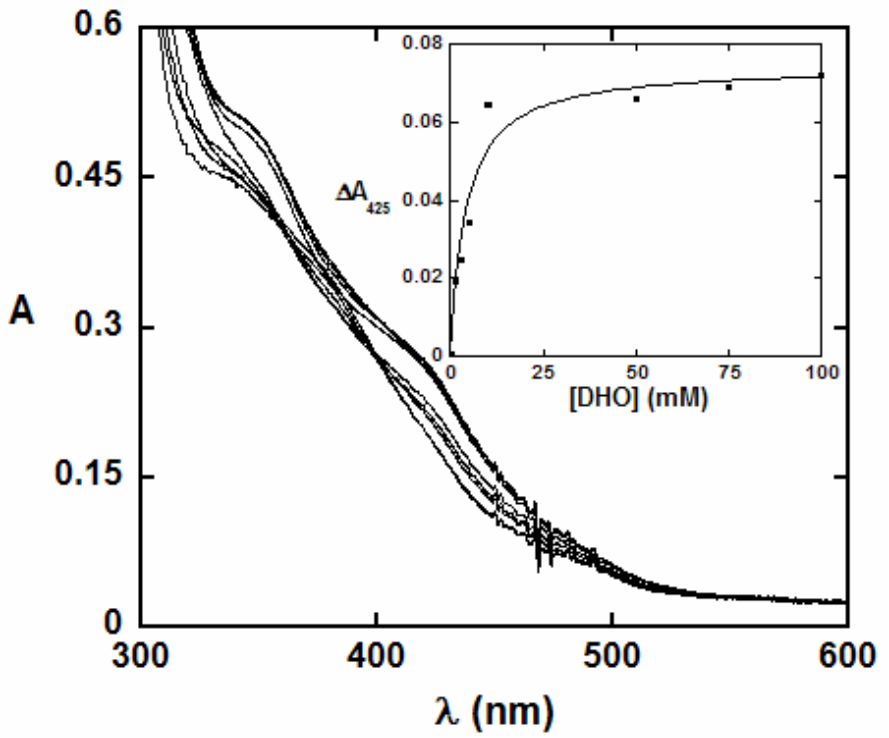

Figure 4.4: Binding to DHO. Dithionite-reduced DHOD (50 μM enzyme) was titrated with increasing amounts of dihydroorotate from 25 μM to 100 mM, causing an increase at 425 nm. The inset shows the plot of the change in absorbance at 425 nm versus dihydroorotate concentration, yielding a 4.1 ± 0.5 mM.

Fumarate Binding to Oxidized Enzyme

Fumarate binding to oxidized enzyme was determined in 100 mM Tris, pH 8.5, at 25 ^{o}C. Enzyme was titrated with increasing concentrations of fumarate and monitored spectrally (Figure 4.5).

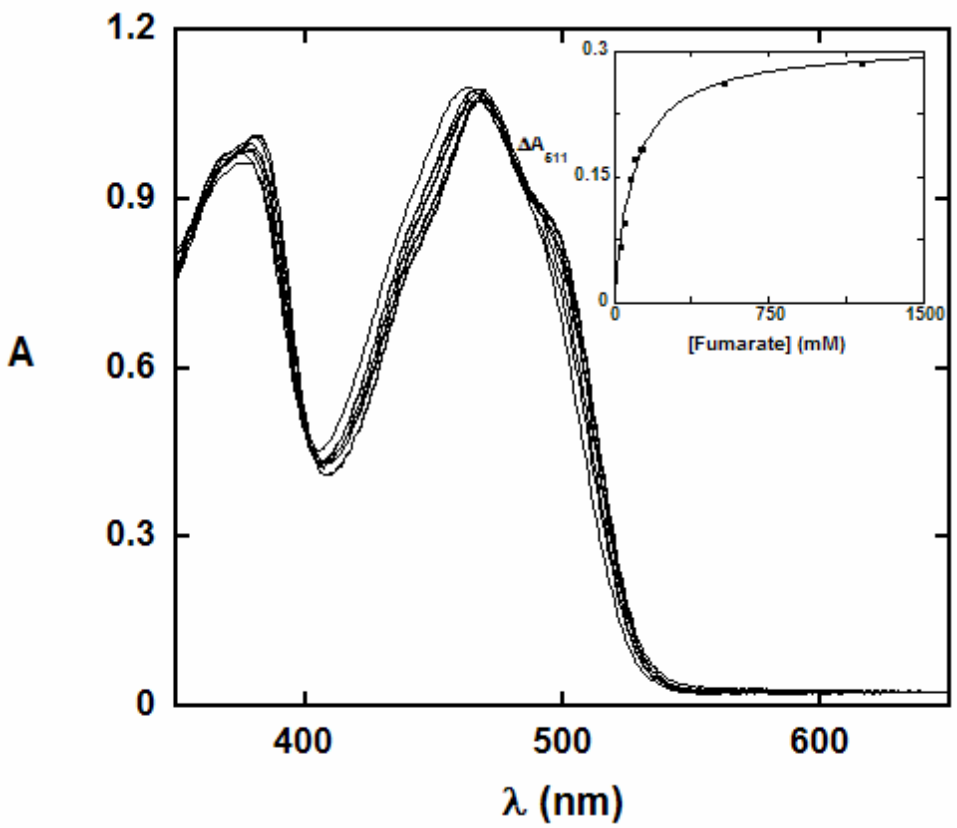

Figure 4.5: Binding to Fumarate. Oxidized DHOD (85 μM enzyme) was titrated with increasing amounts of fumarate from 30 mM to 1.2 M causing a red shift in the flavin peak. The inset shows the plot of the change in absorbance at 511 nm versus fumarate concentration, yielding a K_D of 95 ± 8 mM.

The change in absorbance at 511 nm was fit to (1), giving a K_D of 95 ± 8 mM.

Binding of Succinate to Oxidized Enzyme

A set concentration of enzyme (20 μM final) was added to 1 mL of succinate in 100 mM Tris, pH 8.5, at 25° C (Figure 4.6). Enzyme added to buffer containing succinate showed a discernable spectral shift indicating binding to the oxidized enzyme. Binding was very weak, with a K_D greater than 1 M.

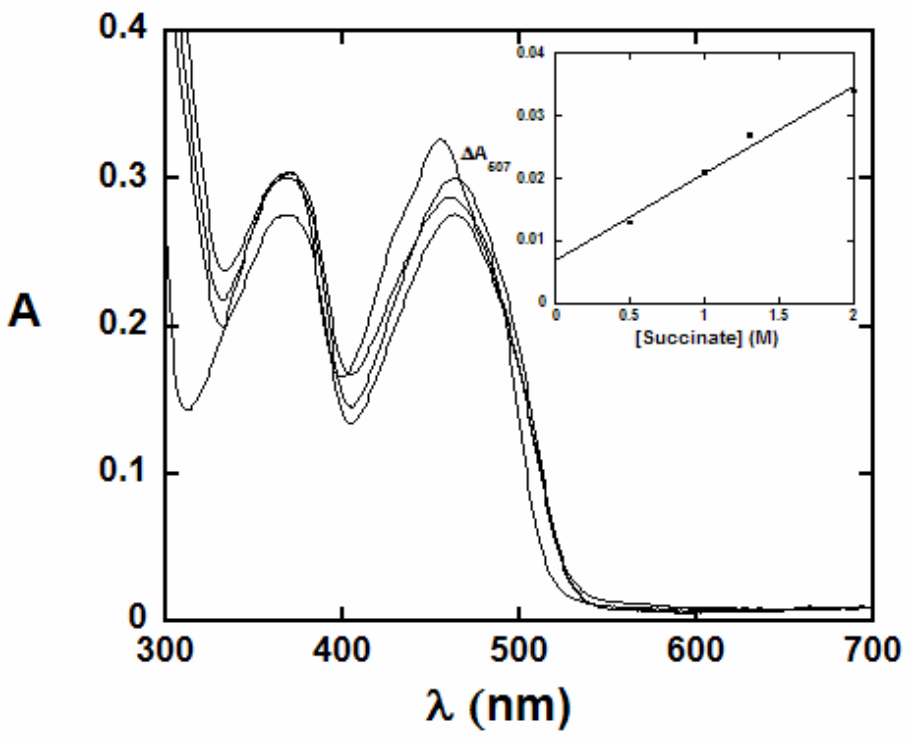

Figure 4.6: Binding to Succinate. Oxidized DHOD (26 μM enzyme) was titrated with increasing amounts of succinate from 500 mM to 2 M, causing a red shift of the flavin peak. The inset shows the plot of the change in absorbance at 507 nm versus succinate concentration, yielding a straight line, indicating a K_D greater than 1 M.

Binding of Hydroxybenzoates

The K_D for 3,5-dihydroxybenzoate was determined from the red shift in the flavin spectrum caused by binding (Figure 4.7). The change in absorbance at 508 nm gave a K_D of 45 ± 5 μM at pH 8.5, 25° C.

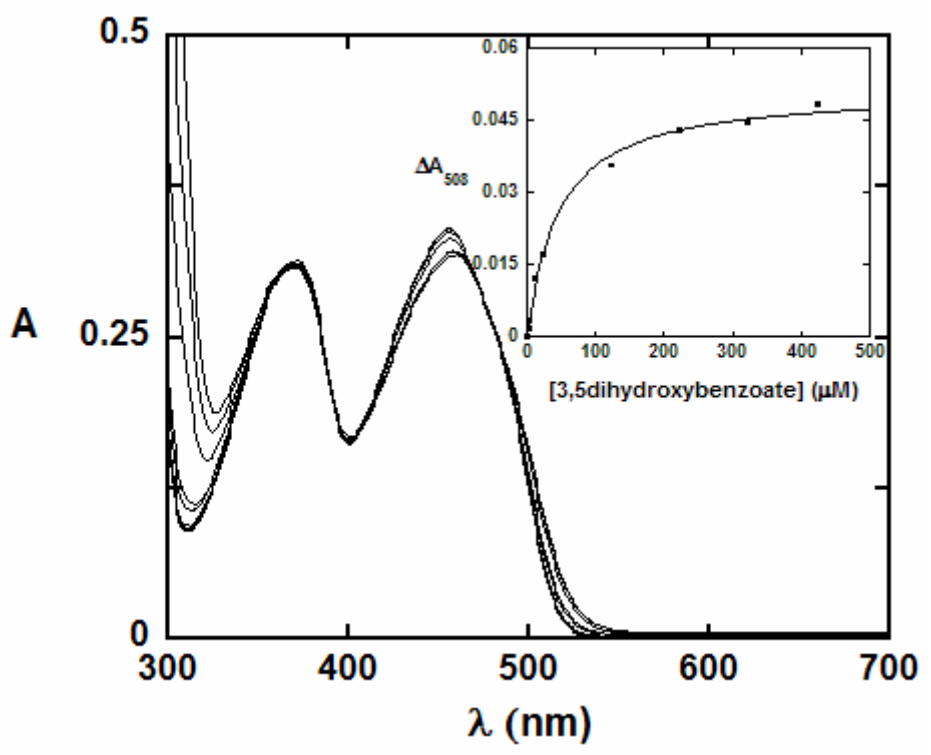

Figure 4.7: Binding to 3,5-Dihdyroxybenzoate. Oxidized DHOD (28 μM enzyme) was titrated with increasing amounts of 3,5-dihydroxybenzoate from 0.2 μM to 422 μM, causing a red shift in the flavin peak. The inset shows the plot of the change in absorbance at 508 nm versus 3,5-dihydroxybenzoate concentration, yielding a K_D of 45 ± 5 μM.

The K_D for 3,4-dihydroxybenzoate was determined by following the formation of a charge-transfer band at 600 nm (Figure 4.8). A K_D value of 260 ± 25 μM at pH 8.5 25° C.

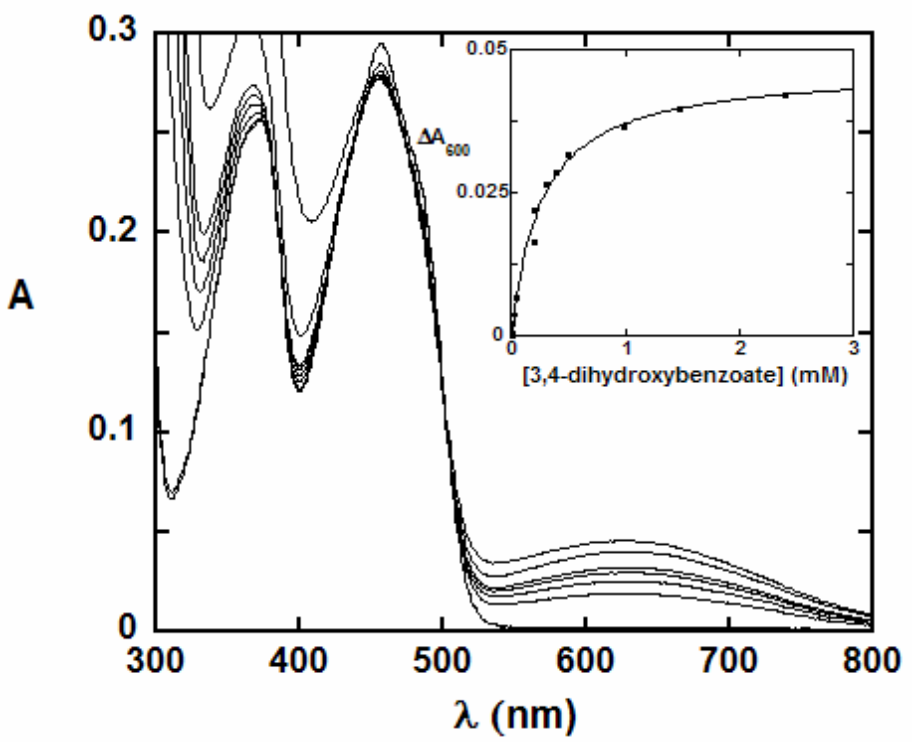

Figure 4.8: Binding to 3,4-Dihydroxybenzoate. Oxidized DHOD (26 μM enzyme) was titrated with increasing amounts of 3,4-dihydroxybenzoate from 0.25 μM to 4.2 mM, causing charge-transfer absorbance at 600 nm. The inset shows the plot of the change in absorbance at 600 nm versus 3,4-dihydroxybenzoate concentration, yielding a K_D of 260 ± 25 μM.

3,4-Dihydroxybenzoate Binding Stoichiometry

The stoichiometry of 3,4-dihydroxybenzoate binding to the oxidized enzyme was determined in 100 mM Tris, pH 8.5, at 25° C. Binding was monitored by observing the formation of the charge-transfer formed when 3,4-dihydroxybenzoate binds to the enzyme at 600 nm. Enzyme (2.57 mM) was titrated with 3,4-dihydroxybenzoate in a 1 mm cell. The stoichiometry of 3,4-dihydroxybenzoate binding to the enzyme was determined to be a single 3,4-dihydroxybenzoate molecule per dimer, suggesting that only half of the enzyme active sites bind to 3,4-dihydroxybenzoate.

Kinetics of Enzyme

Reductive Half-Reaction

The reductive half-reaction was analyzed by mixing various concentrations of DHO with 10 μM of DHOD in a stopped-flow spectrometer at pH 8.5, 4° C. The rate of DHO binding was too fast to determine, but could be detected by a red shift in the flavin spectrum. This red shift occurred within the deadtime of the stopped-flow instrument (<1 ms). After the binding of DHO, the flavin was reduced. This reduction was monitored by a decrease in absorbance of the FMN peak at 450 nm. Flavin reduction was followed by product dissociation, which caused a smaller absorbance decrease at 450 nm. Spectra taken long after the reduction by DHO was complete showed that only half of the flavin absorbance disappeared (4.9).

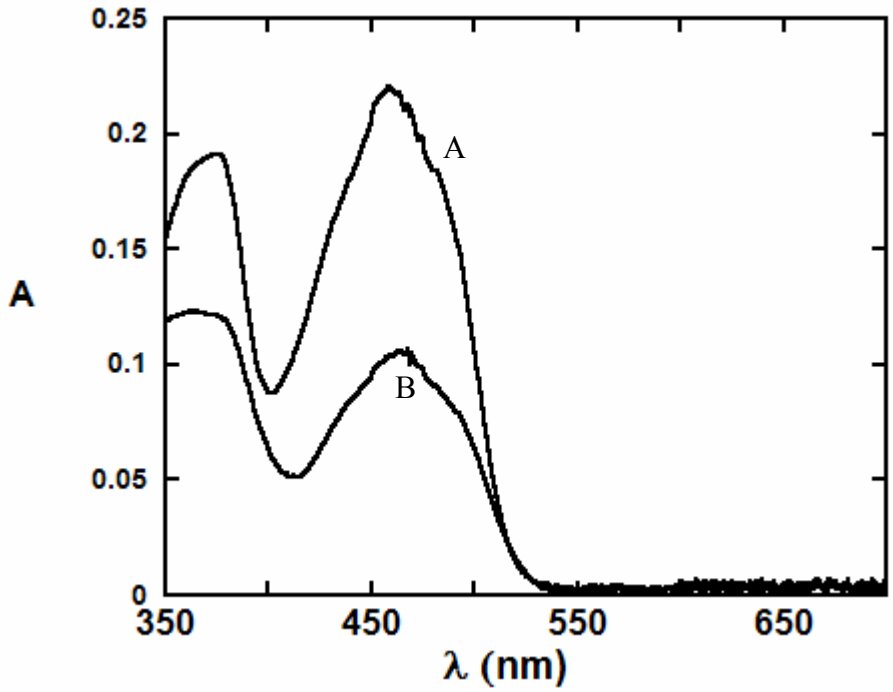

Figure 4.9: Indications of Half-Sites Reactivity. Spectrum (A) shows enzyme oxidized by oxygen (~230 μM final). Spectrum (B) show anaerobic enzyme after mixing with 1 mM dihydrorotate. Upon mixing with saturating amounts of dihydroorotate only half of the flavin is reduced indicating half-sites reactivity.

The extent of reduction was independent of concentration and the half-reduced state was stable for long periods even in the presence of high concentrations of DHO (1 mM). The observed rate constant for the first phase (reduction) increased hyperbolically with respect to DHO, which is consistent with an initial binding of DHO followed by reduction of the flavin (Figure 4.10). The observed rate constants were fit to Equation (4).

$$k_{obs} = \frac{k_{red}[DHO]}{K_D + [DHO]} \qquad (2)$$

The rate constant calculated for reduction with DHO was 53 ± 2 s^{-1} and the K_D was 73 ± 7 μM.

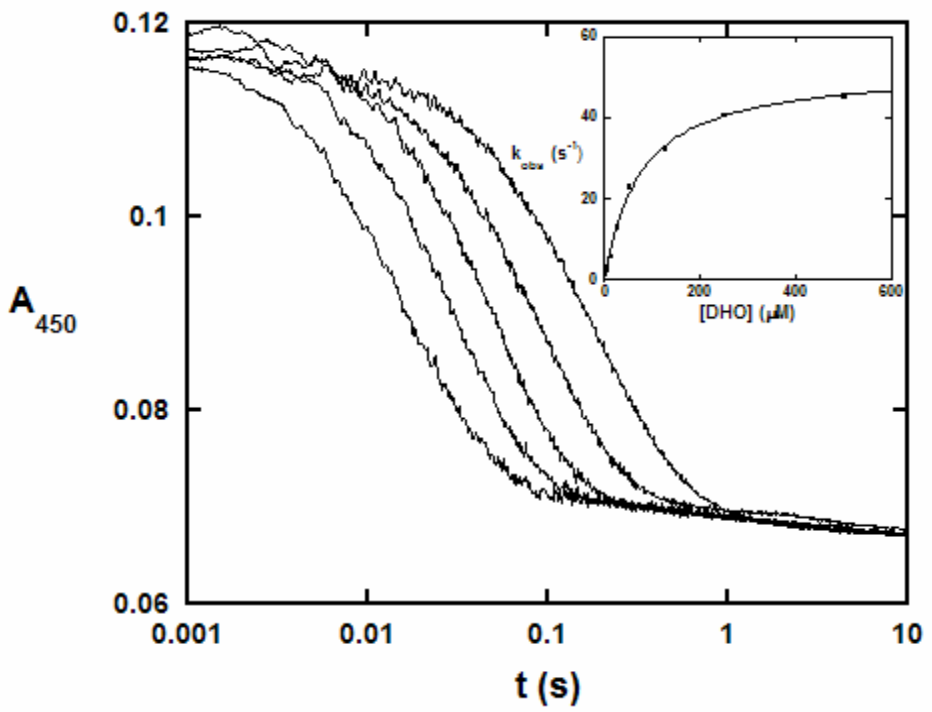

Figure 4.10: Reduction of Oxidized Enzyme with Dihydroorotate. A: Stopped-flow traces watching reduction of oxidized enzyme at 450 nm with increasing concentrations of dihydroorotate from 4 to 500 μM. The traces were fit two exponentials the first of which corresponds to flavin reduction, the second orotate release. The inset shows a plot of concentration dihydroorotate versus rate of reduction giving a reductive rate constant of 52.6 ± 1.6 s^{-1} and a K_D for DHO of 73.6 ± 6.9 μM.

At high concentrations of DHO a charge-transfer band was seen at 550 nm indicating orotate was bound to the reduced enzyme (Figure 4.11). Reaction traces at this wavelength were fit to two exponentials. The observed rate constant of one phase was similar to that for flavin reduction determined at 450 nm, and the other, $16 \pm 0.3\ s^{-1}$ was assigned to the dissociation of orotate from the reduced enzyme.

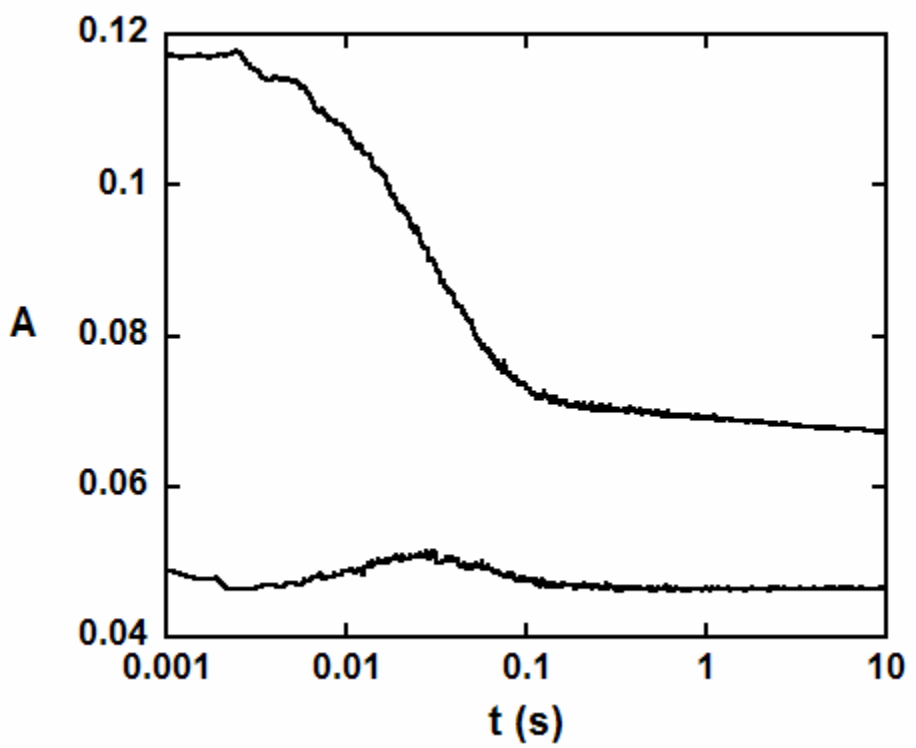

Figure 4.11: Orotate Release. A charge-transfer band is formed in the presence of an orotate reduced-enzyme complex. This charge-transfer band was observed at 550 nm (Bottom Trace). The formation of a reduced enzyme orotate bound species forms at the same rate as flavin reduction followed at 450 nm (Top Trace). The complex quickly disappears giving the rate for orotate release at $16 \pm 0.3\ s^{-1}$.

At low DHO concentrations the formation and dissociation of this charge-transfer complex were not resolved because the observed rate constant for orotate dissociation was larger than that of flavin reduction, thus reducing the amount of charge-transfer complex below the limits of detection.

Oxidation of Reduced Enzyme by Orotate

The rate constant for the oxidation of enzyme by orotate was determined by mixing 26 μM reduced enzyme with varying concentrations of anaerobic orotate. Flavin oxidation was followed at 450 nm. Reaction traces showed an increase in absorbance Traces were fit to one exponential. Observed rate constants were plotted against the concentration of orotate and fit to the equation (3).

$$k_{obs} = \frac{k_{ox}[Orotate]}{K_D + [Orotate]} \qquad (3)$$

The K_D for orotate to reduced enzyme was too low to be determined, indicating tight binding, with an upper estimated limit of 11 μM. A rate constant for oxidation of $1.9 \pm 0.04\ s^{-1}$ was found. The enzyme was only half-oxidized after the reaction with orotate, even at high concentrations of orotate, establishing this was not an equilibrium effect.

pH Dependence of k_{red}

The pH dependence for the reduction of the enzyme by DHO was determined for the reductive half-reaction from pH 6.5 to pH 11 at 4° C. Rate constants for flavin reduction were plotted as a function of pH and fit to Equation (4).

$$k_{red} = k_{\max,red}\left[\frac{10^{-pKa}}{10^{-pKa} + 10^{-pH}}\right] \qquad (4)$$

A pK_a of 8.3 ± 0.1 and a maximum reductive rate of 73.3 ± 2.9 s^{-1} was determined form these data (Figure 4.12).

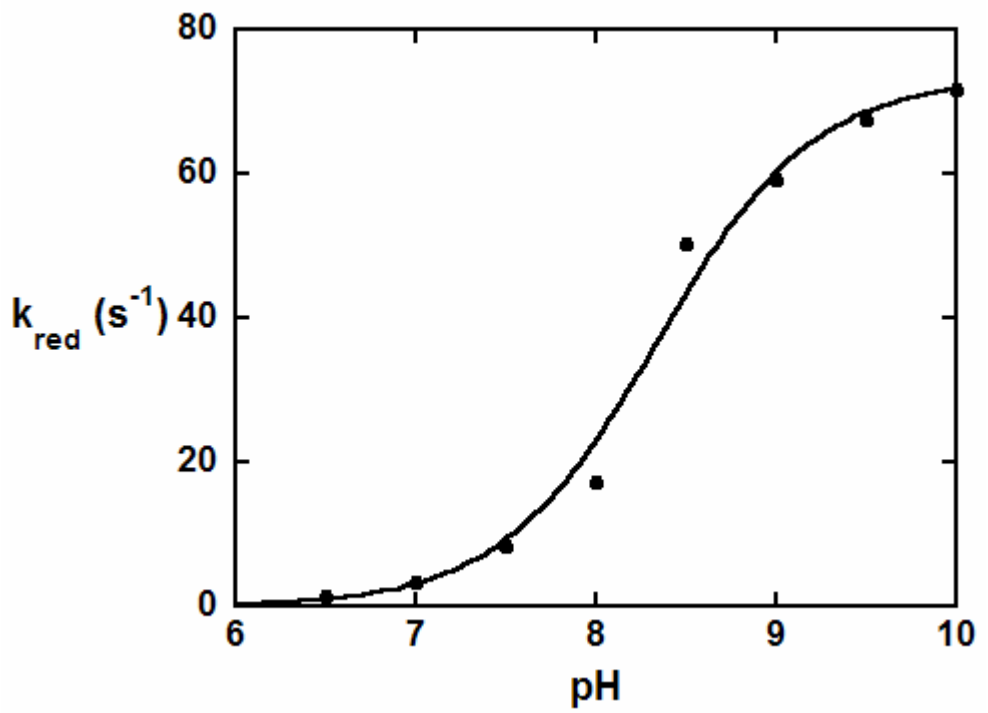

Figure 4.12: Dependence of Reduction on pH. The rate constant of reduction of the enzyme at saturating dihydroorotate was determined over a pH range of 6.5 to 10 and fit to a pK_a of 8.33 ± 0.08.

DHO binding, determined from the half-saturating concentrations of the observed rate constants, increased with increasing pH. The increase in binding showed no plateau making determination of an exact pK_a difficult, with a value above 11 (Figure 4.13). We attribute this to a pK_a potentially on the enzyme, most likely an active site lysine.

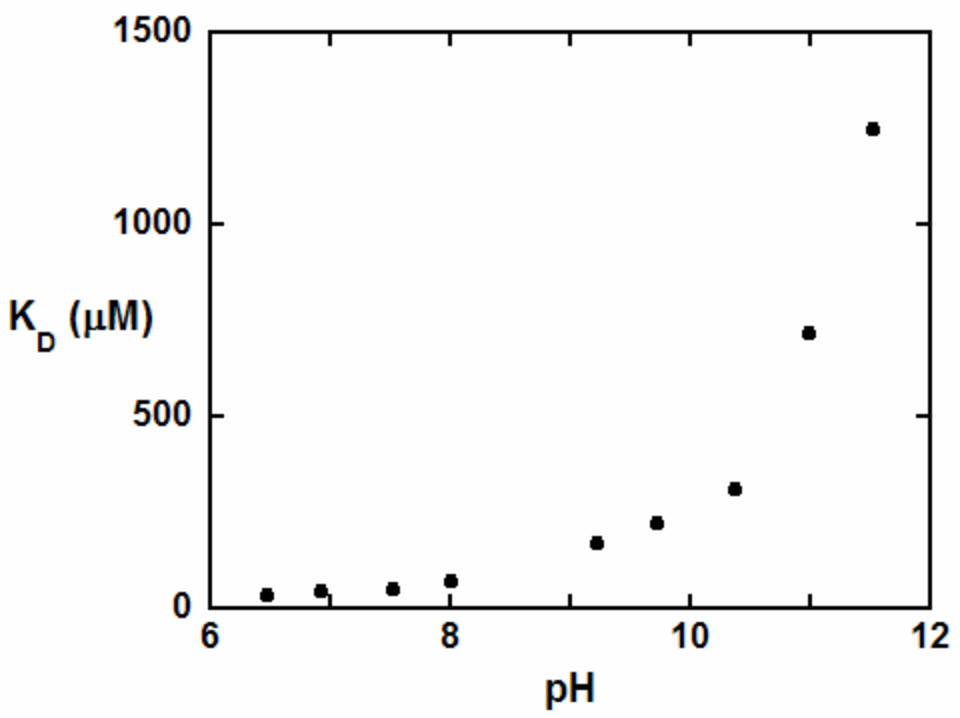

Figure 4.13: Dependence of DHO Binding on pH. The dissociation constant for dihydroorotate to oxidized enzyme was measured as a function of pH from 6.5 to 11.

Oxidative Half-Reaction with Oxonate

Oxidation of the enzyme by oxonate was determined using dithionite-reduced enzyme at 4^{o} C, pH 8.5. Various concentrations of anaerobic oxonate were mixed with enzyme. Flavin oxidation was monitored at 450 nm. Traces were fit to one exponential. The observed rate constants were plotted against oxonate concentration. From these plots a K_D of 4.2 ± 0.4 mM and a k_{ox} of 3.6 ± 0.1 s^{-1} were determined. Half-sites oxidation was observed with oxonate in a fashion similar to that seen for orotate.

Oxidative Half-Reaction with Fumarate

The oxidative half-reaction was analyzed by mixing 26 μM reduced enzyme with various concentrations of fumarate at pH 8.5, 4° C. Flavin oxidation caused an increase in absorbance at 450 nm that was fit to one exponential (Figure 4.14). The observed rate constants were plotted as a function of fumarate concentration and fit to the equation (5)

$$k_{obs} = \frac{k_{ox}[Fumarate]}{K_D + [Fumarate]} \qquad (5)$$

A maximum oxidative rate constant of 5.1 ± 0.7 s^{-1} and a K_D for fumarate to the reduced enzyme of 3.5 ± 0.2 mM were found.

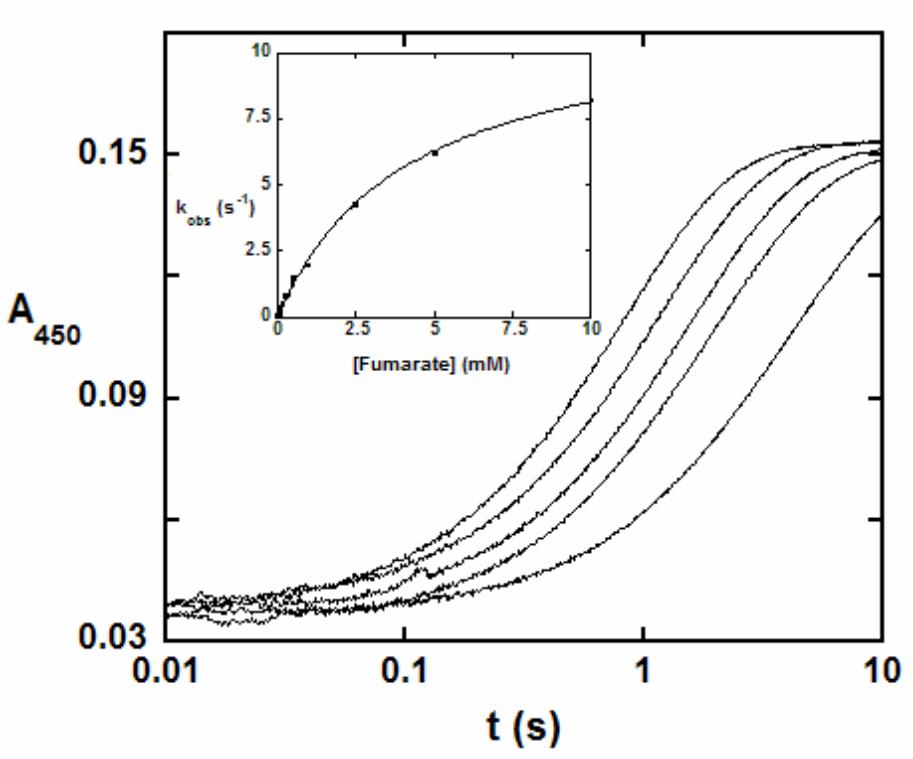

Figure 4.14: Oxidation of Reduced Enzyme with Fumarate. The oxidation of the enzyme was monitored at 450 nm in stop flow experiments by mixing 26 μM reduced enzyme with increasing concentrations of fumarate from 50 μM to 100 mM. The traces were fit to one exponential corresponding to flavin oxidation. The inset shows a plot of the observed rate constant versus fumarate concentration giving the rate constant for oxidation of 5.1 ± 0.3 s^{-1} and a K_D for fumarate to the reduced enzyme of 3.5 ± 0.2 mM.

pH Dependence of k_{ox}

The pH dependence for the oxidative half reaction with fumarate was studied by pH-jump experiments. Reduced enzyme (25 μM) in 0.5 mM KPi, pH 7.0, with ionic strength set to 50 mM with KCl, was mixed against various concentrations of fumarate from pH 6 to pH 11. The rate constant for the reaction of fumarate decreased with increasing pH, controlled by a pK_a of 7.1 ± 0.1, approximately 1 pH unit different than that for the reductive half reaction (Figure 4.15).

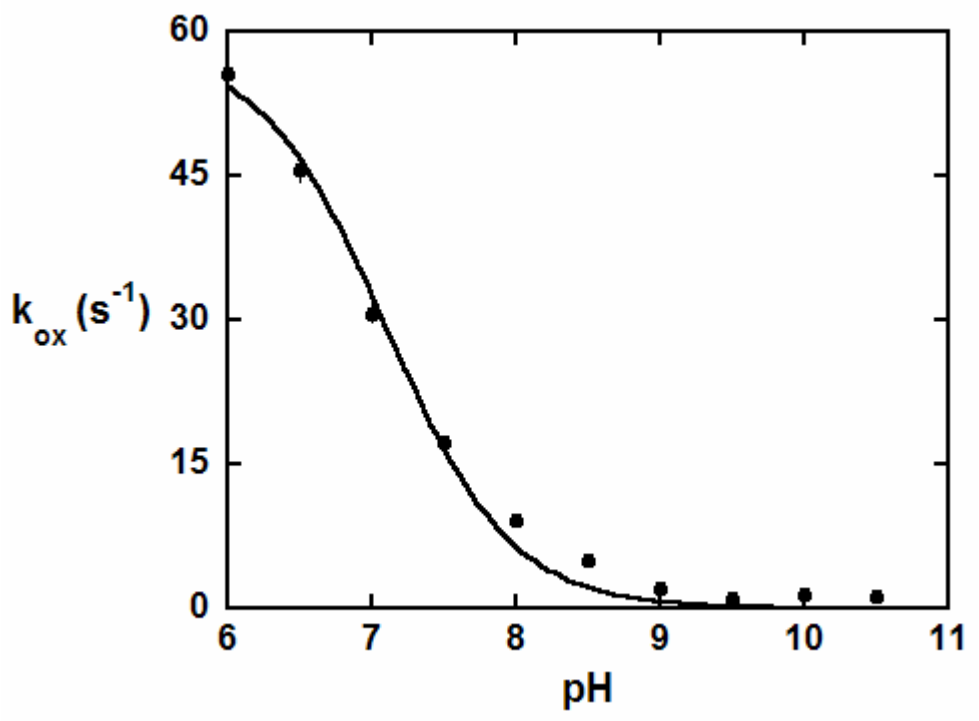

Figure 4.15: Dependence of Oxidation on pH. The rate of oxidation of the enzyme at saturating fumarate was determined over a pH range of 6 to 10.5 and fit to a pK_a of 7.1 ± 0.05.

This indicates that either the substrates change the pK_a of the active site cysteine or another ionizable residue is responsible for the rate limiting step in fumarate reduction.

The K_D for fumarate increased over the pH range from 6 to 11, similar to that for orotate and dihydroorotate, suggesting that this pK_a is due to a group on the enzyme (Figure 4.16).

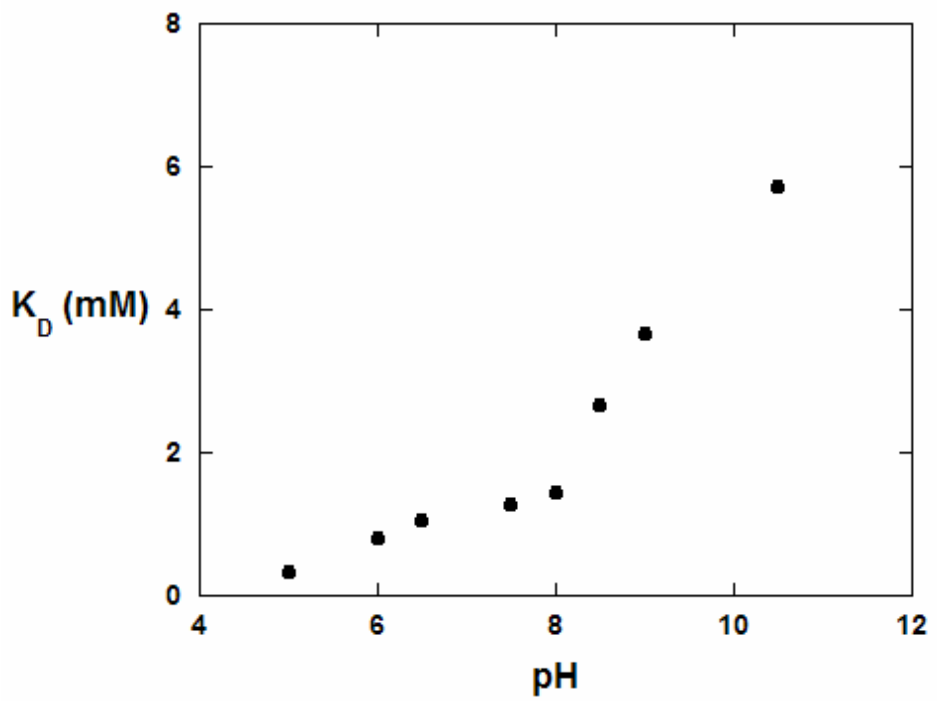

Figure 4.16: Dependence of Fumarate Binding on pH. The dissociation constant for fumarate to reduced enzyme was measured as a function of pH from 5.5 to 10.5.

Reduction of Menedione by Reduced Enzyme

The enzyme was oxidized with menadione in anaerobic stopped-flow experiments using reduced enzyme (25 μM) mixed with increasing concentrations of menadione. The observed rate constant increased linearly with increasing concentrations of menadione (up to its solubility limit of 400 μM). Thus we found no indication of binding prior to reaction as previously postulated (3). A bimolecular rate constant of $9 \times 10^4 \pm 3 \times 10^3$ M^{-1} s^{-1} was found.

Steady-State Kinetics

Steady-state kinetics using fumarate or menadione as oxidizing substrates were determined under aerobic conditions. Menadione reduction at 25 ^{o}C, in 50 mM Tris-HCl, pH 7.5, was detected by using DCIP as a terminal electron acceptor by observing the decrease in absorbance at 610 nm. Menadione and DHO gave a k_{cat} of 56.9 s^{-1} and K_m values of 130 μM for menadione and 68 μM for DHO. These results are similar to those previously obtained for this enzyme (3).

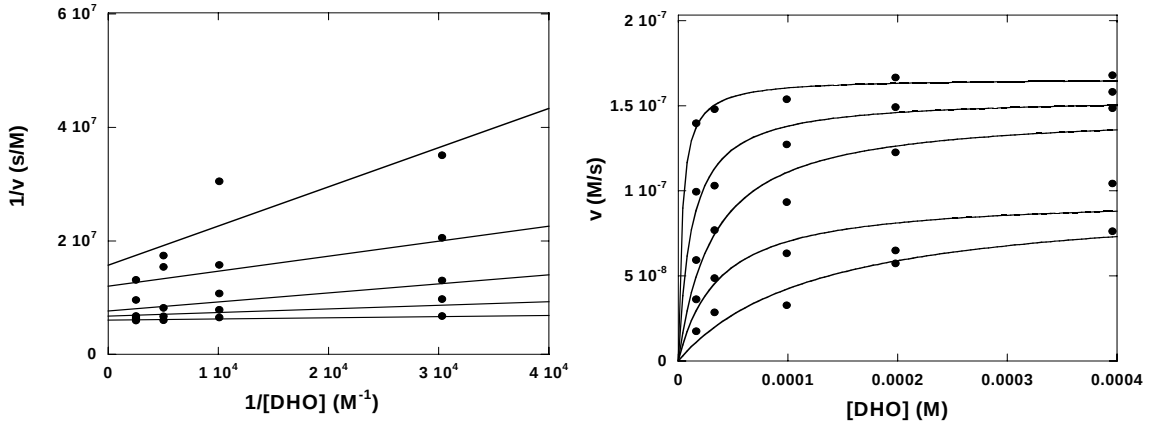

Figure 4.17: Steady-State Kinetics (DHO). The rate of orotate formation as a function of DHO concentration is plotted in both linear and double-reciprocal forms. Note that the DHO curves show saturation at almost every point making the determination of a K_m difficult.

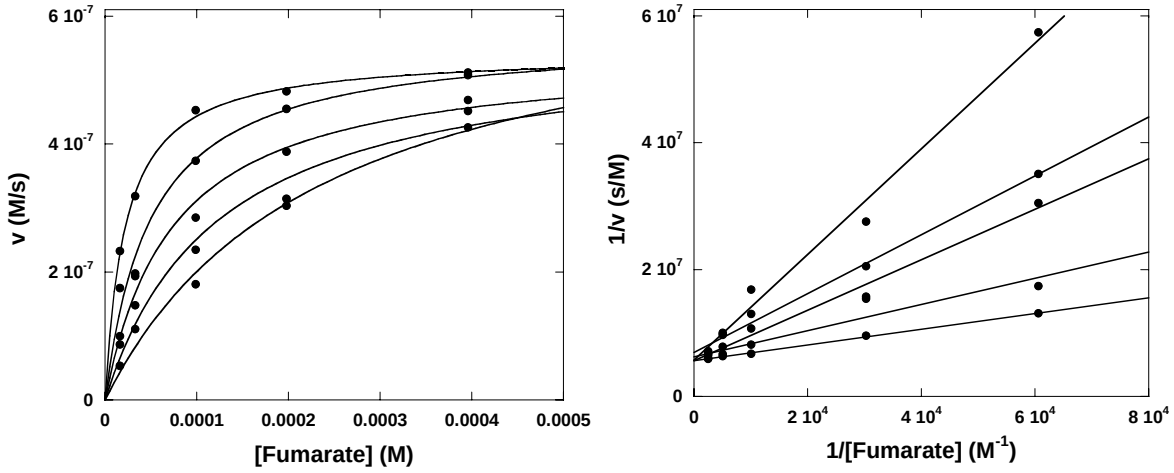

Figure 4.18: Steady-State Kinetics (Fumarate). The rate of orotate formation as a function of fumarate concentration is plotted in both linear and double-reciprocal forms. The Km for fumarate is calculated to be 22 μM.

The natural substrates fumarate and DHO gave different results. The reaction (performed anareobically) at pH 8.5, 4^{o} C, was monitored by the absorbance of orotate at 280 nm. Enzyme (1 μM final) was mixed with various concentrations of fumarate and dihydroorotate (16.5 to 390 μM). Double-reciprocal plots show an intersecting pattern with the best fit to an ordered Bi-Bi mechanism. A k_{cat} of 1.6 ± 0.2 s^{-1} was determined for the reaction with a K_m for fumarate of 22 ± 5 μM. The K_m for DHO was too low to be determined (Figures 4.17 and 4.18).

Enzyme-Monitored Turnover

Enzyme turnover was monitored at pH 8.5, 4 ^{o}C, observing the change in flavin absorbance at 456 nm (Figure 4.19).

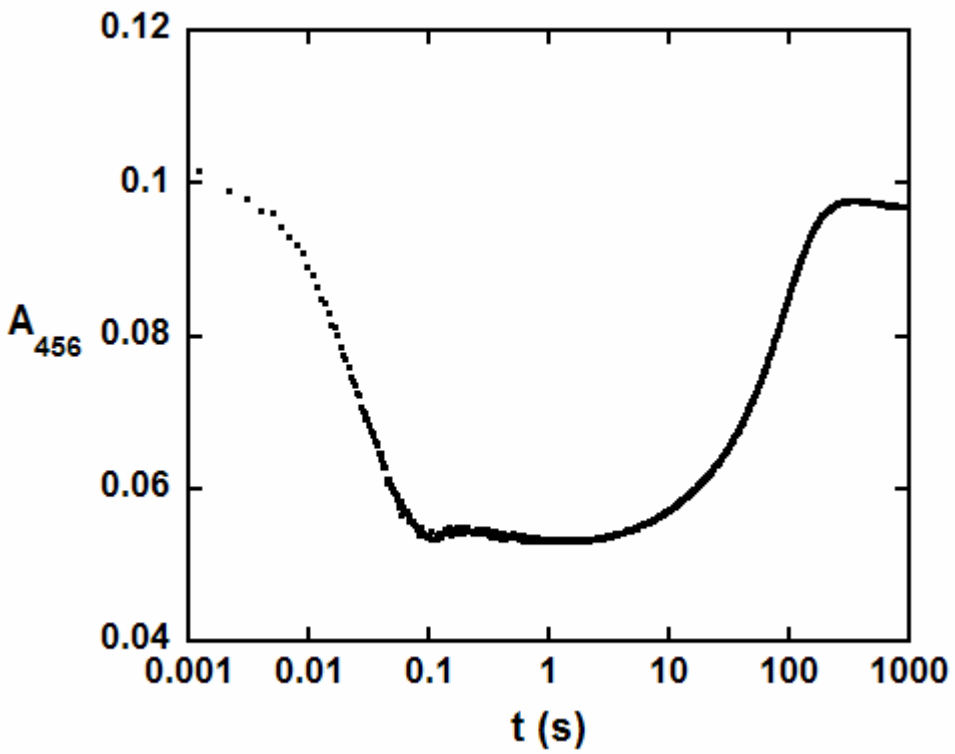

Figure 4.19: Enzyme-Monitored Turnover. An enzyme monitored turnover trace at 456 nm with (22 μM) enzyme, 200 μM DHO, and 400 μM fumarate. Under turnover conditions the enzyme only reduces by half instead of becoming fully reduced.

Oxidized enzyme (22 μM) was reacted with 200 μM DHO, and 400 μM fumarate. The rate constants for the individual half-reactions suggest that under turnover conditions the enzyme should become fully reduced. Under turnover conditions, however, the enzyme only reduces by half.

Discussion

The catalytic cycle of the Class 1A DHOD from *E. faecalis* proceeds through an oxidative and reductive half-reaction (Figure 4.20). The enzymes binds DHO in less than 1 ms. The substrate then reduced the enzymes with a rate constant of 53 s^{-1}. After reduction is complete the product of the half-reaction (orotate) leaves at a rate of 16 s^{-1}, yielding unbound reduced enzyme. The reduced enzyme is then binds to fumarate and with a rate constant of 5 s^{-1}. The product succinate is then released completing the catalytic cycle.

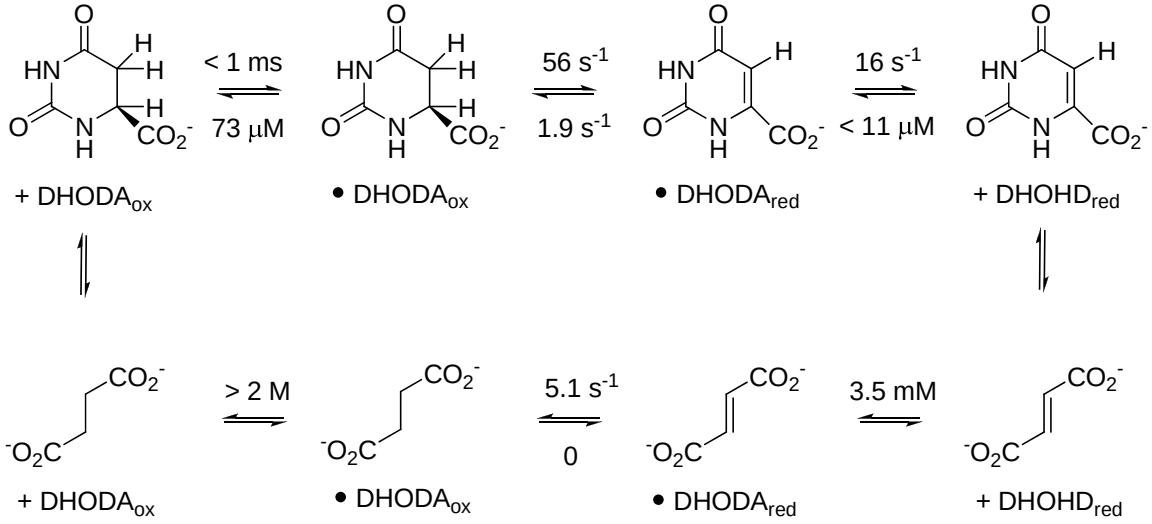

Figure 4.20: Catalytic Scheme of *E. faecalis* DHOD.

Comparing the rate constants for the enzyme one sees that reduction of the flavin by DHO (53 s^{-1}) occurs approximately 10 times faster than oxidation by fumarate (5 s^{-1}) at pH 8.5, 4^{o} C. Though orotate binds relatively tightly to the reduced and oxidized forms, its dissociation from the reduced enzyme is quite fast at 16 s^{-1}. Succinate binding on the

other hand is very weak, >2 M, suggesting that its release is also fast. These results suggest that the rate-limiting step for turnover is fumarate oxidation.

The enzyme k_{cat} (1.6 s^{-1}) is slower than any of the measured rate constants. The enzyme concentration, being calculated by active sites, rather than by the concentration of the dimmer, may therefore be in error. If the enzyme does indeed follow a true half-sites reactivity model, only one of the two active sites would be active at any moment. This would, in effect, decrease the enzyme concentration by half. Doubling k_{cat} to compensate for this change in activity would give a k_{cat} of 3.2 s^{-1}, corresponding with the rate constant for fumarate reduction.

The half-sites-reactivity observed in this enzyme is similar to that reported for the *L. lactis* enzyme (8). Only half of the enzyme is reduced by DHO, regardless of the concentration. In contrast, the unnatural reductant dithionite fully reduces the flavin. The reverse reactions, using orotate or oxonate as oxidants, also show half-sites reactivity, whereas oxidants such as oxygen lead to a fully oxidized enzyme (Figure 4.9). The stoichiometry of binding of orotate to the oxidized enzyme also indicates only half of the dimer is capable of binding orotate.

The structure of the enzyme shows the presence of only one substrate binding pocket, suggesting a Ping-Pong Bi-Bi mechanism. However, the steady-state data obtained using fumarate indicates an ordered sequential mechanism, requiring a reversible step between DHO binding and fumarate binding. One potential explanation is that the active site converts from a DHO-competent site to a fumarate-competent site after each turnover (Figure 4.21). In this model the ligands would induce the changes which convert the monomers into either fumarate or DHO binding sites.

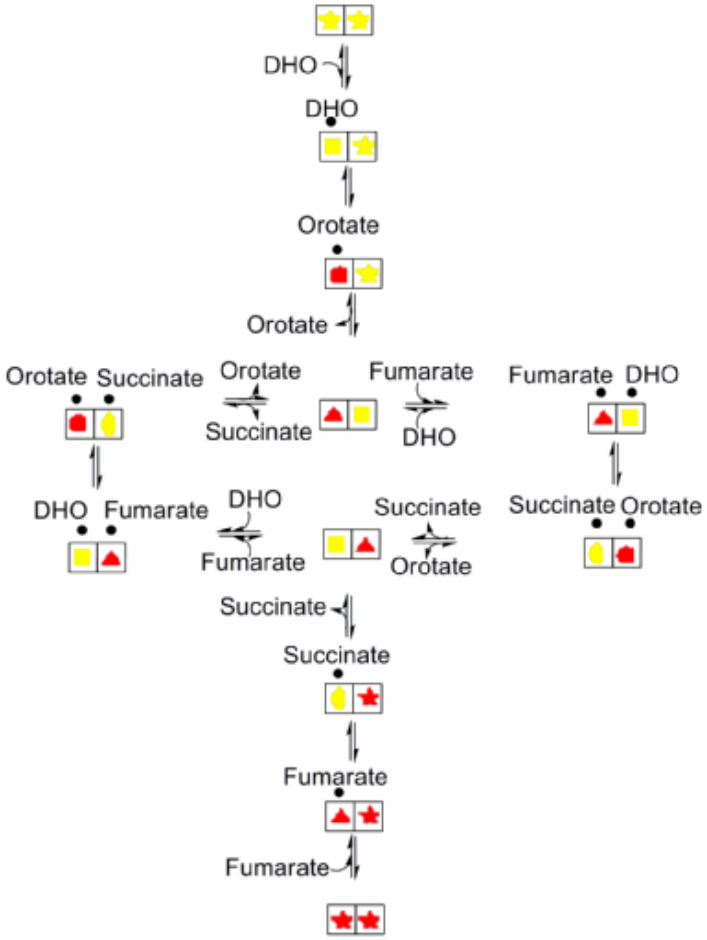

Figure 4.21: Ligand Induced Half-Sites Reactivity Scheme. This mechanistic scheme depicts a potential catalytic cycle in which the enzyme starts in a fully oxidized or reduced form without ligands (stars), and is converted into an enzyme in which one monomer is competent for fumarate (triangles) and one monomer is competent for DHO (squares). The enzyme proceeds through conformations bound to the products succinate (diamonds) and orotate (circles). During this cycle the monomers go from oxidized (yellow) to reduced forms (red).

Another possible model is that active sites are natively different due to the interaction of the monomers themselves, a preexisting asymmetry. In this model the ligands are not the effectors which cause the half-site reactivity. In this model the flavin molecules would have to transfer electrons from the DHO binding site to the fumarate binding site in order for reduction of fumarate to occur (Figure 4.22). This model seems unlikely as there is no other discernable difference between the free enzyme's monomers.

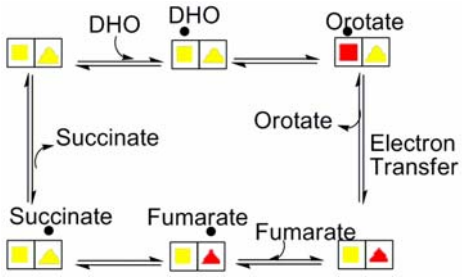

Figure 4.22: Preexisting Asymmetry Half-Site Reactivity Scheme. This mechanistic scheme starts with a preexisting asymmetry in which one monomer of the enzyme is competent for DHO (squares) and one competent for fumarate (triangles). The enzyme proceeds through both oxidized (yellow) and reduced (red) forms. The electrons are passed from the DHO reactive site to the fumrate reactive site which is then reoxidized by fumarate.

Because the rate constant of flavin reduction by DHO is 56 s^{-1} and the rate constant for oxidation by fumrate is 5 s^{-1}, the enzyme should remain in a primarily reduced form. If the enzyme functions using half-sites reactivity, then the enzyme would remain only half reduced during turnover. The latter is seen in enzyme monitored turnover experiments, thus leading to the idea of a homodimer with two functionally non-equivalent halves. Otherwise the enzyme should become almost fully reduced during turnover, which was not seen.

pH Dependence

The pH dependence of flavin reduction indicates that a group with a pK_a of 8.3, consistent with a cysteine as a base. Cys 141 is predicted from the structure (Chapter 5) to be this critical base. The rate constant of fumarate reduction decreases with a pK_a of 7.1. This differnce in pK_a could be caused by the ligands. Both ligands, DHO and fumarate, would be in close proximity to the active site cysteine. Unlike DHO fumarate

would likely bring in a second nearby negative charge with its other carboxylate. This however should increase, not decrease the pK_a of the cysteine.

The pH dependence of the binding of orotate, DHO, and fumarate indicate that there is a pK_a above 12 which affects ligand binding to the enzyme. The difference in these substrates strengthens the argument that this is an enzyme-related pK_a and not a substrate pK_a, since fumarate has pK_a values of 3.5 and 4.0 for its carboxylates, far away from 12. As the pH increases, the affinities for all these ligands decrease. The most likely candidate for the pK_a controlling binding is Lys 55 which is near the N5 of the flavin and hydrogen-bonds to the carboxylates of the ligands.

Ligand Binding

The reduction potential of the flavin of the free enzyme is -262 mV, essentially the same as the midpoint potential of the dihydororotate/orotate couple (-258 mV). However, the extent of reduction was not sensitive to DHO concentrations above 10 μM, suggesting that DHO binding may change the potential of the flavin.

This change in redox state of the flavin seems to cause changes in the active site in both oxidized and reduced forms. Large differences are seen in the binding of ligands to the oxidized and reduced forms of the enzyme. The K_D of fumarate changes from 3.5 mM when binding to the reduced enzyme to 95 mM for the oxidized enzyme. This difference also occurs for DHO, with a K_D of 73 μM to the oxidized enzyme and a K_D of 3 mM to the reduced form (Table 4.1). Though obvious changes in binding affinity are seen, few changes, if any, are seen in crystal structures when comparing oxidized and reduced enzymes.

Table 4.1 Ligand Binding to *E. faecalis*

Ligand	$K_{D\ ox}$	$K_{D\ red}$
3,5-diHOB	45 ± 5 μM	N. D.
3,4-diHOB	260 ± 25 μM	N. D.
Orotate	151 ± 32 μM	< 11 μM
DHO	73 ± 7 μM	4.1 ± 0.5 mM
Fumarate	95 ±8 mM	3.5 ± 0.2 mM
Succinate	> 1 M	N. D.
Oxonate	N. D.	4.2 ± 0.4 mM

In a previous study of this enzyme the authors reported that menadione was a substrate for the enzyme (3). They predicted a menadione binding site, perhaps distinct from the pyrimidine binding site. There was no observed saturation for the rate constant for the reaction with menadione (Table 4.2). The crystal structure of the enzyme also shows no secondary site for the enzyme to bind menadione (Chapter 5).

Table 4.2 Rate Constants for Oxidants of *E. faecalis*

Oxidant	Rate Constant
Fumarate	$5.1 \pm 0.7\ s^{-1}$
Orotate	$1.9 \pm 0.04\ s^{-1}$
Oxonate	$3.6 \pm 0.1\ s^{-1}$
Menadione	$9 \times 10^4 \pm 3 \times 10^3\ M^{-1}s^{-1}$

The lack of a menadione binding to the enzyme, and the absence of a secondary site for it to bind to indicates that it is unlikely that menadione is the physiological substrate. Most likely the enzyme utilizes fumarate as its physiological substrate.

The previously reported inhibitors 3,4-DHB and 3,5-DHB also bind to this enzyme with relatively high affinities (9). Though the product orotate has a lower K_D than these compounds, both bind to the oxidized enzyme with affinities similar to those of DHO, with 3,5-DHB having a slightly higher affinity than DHO.

Conclusions

A number of details about the function of this enzyme have come out through its characterization. Contrary to previous reports, there is no observable binding for menadione to the enzyme, making quinones unlikely physiological substrates of the enzyme. This indicates fumarate is the much more likely substrate of the enzyme. From the transient state kinetic data we can conclude that the rate limiting step in the catalytic cycle is the oxidation of the enzyme by fumarate.

The pH dependence of the enzyme also allowed us to understand more about how the enzyme functions. The rate constants for the oxidation and reduction of the enzyme show a pKa indicative of a cysteine residue. The shift in this pK_a between the oxidative and reductive half-reactions also indicates that the substrates affect this pK_a. The effect of pH on ligand binding indicated a second pK_a corresponding to a potential active site lysine.

During catalysis a strong negative cooperativity is observed. This half-sites-reactivity has also been observed in the *L. lactis* Class 1A enzyme (8). This effect seems to be related to substrate binding to the enzyme, and not simply due to the redox state of the flavin. Though large changes in ligand binding occur between the oxidized and reduced forms, this effect is also seen in orotate binding to the oxidized enzyme, indicating substrate binding may be a controlling factor. In the next chapter we will look at this half-sites reactivity through both multidimensional NMR and x-ray crystallography in an attempt to understand how this asymmetry is imposed.

References

1. Pinheiro, M.P., Iulek, J., Nonato, M.C., "Crystal structure of *Trypanosoma cruzi* dihydroorotate dehydrogenase from Y strain" (2008) *Biochem. Biophys. Res. Comm.*, 369, 812-817

2. Feliciano, P.R., Cordeiro, A.T., Costa-Filho, A.J., Nonato, M.C., "Crystallization and preliminary X-ray diffraction analysis of *Leishmania major* dihydroorotate dehydrogenase " (2006) *Prot. Exp. and Purif.*, 48, 98-103

3. Marcinkeviciene, J., Jiang W., Locke, G., Kopcho, L. M., Rogers, M. J., Copeland, R.A."A Second Dihydroorotate Dehydrogenase (Type A) of the Human Pathogen *Enterococcus faecalis:* Expression, Purification, and Steady-State Kinetic Mechanism" (2000) *Arch. Biochem. Biophys*., 377, 178-186

4. Nørager, S., Arent, S., Björnberg, O., Ottosen, M. B., Leggio, L.L., Jensen, K. F., Larsen, S., "Lactococcus lactis dihydroorotate dehydrogenase A mutants reveal important facets of the enzymatic function" (2003) *J. Biol. Chem.,* 278, 28812-28822

5. Rowland, P., Nielsen, F.S., Jensen, K.F., Larsen, S., "The crystal structure of the flavin containing enzyme dihydroorotate dehydrogenase A from *Lactococcus lactis*" (1997) *Structure* 15:239-252

6. Ottosen, M. B., Björnberg, O., Nørager, S., Larsen, S., Palfey, B. A., and Jensen, K. F. "The dimeric dihydroorotate dehydrogenase A from *Lactococcus lactis* dissociates reversibly into inactive monomers" (2002) *Prot. Sci.*, 11:2575-2583

7. Massey, V., "A Simple Method for the Determination of Redox Potentials." (1991) In: Flavins and Flavoproteins, edited by Curti B., Ronichi S., and Zanetti G., Berlin: Walter de Gruyter, pp. 59-66

8. Shi, J., Dertouzos, J., Gafni, A., Steel, D., and Palfey, B. A. "Single-molecule kinetics reveals signatures of half-sites reactivity in dihydroorotate dehydrogenase A catalysis" (2006) *Proc. Nat. Acad. Sci.* U.S.A., 103:5775-5780

9. Wolfe, A.E., Thymark, M., Gattis, S.G., Fagan, R.L., Hu, Y., Johansson, E., Arent, S., Larsen, S., Palfey, B.A., "The Interaction of Benzoate Pyrimidine Analogs with the Class 1A Dihydroorotate Dehydrogenase from *Lactococcus lactis*" (2007) *Biochemistry*, 46:5741-5753

Chapter 5

Dynamics and Structure of the Class 1A Dihydroorotate Dehydrogenase from *Enterococcus faecalis*

Introduction

Dihydroorotate dehydrogenases (DHODs) catalyze the oxidation of (S)-dihydroorotate to orotate, one of the critical reactions in the de novo biosynthesis of pyrimidines. The Class 1A DHOD from *Enterococcus faecalis* is a homodimer composed of two polypeptide chains each containing a bound FMN cofactor. Comparison of the sequence of this enzyme the Class 1A DHOD from *Lactococcus lactis* shows 68% identity.

The Class 1A DHOD from *L. lactis* has half-sites reactivity (1). Also, the dissociation of the homodimer into monomers causes inactivation (2), indicating the importance of interactions between the two monomers. Furthermore, single-molecule studies have shown that there are two major populations of enzyme, which react either from the fully reduced state to the half-oxidized state, or from the fully-oxidized state to the half-oxidized state (1). The simplest mechanism compatible with the single-molecule studies indicates that the two subunits interconvert between active and inactive states.

Studies onthe *E. faecalis* enzyme have also shown evidence for half-sites reactivity. When the fully reduced enzyme is oxidized by fumarate or fully oxidized

enzyme is reduced by dihydroorotate (DHO), reactions only go to 50 percent completion (Figure 5.1). The reverse reaction - orotate with reduced enzyme to form DHO and oxidized enzyme - also shows half-sites reactivity.

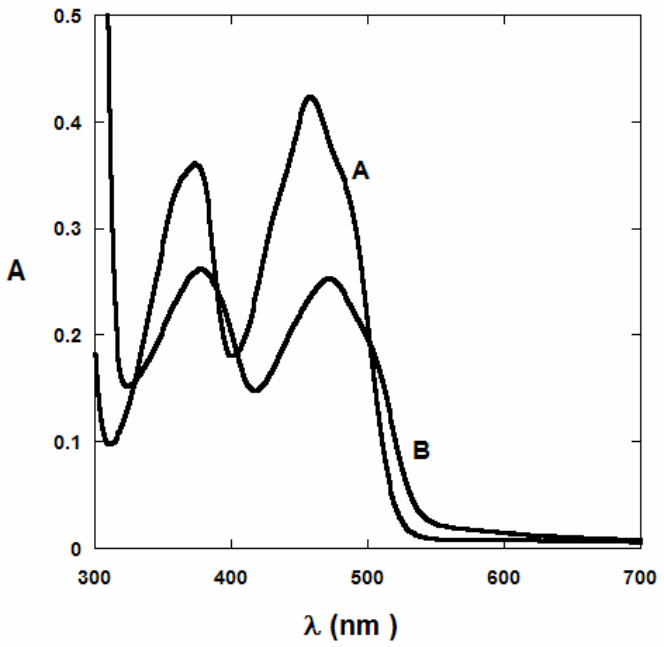

Figure 5.1: Half-Sites-Reactive of *E. faecalis* DHOD. A: Absorbance spectrum of 42 μM fully oxidized DHOD from *E. faecalis* in 100 mM TRIS, pH 8.5. B: Absorbance spectrum of 42 μM anaerobic enzyme in 100 mM TRIS, pH 8.5 after reaction with 10 mM DHO. Note only half of the absorbance at 456 disappears, indicating only partial reduction of the enzyme. A similar spectrum is seen upon oxidation of reduced enzyme with fumarate.

Under turnover conditions it is also seen that the enzyme only reduces halfway even with saturating DHO. In contrast, chemical reductants such as dithionite completely reduce the oxidized enzyme, and chemical oxidants such as DCIP completely oxidize reduced enzyme. These results clearly indicate that the half-sites reactivity is dependent on the type of substrate used.

Though half-sites reactivity seems to be common in Class 1A DHODs, its mechanism is not understood. The enzyme is a homodimer, suggesting that asymmetry is imposed either by the binding of the monomers to one another, or by interactions with the

substrates or ligands. The preexisting asymmetry model, in which the homodimers impose asymmetry on one another through their interactions, or the ligand-induced asymmetry model, where binding of substrates or products induce asymmetry, are both compatible with the current data. Previous crystal structures of the *L. lactis* enzyme have shed little light on this asymmetry, with the exception of a structure of a mutant enzyme which shows differences between the active site loops of the two monomers (3).

In order to better understand the origin of this asymmetry, crystal structures were solved with, L-malate, 3,4-dihydroxybenzoate, 3,5-dihydroxybenzoate, orotate, and dihydroorotate bound. NMR studies were also carried out in order to understand the dynamics of the enzyme. Obtaining chemical shifts for residues in both the free enzyme and enzyme-product complex in solution was undertaken to identify the residues causing asymmetry. If there is pre-existing asymmetry, the free enzyme will show two sets of shifts for the residues involved. If the asymmetry is ligand-induced, resonances should split into two peaks for those residues of the protein affected by ligand binding. [^{1}H,^{15}N]-TROSY experiments on the enzyme in the presence and absence of the ligands 3,4-dihydroxybenzoate, 3,5-dihydroxybenzoate, and orotate show large conformational effects on the tertiary structure of the enzyme upon ligand binding. Through the combination of 3D [^{1}H,^{15}N,^{13}C] HNCO, HN(CO)CA, HN(CA)CB, and specifically labeled [^{1}H,^{15}N]-TROSY spectra, the resonances of the ligand-free enzyme have been partially assigned, illuminating a generally static core of residues.

Materials and Methods

Expression of the Class 1A *Enterococcus faecalis* DHOD

BL21 DE3 cells were transformed by heat shock with the plasmid expressing the Class 1A *E. faecalis* DHOD (Chapter 4) and plated on LB-kanamycin plates. Single colonies were picked to inoculate overnight cultures of 5 mL LB, and 1 mL of this culture was added to 1 L LB media. The cells were gown to an OD of 0.6 at 600 nm and induced using 1 mM IPTG (final concentration) and grown for 24 hours at 37^{o} C.

Expression of ^{15}N-labeled Class 1A *Enterococcus faecalis* DHOD

For production of ^{15}N-labeled enzyme, 1 mL of an overnight culture was added to 1 L of ^{15}N ammonium chloride-substituted M9 minimal medium . The cells were gown to an OD of 0.6 at 600 nm, induced using 1 mM IPTG (final concentration), and grown for 24 hours at 37^{o} C.

Expression of ^{15}N, ^{13}C, ^{2}H *Enterococcus faecalis* DHOD

BL21 DE3 cells were transformed by heat shock using the plasmid expressing the Class 1A *E. faecalis* DHOD and plated on M9 minimal media kanamycin plates made with D_2O in place of H_2O and grown overnight at 37^{o} C. Colonies were streaked onto these M9 minimal media for 3 subsequent times to allow colonies to adapt to growth in deuterium. After 3 days of restreaking, single colonies were picked and used to inoculate 5 mL overnight cultures of M9 minimal medium containing ^{15}N ammonium chloride, D_2O, and ^{13}C-d-glucose; 1 mL of this culture was added to 1 L of M9 minimal medium containing ^{15}N ammonium chloride, D_2O, and ^{13}C-d-glucose. The cells were gown to an

OD of 0.6 at 600 nm and induced using 1 mM IPTG (final concentration) and grown for 48 hours at 37^{o} C.

^{15}N Valine and ^{15}N Leucine Labeled Protein

Proteins selectively labeled with ^{15}N at the amide nitrogen of leucine and valine residues were obtained by expressing the protein in the auxotrophic strain DL39avtA/DE3. Single colonies were picked and grown overnight in 5 mL LB, and 1 mL of this culture was added to a rich media. The media was made from 950 mL of H_2O containing the amino acids in the following amounts; 500 mg alanine, 400 mg arginine, 400 mg aspartate, 50 mg cysteine, 400 mg glutamine, 650 mg glutamate, 550 mg glycine, 100 mg histidine, 230 mg isoleucine, 420 mg leucine, 420 mg lysine, 250 mg methionine, 130 mg phenylalanine, 100 mg proline, 2100 mg serine, 230 mg threonine, and 170 mg tyrosine. Nucleotides were added in the amounts of 500 mg adenine, 650 mg guanosine, 200 mg thymine, 500 mg uracil, and 200 mg cytosine. Additional carbon sources beyond glucose were added consisting of 1500 mg sodium acetate (anhydrous), and 1500 mg succinate. The nitrogen source consisted of 750 mg ammonium chloride. The media was buffer with 850 mg sodium hydroxide, and 10,500 mg of dibasic potassium phosphate yielding a final pH of approximately 7.4. The final solution was sterilized by autoclaving, mixed with 10 mL of a second, filtered-sterilized solution containing the micronutrients 2 mg calcium chloride, 2 mg zinc sulfate, 2 mg manganese sulfate, 50 mg l-tryptophan, 50 mg thiamine, 50 mg niacin, and 0.75 mg biotin. The selectable antibiotic kanamycin was used at a concentration of 0.5g/mL. Finally 50 mL of 40% glucose, 4 mL 1M magnesium sulfate, and 1 mL of 0.01 M iron(III) chloride were added. For either the leucine or valine

labeled protein, the corresponding amino acid in the media was replaced with the same amount of ^{15}N-labeled amino acid. The cells were grown to an OD of 0.6 at 600 nm and induced using 1 mM IPTG (final concentration) and grown for 24 hours at 37^{o} C.

Purification of *Enterococcus faecalis* DHOD

The DHOD-containing cells were pelleted by centrifugation (16,000 x g for 20 minutes) and resuspended in 100 mM Bis-Tris pH 6.5 buffers. The cells were then sonicated for 15 minutes on ice. Cell debris was removed by centrifugation (20,000 x g for 20 minutes) at 4^{o}C. Solid ammonium sulfate was added to 50% saturation, and the precipitated proteins were removed by centrifugation (16,000 x g for 20 minutes) at 4 ^{o}C. The supernatant was dialyzed against 2 L 100 mM Bis-Tris pH 6.5 at 4^{o} C. The dialyzed protein was then applied to a DEAE sepharose column 25^{o} C (70 mL equilibrated in 100 mM Bis-Tris pH 6.5). The column was washed extensively with 100 mM Bis-Tris pH 6.5, 100 mM NaCl. The protein was then eluted with 100 mM Bis-Tris pH 6.5, 250 mM NaCl and fractions were collected. Fractions containing the protein were identified by their yellow color. Enzyme fractions were then pooled, concentrated, and dialyzed against 100 mM Bis-Tris pH 6.5 and precipitated with 0.472 g/mL ammonium sulfate and stored at 4^{o} C. Single bands of approximately 35 kDa were seen on an SDS PAGE (12%) using Coomassie Blue staining, indicating that the enzyme was greater than 95% pure. Enzyme concentrations for these proteins were determined as outlined in chapter 4.

Protein Crystallization and Data Collection

Protein crystals were grown within 3-4 days at 4^{o} C via sitting drop vapor diffusion with equal volumes of protein [6 μL, 30 mg/mL DHODA, 1 mM KPi, pH 7.0] and reservoir [6 μL, 2.5 M L-malate, pH 7.7] over 0.5 mL of the reservoir solution. Crystals were transferred to solutions of 2.5 M L-malate, pH 7.7, containing either 10 mM orotate, 5 mM 3,4-dihydroxybenzoate, or 5 mM 3,5-dihydroxybenzoate. Crystals containing dihydroorotate were soaked with a 10 mM solution of dihydroorotate made anaerobic by bubbling with argon. The crystals were all soaked for approximately 30 minutes with ligands and then flash-frozen in liquid nitrogen. Diffraction data were collected at the APS LS/CAT beam line using 0.9785 Å radiation and recorded on a marCCD 165 detector. All crystals belonged to the H32 space group.

Crystal Structure Determination and Refinement

Crystallographic data sets were indexed, reduced, and processed with HKL 2000. The scaled data were converted to mtz files using scalepak2mtz in CCP4 (4). The structure was modeled by molecular replacement using a homology model of the *E. faecalis* protein based on the previously determined *L. lactis* DHODA structure in the program Phaser. Refinement was performed with iterative cycles of manual model building in COOT (5) and REFMAC (5-8) with 5% of all data set aside for R_{free} calculation. Quality assessment of the model was preformed with PROCHECK (9), WHATCHECK (10), and SF-CHECK (11) (Table 5.1). Figures were created using Pymol (12).

Table 5.1: Crystal Structure Data and Refinement Statistics

	DHO	35 DHB	34 DHB	OROTATE	L-MALATE
Space Group	H 3 2	H 3 2	H 3 2	H 3 2	H 3 2
Cell dimensions (Å)					
a	98.07	99.154	99.284	100.028	99.21
B	98.07	99.154	99.284	100.028	99.21
c	215.64	215.936	214.389	213.426	213.92
Molecules per Asymmetric Unit	2	2	2	2	2
Wavelength (Å)	0.9785	0.9785	0.9785	0.9785	0.9785
Overall Resolution Limits (Å)	79.06-1.5	22.85-1.4	20.84-2.0	23.44-1.55	22.26-1.6
Number of reflections collected	116825	145983	48560	117453	101889
Number of Unique Reflections	483014	559773	196357	442123	384274
Overall redundancy of Data	3.9	4.1	7.2	7.5	3.8
Overall completeness of data (last shell)	99.13 (93.4)	98.56 (97.4)	96.28 (89.8)	98.3 (88.9)	97.6 (95.6)
Overall R_{sym} (last shell)	0.029 (0.312)	0.037 (0.416)	0.037(0.265)	0.033(0.178)	0.042 (0.057)
Overall I/_(I) (last shell)	17.5 (0.2)	11.5 (2.2)	14.4 (3.3)	9.3(8.1)	15.2 (1.4)
Model Refinement					
Model Total Number of atoms	5560	5756	5047	5603	5586
Number of water molecules	747	983	153	903	994
Crystal Solvent content					
Refinement Resolution Limits (Å)	79.06-1.5	22.85-1.4	20.84-2.0	23.44-1.55	22.26-1.6
Number of reflections used	109735	117453	48372	106356	96775
Completeness	99.13	98.6	96.2	96.9	97.6
R-factor for all reflections	0.17075	0.19301	0.18303	0.1787	0.184
$R_{working}$	0.16947	0.19189	0.18095	0.1775	0.183
R_{free}	0.19428	0.2145	0.22217	0.1999	0.209
Validation					
Phi-Psi in most favored region	94	94	93.4	94	93.6
Phi-Psi in allowed region	6	6	6.6	6	6.4
Phi-Psi in generously allowed region	0	0	0	0	0
Phi-Psi in disallowed region	0	0	0	0	0
RMSD from ideal bond length	0.014	0.014	0.13	0.014	0.015
RMSD from ideal bond length	1.4	1.4	1.4	1.4	1.5

$R_{sym} = \Sigma|Ii-\langle I\rangle|/\Sigma|Ii|$, for equivalent reflections.
$R_{working} = (\Sigma||Fo|-|Fc||) / \Sigma|Fo|)$, calculated without free reflections.
$R_{free} = (\Sigma||Fo|-|Fc||) / \Sigma|Fo|)$, calculated with free reflections.

NMR Experiments

Samples were prepared by dialyzing the protein in 10 mM potassium phosphate (pH 7.7), 1 mM EDTA, 1 mM TCEP, 1 mM PMSF, and 0.1% Azide. The protein concentration was ~0.3 to 0.5 mM in 95% $^{1}H_2O$ and 5% $^{2}H_2O$. NMR experiments were performed at 303 K on an 800 MHz Varian spectrometer equipped with a [^{1}H, ^{13}C, ^{15}N] cryoprobe with a single-axis pulsed-field gradient capability. [^{1}H, ^{15}N] TROSY spectra were collected on uniformly and specifically labeled enzyme. 3D triple-resonance HNCO, HN(CO)CA, and HNCACB experiments were performed on [^{2}H, ^{13}C, ^{15}N]- uniformly-labeled protein. Data were collected using VnmrJ. FIDs were phased and processed in NmrDraw and converted into *.ucsf files using NMR Pipe (13). The subsequent *.ucsf files were analyzed using Sparky (14).

Results and Discussion

Crystal Structures were determined for the enzyme complexed with orotate, dihydroorotate, 3,4-dihydroxybenzoate, 3,5-dihydroxybenzoate, and L-malate. The models have similar structures consisting of two polypeptide chains and two flavin molecules, consistent with the *L. lactis* enzyme, and the proposed biological unit for class 1A DHODs. In all cases soaked ligands were found bound in both active sites of the protein. Models range in resolution from 1.4 to 2.0 Å with $R_{working}$ values from 0.17 to 0.19 and R_{free} values from 0.19 to 0.22 (Table 5.1).

The active sites of the enzymes are shown in Figures 5.2-5.6. The active site residues shown are asparagines 143, 79, 204, and 138 which surround the binding pocket for the ligands along with the likely active site base, cysteine 141 and lysine 55, which hydrogen bonds to N5 of the isoalloxazine ring system.

One of the major differences in the structures are changes in the loop covering the active site of the enzyme. With 3,5-dihydroxybenzoate, orotate, and L-malate bound, the whole loop was observed. In the dihydroorotate complex, the loop appears more flexible and residues 147 and 148were not observed in the electron density. In the 3,4-dihydroxybenzoate complex, residues 142-148 were not observed. This includes one of the highly conserved active site residues, asparagine 143. The B-factors of this loop are the highest in every structure and, given the resolution of these structures, the loss of density is most likely due to thermal motion.

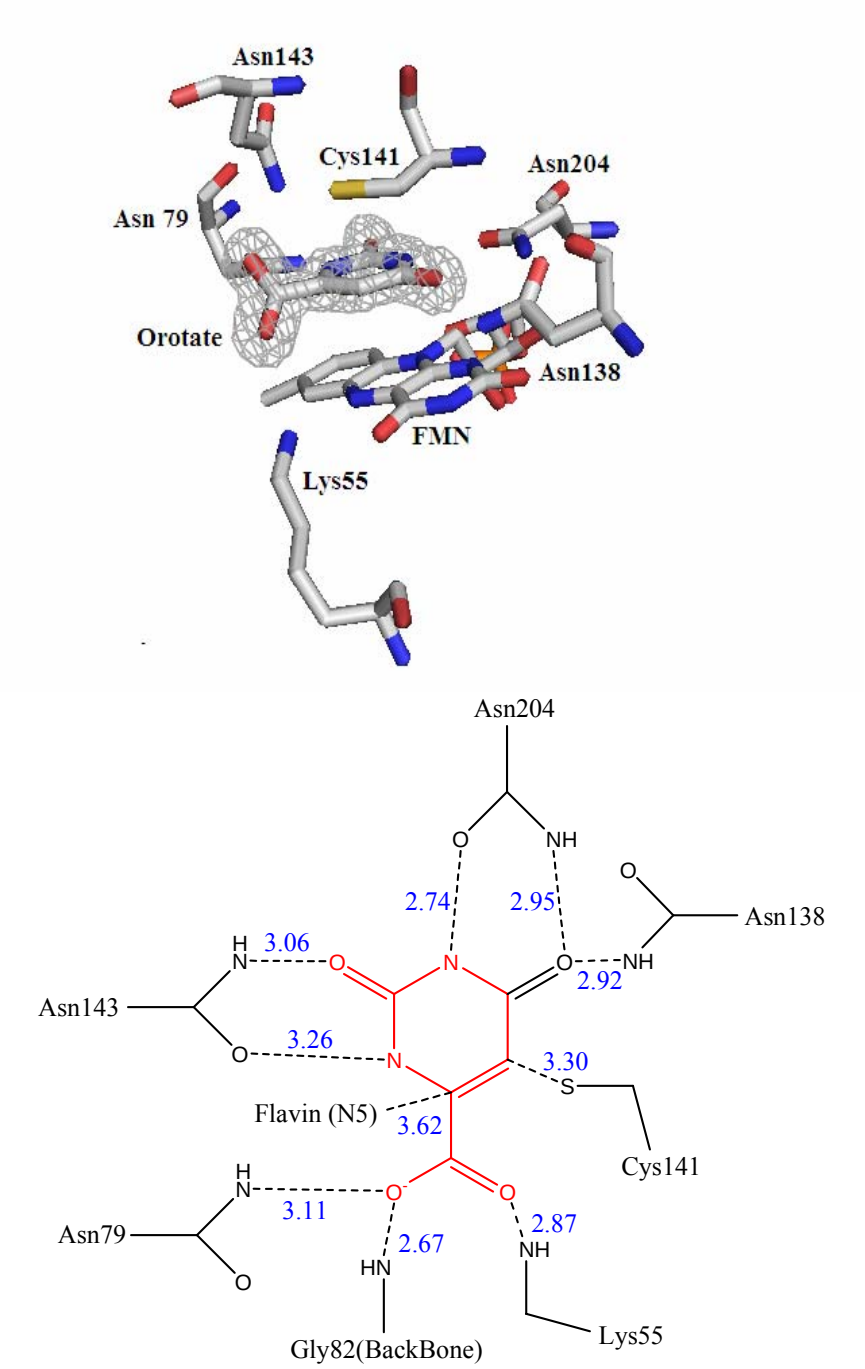

Figure 5.2: Crystal Structure of the *E. faecalis* DHOD with Orotate. The top panel shows the active site residues and FMN prosthetic group with the ligand depicted with its electron density shown in grey. The lower panel shows the distances of the active site residues from the ligand in angstroms.

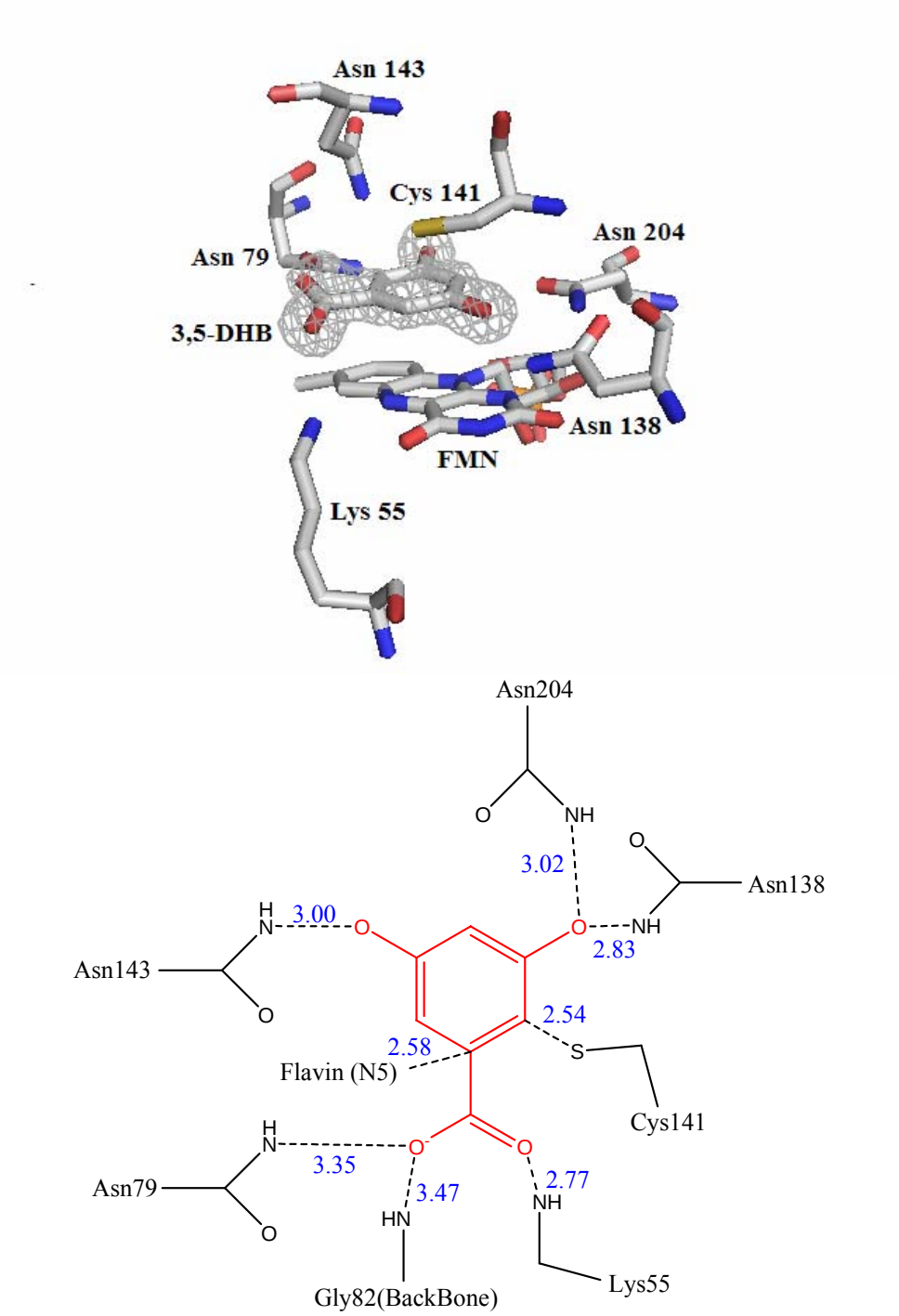

Figure 5.3: Crystal Structure of the *E. faecalis* DHOD with 3,5-Dihydroxybenzoate. The top panel shows the active site residues and FMN prosthetic group with the ligand depicted with its electron density shown in grey. The lower panel shows the distances of the active site residues from the ligand in angstroms.

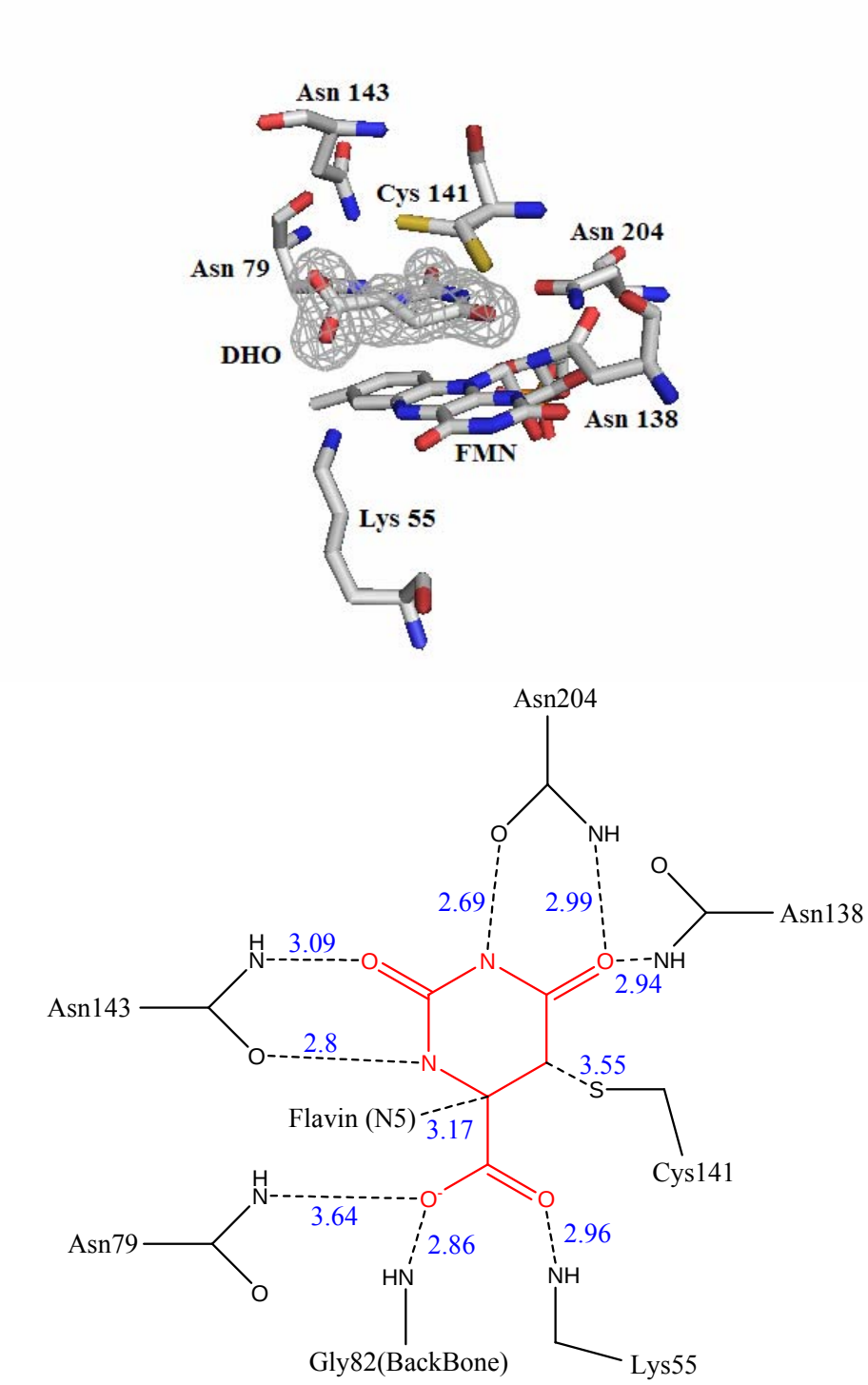

Figure 5.4: Crystal Structure of the *E. faecalis* DHOD with Dihydroorotate. The top panel shows the active site residues and FMN prosthetic group with the ligand depicted with its electron density shown in grey. The lower panel shows the distances of the active site residues from the ligand in angstroms.

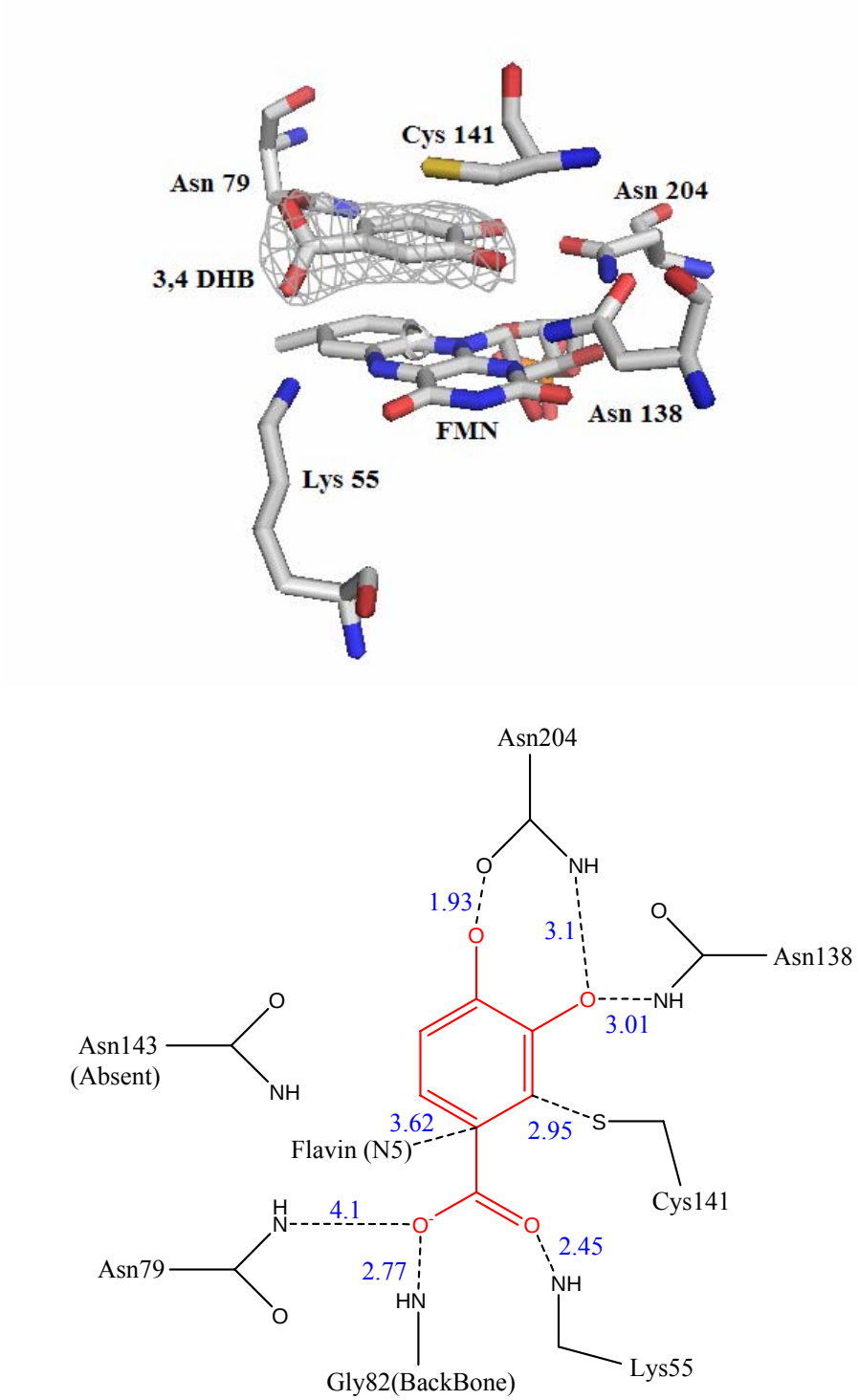

Figure 5.5: Crystal Structure of the *E. faecalis* DHOD with 3,4-Dihydroxybenzoate. The top panel shows the active site residues and FMN prosthetic group with the ligand depicted with its electron density shown in grey. The lower panel shows the distances of the active site residues from the ligand in angstroms.

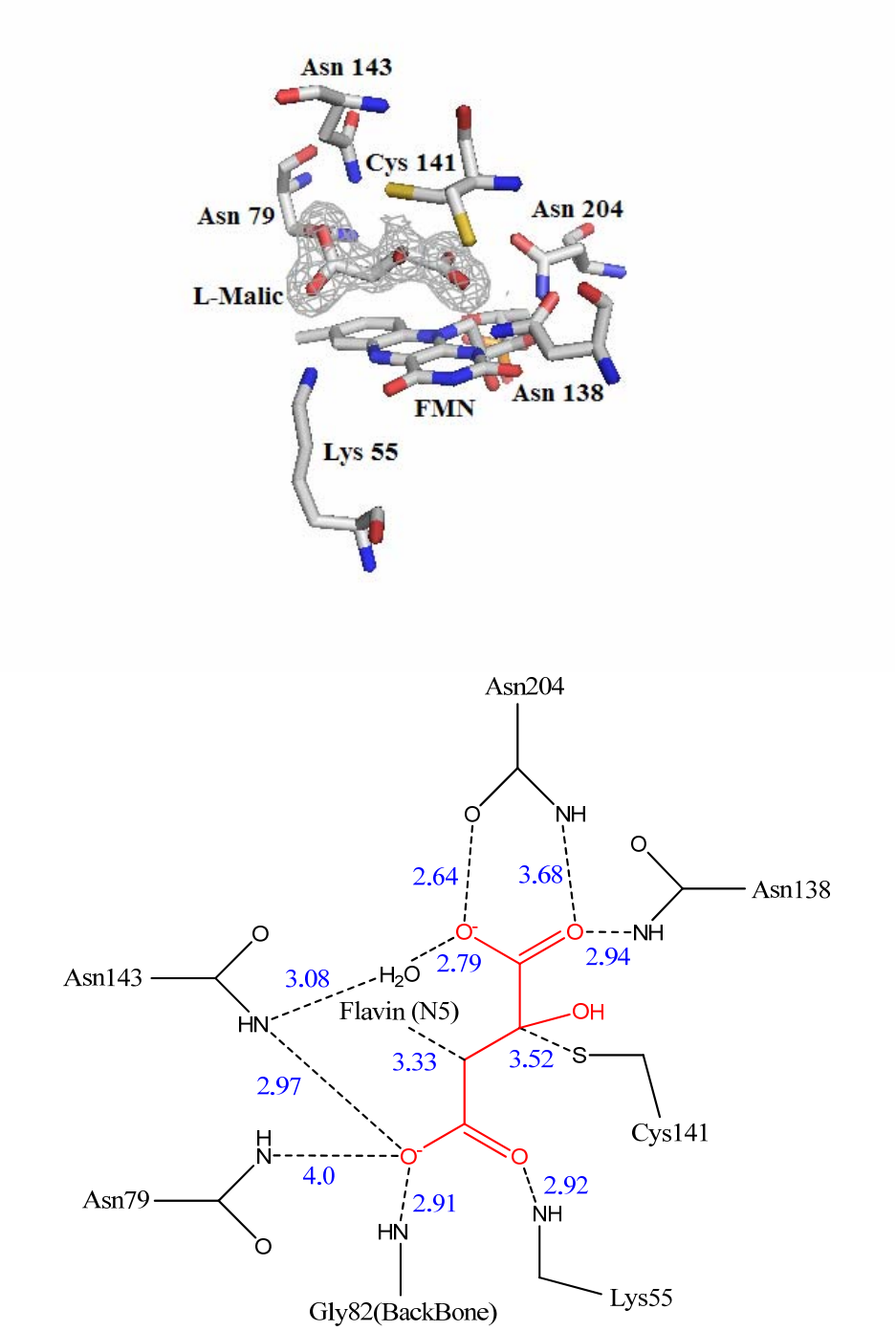

Figure 5.6: Crystal Structure of the *E. faecalis* DHOD with L-Malate The top panel shows the active site residues and FMN prosthetic group with the ligand depicted with its electron density shown in grey. The lower panel shows the distances of the active site residues and their distance from the ligand in angstroms.

The B-factors for most of the complexes show a similar pattern for both molecules of the dimer with high B-values for the loop region in the 60-110 range and lower B factors for the rest of the structure. In the L-malate structure, however, there is a difference in B-factors at the two active sites (Figure 5.7). One active site loop shows far more variation than is seen for the other active site loop. The rmsd difference between the two molecules was calculated using the program Superpose (16). The rmsd is only 0.25 Å between all of the heavy atoms in the structure, a very minor difference between the monomers.

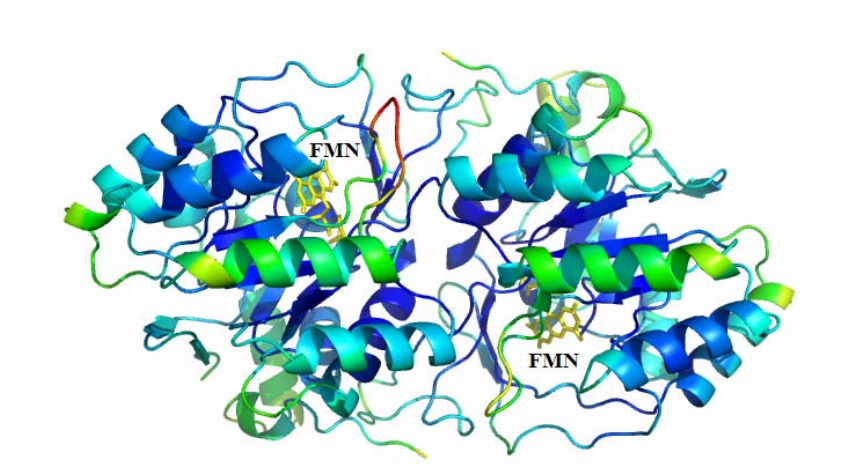

Figure 5.7. Loop Mobility. The crystal structure for the L-malate bound enzyme is shown. B-factors ranging in magnitude from 6 to 139 are shown from blue (lowest) to red (highest). The FMN prosthetic groups are labeled. Note the non-equivalent B factors for the two separate active site loops of each molecule.

This difference could be caused due to either slight changes in the active sites of the enzyme, a perturbation which causes the half-sites reactivity seen in solution, or crystal packing contacts (Figure 5.8). Crystal packing forces seems less likely because this perturbation is not seen in the other crystal structures and all pack in the same fashion in the crystal cell.

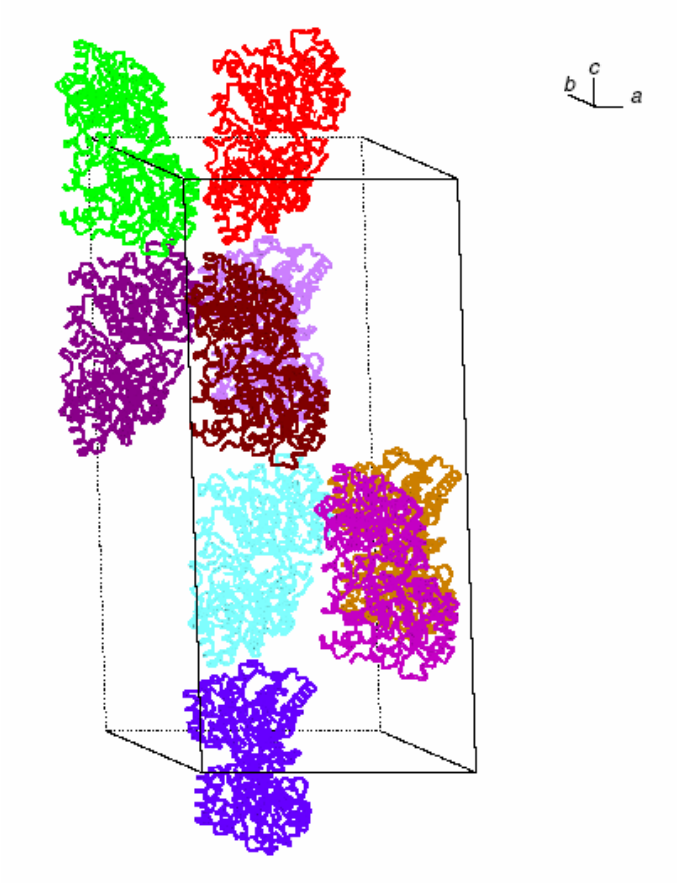

Figure 5.8: Crystal Packing. The crystal packing for the enzyme is depicted. Note that the active site loops are far from any packing contacts. The loops are at the dimer interface and packing contacts are at the ends of the dimer.

Comparison of the L-malate structure and the other 4 structures shows that the enzyme undergoes minor changes in accommodating L-malate in the active site. In this structure the active site cysteine occupies two locations with nearly equal density for both positions. Only one position for cysteine 141 is seen for the majority of structures. However in the L-malate and dihydroorotate-bound structures the cysteine also adopts a conformation in which it is pushed off to the side by ~1.5 Å in what would seem to be an inactive conformation. The dihydroorotate bound enzyme, by virtue of having high concentrations of dihydroorotate present, had its flavin cofactor in a reduced state. This reduction was observable in the macroscopic crystals due to a color change from yellow

to light-red. No change in the flavin cofactor was observed in this dihydroorotate bound complex. The L-malate structure also has a water molecule bound in the active site where the orotate ring would be found. The final difference between this structure and the others is the change in position of asparagine 204. This residue hydrogen bonds to N3 and the C4 carbonyl oxygen of orotate and dihydroorotate. In the L-malate complex the asparagine rotates to hydrogen bond to the carboxylate of L-malate.

Comparison of these crystal structures to the crystal structures for other Class 1A DHODs was performed using DALI and Superpose (15, 16). The *E. feacalis* orotate bound structure showed high similarity to the Class 1A DHODs from *L. lactis*, *P. falciparum*, and *T. cruzi* with root mean square differences of the backbone atoms from 0.75 Å for the *L. lactis* enzyme to 1.54 Å for the *T. cruzi* enzyme. The orotate bound structure also showed similarity to the Class 2 human and *E. coli's* but with rmsd values of 2.3 Å and 2.4 Å, and the *L. lactis* Class 1B enzyme with an rmsd of 2.5 Å for the backbone atoms. An rmsd of < 1.1 Å indicates very high structural alignment of the proteins. Here the *L. lactis* and *P. falciparum* structures show such an agreement, whereas the farther removed structures of the Class 2 and 1B enzymes show a greater difference and therefore less structural homology.

Changes Induced by Ligand Binding

[^{1}H,^{15}N]-TROSY spectra of the enzyme in the presence and absence of the ligands 3,4-dihydroxybenzoate, 3,5-dihydroxybenzoate, and orotate are shown in Figure 5.9. These spectra show large changes in the enzyme upon binding of ligands. A large central mass of signals in the free enzyme becomes more dispersed and forms into sharp

peaks upon binding of all ligands. This is an indication that the majority of these residues are in a state of dynamic motion prior to ligand binding, leading to the amassing of signal near the center of the spectrum.

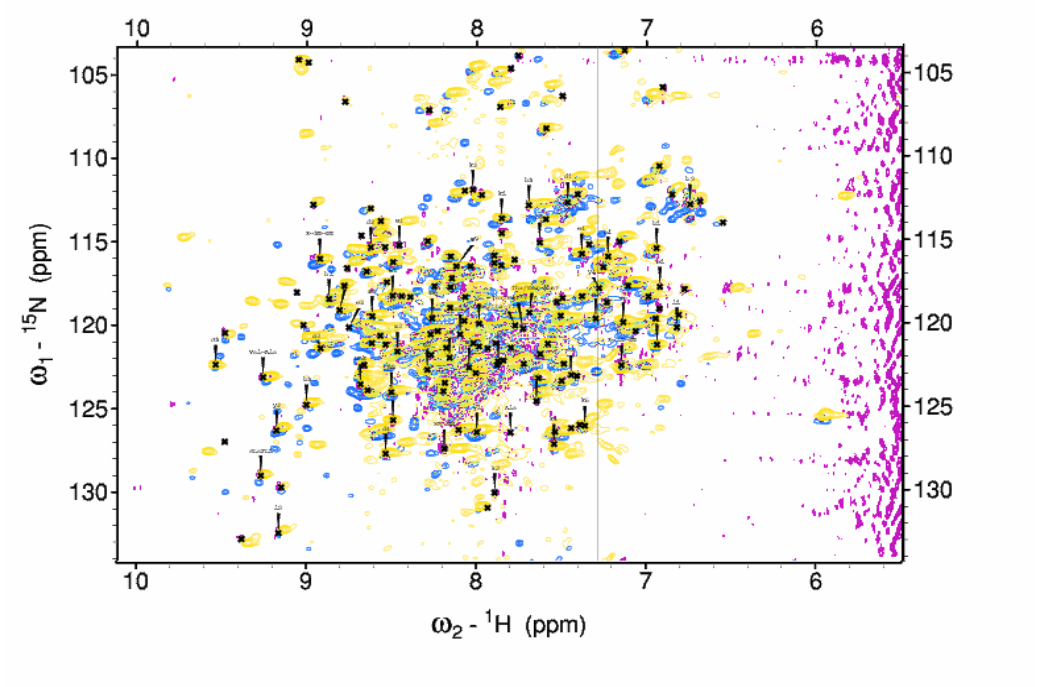

Figure 5.9: Effects of Ligands on *E. faecalis* NMR Resonances. Depicted is the [^{1}H,^{15}N]-TROSY spectra of uniformly labeled DHODA in the absence of ligands (purple), with 3,5-dihydroxybenzoate bound (yellow), with orotate bound (blue), and with 3,4-dihydroxybenzoate bound (green).

Binding of each ligand causes very similar changes in the spectral dispersion of residues indicating similar structures for all of these protein-ligand complexes. The most dispersed spectra are those of the orotate and 3,5-dihydroxybenzoate complexes. The number of discernable peaks increases from ~180 in the ligand-free spectrum to ~400 in the spectrum of the 3,5-dihydroxybenzoate complex. This indicates that a large portion of the free enzyme is dynamic and that the ligand-bound enzyme should provide a better starting structure for assigning resonance of residues. A similar experiment obtaining

[^{1}H,^{15}N]-TROSY spectra of the specifically labeled leucine and valine enzymes in complex with orotate was carried out (Figures 5.10 and 5.11).

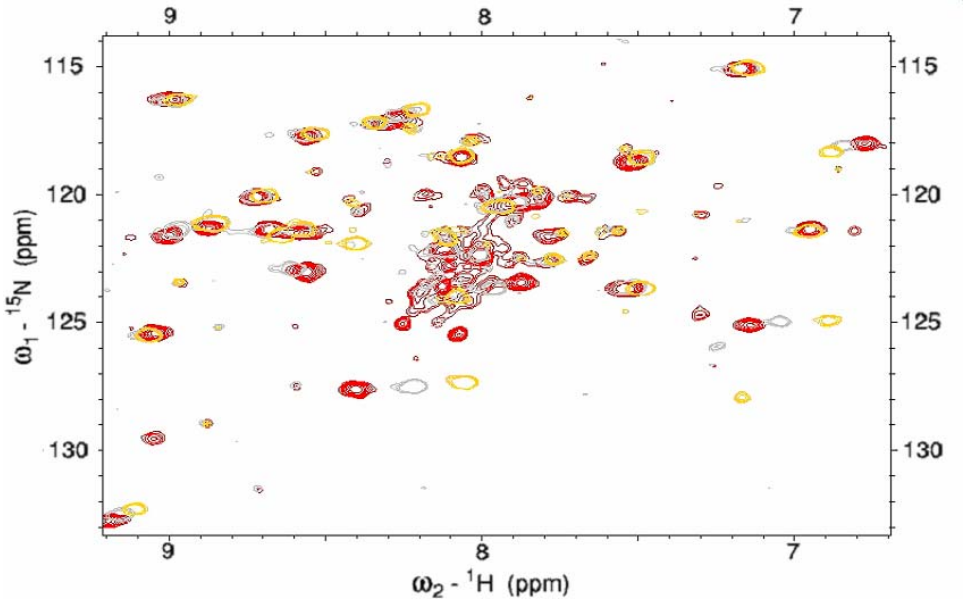

Figure 5.10: Effects of Ligands on Leucine Residues. The [^{1}H,^{15}N]-TROSY spectra of ^{15}N-leucine labeled DHODA with no ligand bound (red), approximately half bound (grey), and fully bound (yellow) is shown. Note the large chemical shifts seen for many of the residues.

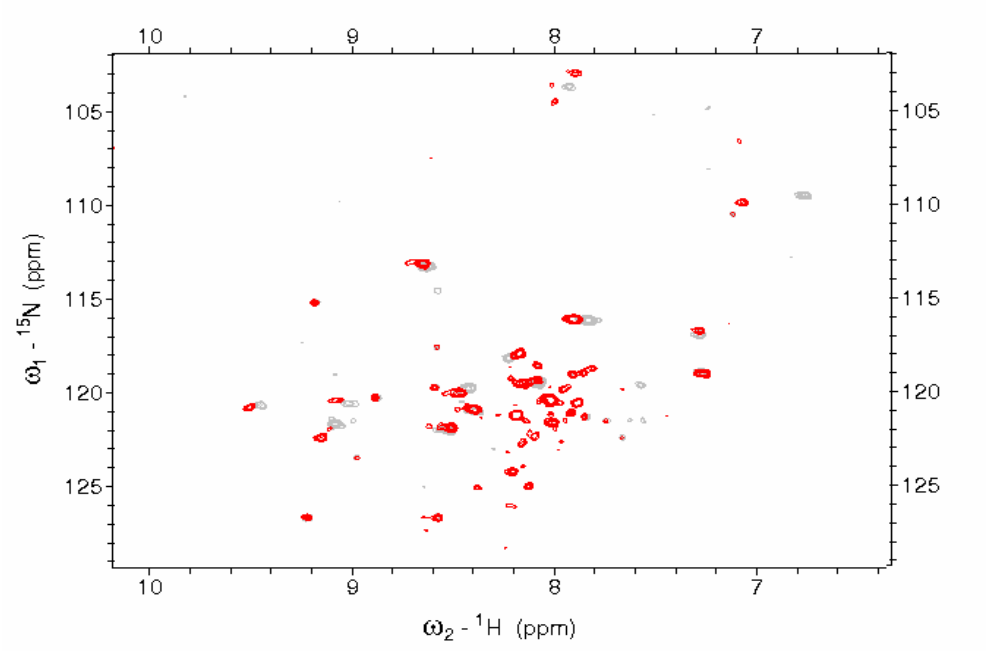

Figure 5.11: Effects of Ligands on Valine Residues. The [^{1}H,^{15}N]-TROSY spectra of ^{15}N-valine labeled DHODA with no ligand bound (red), and bound (grey. Note the large chemical shifts seen for many of the residues.

When the enzyme labeled at leucine residues is titrated with orotate, the 32 peaks, with a visible large mass of signals in the center of the spectrum, disperse into 35 peaks upon orotate binding. There are fewer signals at the center and all peaks become well-resolved. This is consistent with the hypothesis that these residues are in a state of dynamic flux, and therefore are un-resolvable in ligand-free enzyme. It also shows that 13 leucine residues have a change in their chemical environment, indicating potential residue movement upon titration with orotate, indicating a large change in the structure. This is in contrast somewhat with what is seen for the crystal structures of other Class 1A DHODs. Though we do not have a crystal structure of the unbound form of the enzyme, the differences between each ligand-bound form are not so widespread, occurring mainly in the active site loop. Structures of the *L. lactis* enzyme have been determined in the presence and absence of ligands (17,18). Comparisons of these structures show almost no change between the ligand bound forms and the free enzyme.

Peak Assignment

Three dimensional [^{1}H,^{15}N,^{13}C] HNCO, HN(CO)CA, HN(CA)CB, and [^{1}H,^{15}N]-TROSY spectra of the ligand-free enzyme were obtained in order to assign the amino acid residues present in the NMR spectra. The protein consists of two-320-residue polypeptides forming a homodimer of ~70 kDa. Because of the large size and the presence of some dynamic regions which become uninterruptible in the NMR spectra, the resonances were difficult to assign. To assist in the assignment, specifically labeled [^{1}H,^{15}N]-TROSY spectra of the ligand-free enzyme were obtained. Through analysis of

these spectra a partial assignment was made, covering ~15% of the resonances visible in the NMR spectrum (Table 5.2).

Table 5.2: Residues assigned via NMR

Leu 23 – Leu 27
Leu 197 - Val 200
Leu 239 – Ala 240
Leu 278 – Val 279
Ala 294 – Ala 297

These resonances for the residues highlighted in red (Figure 5.12), change little in position from the ligand-free enzyme to the ligand-bound enzyme, indicating that this is a static region of the enzyme. The resonances of the two leucine residues highlighted in green show some change in position, but are far from the most dynamic residues in the structure.

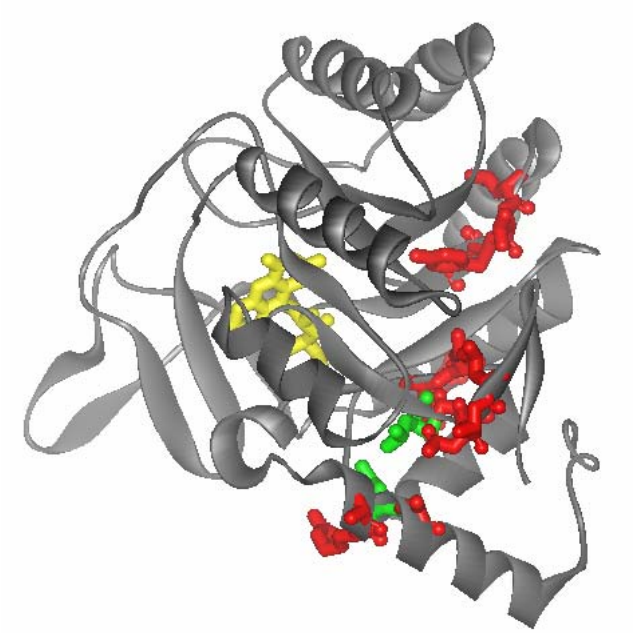

Figure 5.12: Assigned residues mapped onto the *E. faecalis* crystal structure. The assigned residues are shown in stick form on the structure indicating those undergoing chemical shift changes (green) and those remaining static (red).

Both the crystal structure and the NMR data indicate that this enzyme has flexible regions. The NMR data suggest extensive flexibility, but the crystallographic data suggests less flexibility. The areas of rigidity are the same in both methods, showing that at least part of the DHOD structure acts as a static core. The crystal structures indicate that the active site of the enzyme, especially the loop region, has conformational flexibility, but this has not yet been verified by NMR.

Conclusions

The data obtained show that L-malate, pyrimidine and dihydroxybenzoate ligands all hydrogen bond with Asn 204, Asn 79, and Lys 55, as well as the backbone amide of Gly 82. The last three interactions Asn 79, Lys 55, and Gly 82, all interact with the carboxylate of these ligands helping to position the substrates in approximately the same orientation. Both of the pyrimidine-like and fumarate-like ligands are positioned between N5 of the flavin and the active site cysteine. As the pH data from the previous chapter indicated, an ionizable cysteine (Cys 141) residue is in a position to catalyze proton abstraction, and an ionizable lysine (Lys 55) is in a position to bind the carboxylate of both the pyrimidine-like and fumarate-like substrates.

Some evidence for behavior half-sites reactivity is seen in the crystal structure of the enzyme with L-malate bound. There are differences in the B-factors, or dynamic motion of the loop regions of the two monomers. The change in position of Asn 204 is the largest difference seen in this structure, very minor changes are seen in the structure elsewhere. Comparison of the crystallographic data and the NMR data indicate that the crystal structures are far less dynamic than the enzyme is in solution. The NMR data show large changes in the dynamics and structure of many residues in the enzyme upon ligand binding. The NMR assignment and crystallographic data, though indicating changes are induced in the enzyme upon ligand binding, do not elucidate a mechanism for the half-sites reactivity seen in kinetics experiments. Further NMR experiments looking at the oxidized and reduced states of the enzyme, along with further assignment of the forms of the enzyme already examined may lead to better understanding of this asymmetry.

References

1. Shi, J., Dertouzos, J., Gafni, A., Steel, D., and Palfey, B. A. "Single-molecule kinetics reveals signatures of half-sites reactivity in dihydroorotate dehydrogenase A catalysis" (2006) *Proc. Nat. Acad. Sci.* U.S.A., 103:5775-5780

2. Ottosen, M. B., Björnberg, O., Nørager, S., Larsen, S., Palfey, B. A., and Jensen, K. F. "The dimeric dihydroorotate dehydrogenase A from *Lactococcus lactis* dissociates reversibly into inactive monomers" (2002) *Prot. Sci.*, 11:2575-2583

3. Nørager, S., Arent, S., Björnberg, O., Ottosen, M. B., Leggio, L.L., Jensen, K. F., Larsen, S., "*Lactococcus lactis* Dihydroorotate Dehydrogenase A Mutants Reveal Important Facets of the Enzymatic Function" (2003) *J. Biol. Chem.,* 278:28812-28822

4. CCP4. "The CCP4 suite: programs for protein crystallography" (1994) *Acta Cryst.Sect. D –Biol. Cryst.*. 50:760-763.

5. Emsley, P., Cowtan, K., "Coot: Model-Building tools for molecular graphics" (2004) *Acta Cryst. Sect. D – Biol. Crys.,* 60:2126-2132

6. Winn, M.D., Mushudov, G.N., Papiz, M.Z., "Macomolecular TLS refinement in REFMAC at moderate resolutions" (2003) *Meth. Enz.*, 374:300-321

7. B.Howlin, S.A.Butler, D.S.Moss, G.W.Harris and H.P.C.Driessen, "TLSANL: TLS parameter analysis program for segmented anisotropic refinement of macromolecular structures." (1993) *J. Appl. Cryst.*, 26:622-624

8. Perrakis A, Morris R, Lamzin "VS. Automated protein model building combined with iterative structure refinement." (1999) *Nat. Struct. Biol.,* 6:458-463.

9. Laskowski RA, Macarthur MW, Moss DS, Thornton JM. Procheck-a program to check the stereochemical quality of protein structures. (1993) *J. Appl. Cryst.,* 26:283-291.

10. Vriend G. "What if - a molecular modeling and drug design program." (1990) *J. Mol. Graph.,* 8: 52-56.

11. Vaguine AA, Richelle J, Wodak SJ. "SFCHECK: a unified set of procedures for evaluating the quality of macromolecular structure actor data and their agreement with the atomic model." (1999) *Acta Crystr. Sect. D - Biol. Cryst.,* 55:191-205.

12. DeLano WL. "The PyMOL molecular graphics system." (2002) San Carlos, CA: DeLano Scientific

13. Delaglio, F., Grzesiek, S., Vuister, G.W., Zhu, G., Pfeifer, J., Bax, A., "NMRPipe: a multidimensional spectral processing system based on UNIX pipes. (1995) *J. Biomol. NMR.,* 6:277-293

14. T. D. Goddard and D. G. Kneller, SPARKY 3, University of California, San Francisco

15. Holm, L., Kaarianen, S., Rosenstron, P., Schenkel, "Searching Protein Structure Databases with DaliLite v.3" (2008) *Appl., Bioinfor.,* 10:1039-1057

16. Rajarshi M., Gary H. V., Haiyan Z., and David S. W., "SuperPose: a simple server for sophisticated structural superposition" (2004) *Nucleic Acids Res.*; 32 (Web Server issue): W590W594.

17. Rowland, P., Bjornberg, O., Nielsen, F.S., Jensen, K.F., and Larsen, S., "The crystal structure of *Lactococcus lactis* dihydroorotate dehydrogenase A complexed with the enzyme reaction product throws light on its enzymatic function" (1998) *Prot. Sci.,* 7:1269-1279

18. Rowland, P., Nielsen, F.S., Jensen, K.F., Larsen, S., "The crystal structure of the flavin containing enzyme dihydroorotate dehydrogenase A from *Lactococcus lactis*" (1997) *Structure,* 15:239-252

Chapter 6

Conclusions and Future Directions

Overall Conclusions

All known enzymes that reduce or oxidize the carbon 5 and carbon 6 positions of the pyrimidine, are flavoenzymes. In the previous chapters we explored the mechanisms of carbon double-bond forming and breaking enzymes. Both dihydrouridine synthases and dihydroorotate dehydrogenases were examined through kinetics as well as structural biology. The similarity of these mechanisms will be explored in the context of the studies presented in this thesis.

The general mechanisms for these enzymes can be broken-down into and an oxidative half-reaction and a reductive half-reaction. The enzymes studied transfer a hydride to and from the flavin at the 5-position and use an active site cysteine to protonate/deprotonate the pyrimidine, likely at the carbon-6 position. Though the dihydrouridine synthases and dihydroorotate dehydrogenases share half-reactions that are essentially the reverse of one another, the necessity for a redox-capable center and an acid/base catalyst are shared.

The redox potentials of the flavins and the substrate pyrimidines for both dihydrouridine synthase and dihydroorotate dehydrogenase reactions are similar. This is extrapolated from the fact that the reduction potentials for the dihydroorotate dehydrogenase from *E. faecalis*, and the dihydrouridine synthase from *T. maritima* were

similar (-262 mV and -252 mV, respectively). The reactions performed by these enzymes were reversible when high concentrations of the reduced or oxidized pyrimidine substrates/products were present. This indicates that the potentials for both pyrimidines are close to their cognate flavin potentials. The dihydroorotate/orotate couple is -250 mV (1), and the uridine/dihydrouridine couple may also lies close to this value at -256 mV (2).

Given the similarities seen between the reaction mechanisms, it is little surprise that the structures of the two enzymes share homology. The active site regions of both families of enzymes consist of a flavin binding (β/α)8-barrel domain. The dihydrouridine synthases are monomers and have secondary tRNA binding domains, and open active sites. The class 1A dihydroorotate dehydrogenases consist of a dimer of two (β/α)8-barrel domains with a flexible loop that closes the active site.

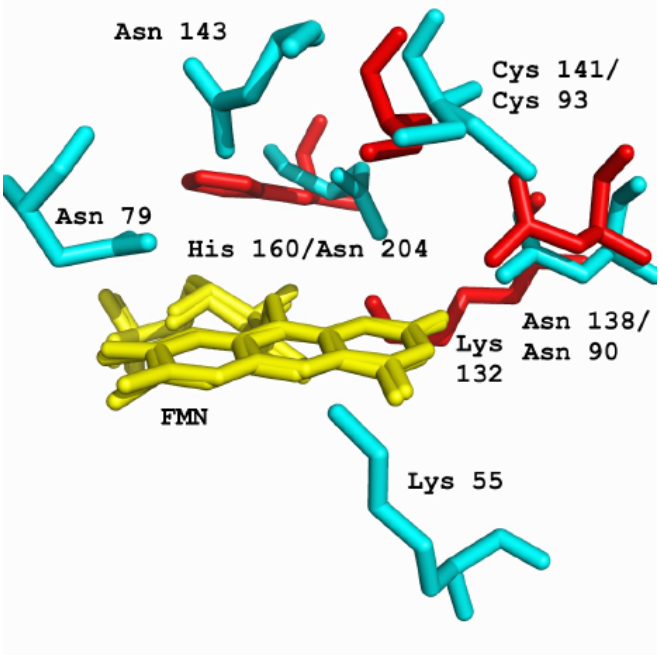

Figure 6.1: Comparison of Dihydroorotate Dehydrogenases and Dihydrouridine Synthase Active Sites. The C-alpha backbones of the *E. faecalis* DHOD (blue) and the *T. maritima* DUS (red) were superimposed using the program Superpose. The active site residues and flavin cofactor of both proteins are depicted.

The active site residues pictured above show the similarity between the enzymes. The C-alpha backbone of both (β/α)8-barrel domains overlay similarly, with the flavin prosthetic group in almost the same identical position. Both enzymes hydrogen bond to the flavin using at least one active site lysine: Lys 132 and Lys 175 at N1 for dihydrouridine synthase and dihydroorotate dehydrogenase respecitively. This puts a positive charge next to the flavin ring and probably has a large affect upon its reduction potential. Both enzymes also have an asparagine residue that probably hydrogen-bonds to and orients the pyrimidine. In the *E. faecalis* dihydroorotate dehydrogenase this residue hydrogen bonds to the C4 carbonyl of orotate, suggesting that this residue might also bind to the C4 carbonyl of dihydrouridine in the *T. maritima* dihydrouridine synthase.

Dihydrouridine Synthases

The second chapter we examined the dihydrouridine synthase 2 from *Saccharomyces cerevisiae*. The reactions of this enzyme were examined using transient kinetics. The results of these experiments show that the reduction of tRNA is the slowest step for the reaction. Efficient reduction of tRNA requires a prior modification of the tRNA substrate. Site-directed-mutagenesis indicates that an cysteine 117 acts as an active-site acid in the reduction of tRNA. These experiments show a detailed picture of how this enzyme modifies tRNA substrates.

The studies of the putative dihydrouridine synthase from *Thermotoga maritima* showed that this enzyme forms dihydrouridine, validating the predicted function of this gene. Kinetics and crystallographic studies of this enzyme were undertaken. This enzyme has low reactivity for both reduction by NADPH and oxidation by tRNA at 35 ^{o}C. A comparison of reaction rates and kinetic isotope effect studies indicates that chemistry is

not rate determining for this enzyme. This low reactivity is probably caused by a slow isomerization step. This isomerization is hypothesized to be the unblocking of the active site by the second, flexible domain. Crystallization of the enzyme in the presence and absence of this domain shows that separation of this domain from the rest of the enzyme causes no major perturbations in the structure. No major structural rearrangements are seen, even at the interface of these two domains. This indicates that the interactions between these domains are not significant to the overall structure of the (β/α)8-barrel and would allow this domain to move without considerable change to the rest of the enzyme. Therefore this domain may be mobile enough to fold over the active site of the enzyme.

Some general themes have come out of the studies of these two enzymes. The enzymes seem to bind to tRNA in a similar manner. The reduction potentials for both enzymes seem to be in the same range, both enzymes use NADPH in a *proR*-specific fashion, and both enzymes show a similar tight binding to modified tRNAs. All of these points together give a general scheme for how this family of enzymes functions.

The binding of co-purifying tRNAs was studied for both of these enzymes. From these data we were able to see that the enzymes both bound to almost every isotype of tRNA found in *E. coli*. For both enzymes, tRNA binding seems to be generalized. These enzymes must bind a common set of residues or a structural motif found in all the tRNAs of *E. coli*. The enzyme from *S. cerevisiae* has been shown to modify tRNAs at the U16/17 position in the D-loop, a ubiquitously modified position in yeast, indicating the enzyme should act on a broad range of tRNAs. The enzyme from *T. maritima* should also act upon a broad range of tRNA substrates as it is the only dihydrouridine synthase found in *T. maritima*. Both enzymes bind much more tightly to *E. coli* tRNAs than to *in vitro*

transcribed tRNAs. As both enzymes seem affected by the presence of tRNA modifications, allowing for tight binding of these tRNAs, these enzymes may share a common mechanism for recognizing these tRNAs. This may therefore explain one of the major aspects of the substrate recognition of dihydrouridine synthases, that prior modifications are a general recognition method used by these enzymes. Some alternate mechanisms controlling tRNA recognition may also exist for dihydrouridine synthases that only recognize specific tRNAs, such as the DUS 1 from *E. coli* that only recognizes $tRNA^{fMet}$ (3).

Another characteristic that both enzymes share is that tRNA reduction is reversible for both enzymes. This indicates that both enzymes have similar potentials. This seems logical given both enzymes perform the same chemical reaction. The affects of temperature on reduction potential have not been looked at for either enzyme, but it is possible the reduction potential of the *T. maritima* enzyme may shift when the temperature is increased to its physiological level. Though not fully explored, the general role of the flavin cofactor in both enzymes seems to be conserved, as are their general reduction potentials.

Both enzymes use the substrate NADPH. Upon reduction with this substrate both enzymes also show a similar stereochemical preference for this substrate using the *proR* hydride of NADPH. This indicates that both enzymes likely interact with NADPH in a similar manner.

The final similarity relates to the interaction of these enzymes with their tRNA substrates. When the *S. cerevisiae* enzyme was reacted with tRNA substrates containing or lacking modifications a large change in reactivity was seen. The modified tRNA

substrate binds to the enzyme with a much higher affinity than the non-modified tRNA. Though these experiments were not performed with the *T. maritima* enzyme a similar mechanism might be utilized. Both enzymes showed high affinity for the modified *E. coli* tRNA and low affinity for *in vitro* transcribed tRNA. This may indicate that the need for modification of the tRNA substrate is universal for this enzyme family.

Future Directions Dihydrouridine Synthases

A number of important questions have been raised from the studies presented in this thesis. The first and most prominent question is the role of post-transcriptional modification of the substrate tRNA in the reaction. Though likely candidates for this modification were mentioned (Chapter 2), the specific modification or modifications required for activity have not yet been determined. There are a few ways to address this question. One way would be to examine the effects on the kinetics of the reaction with tRNAs from *S. cerevisiae* deletion strains lacking both dihydrouridine synthase activity as well as other secondary modifications. Another way to address this question would be to obtain the proteins responsible for the likely modifications, use them to process *in vitro* transcribed tRNA, and dissect which modifications can increase the reactivity of the tRNA substrates. Either of these methods should give a better understanding of the specific modifications needed to increase reactivity.

An interesting question that arose was the nature of the slow isomerization step seen in the *T. maritima* enzyme. One hypothesis is that the 4-helix-bundle of this enzyme was the cause of this slow isomerization, with uncovering the active site being the rate-limiting step for the enzyme. One potential way to address this question would be to analyze the enzyme in the absence of this domain. A truncated form of this enzyme could

be used in kinetic assays to see whether the reaction rate was faster or slower with or without this domain. In particular it would be interesting to see if the enzyme was reduced faster by NADPH without this domain. The binding of tRNA requires this domain because it has a RNA binding motif. The loss of this domain may thereby inhibit the oxidation of the enzyme by tRNA, instead of increasing the oxidation rate. In either case understanding the effect of this domain upon both NADPH and tRNA reactivity would give us more insight into how the enzyme functions. It would also be interesting to test the reduced form of this enzyme with various bulky redox-reactive dies in the presence and absence of this domain. This would give a general sense of whether the slow rate seen was indeed due to the enzyme opening up to expose the flavin.

The truncated form of the enzyme could also prove useful in other ways. In the crystal structure of this enzyme (Chapter 5) the protein contains bicine in its active site. In the other crystallized form of the enzyme, no co-complex was formed by soaking with NADP(H) or uracil. This truncated form of the enzyme however seems capable of binding to substrates and may allow the formation of co-complexes with NADPH or uracil.

Dihydroorotate Dehydrogenases

The last two chapters focus on the dihydroorotate dehydrogenase from the pathogenic bacterium *Enterococcus faecalis*. The kinetics of the *Enterococcus faecalis* enzyme examined in Chapter 4 show that the oxidative half-reaction with fumarate is rate limiting at pH 8.5. The effect of pH upon the half-reactions indicated that an active site cysteine was important in protonation of fumarate and deprotonation of dihydroorotate.

An active site lysine is also involved in binding to the carboxylates of both fumarate and dihydroorotate.

The structures of the enzyme complexed to orotate, dihydroorotate, L-malate, 3,4-dihydroxybenzoate, and 3,5-dihydroxybenzoate were determined. Minor alterations in the enzyme are seen upon binding to different substrates, with the largest changes caused by L-malate. Even larger dynamic changes are seen upon binding of substrates to the enzyme in solution by NMR. Partial assignment of the resonances yielded information about a static core of protein residues which change little during the binding of ligands to the enzyme.

All of these results show a detailed picture of the turnover of the enzyme. The enzyme is a dynamic molecule with high flexibility, especially at the two active site loops. During turnover this enzyme shows very strong negative cooperativity, indicating two non-equivalent dimers are present. Comparison of the steady-state and transient-state kinetic data may indicate half-sites reactivity, because k_{cat} is half the rate of the slowest transient step (oxidation), exactly the rate expected if only half of the enzyme was functioning. The crystal structures and the kinetics of the enzyme flesh out a detailed picture of the enzymes kinetic mechanism and show potential snapshots of the enzyme at different stages of this mechanism.

Future Directions Dihydroorotate Dehydrogenase

In the study of this enzyme many important aspects of its function have been explored. The main question remaining revolves around how half-sites reactivity occurs in this enzyme. There are a number of possible approaches which could further clarify how this negative cooperativity occurs. One way would be to purify mixed dimers that

have an active monomer on one side, and an inactive monomer on the other. This would help to explain whether the enzymes have a true preexisting asymmetry, with each monomer being utilized only for fumarate or dihydroorotate.The dissociation of the enzyme into monomers poses a limitation to this experiment but may be surmountable. Another way to examine this would be to unfold and reconstitute the enzyme with modified flavins. A flavin such as 5-carba-deazaflavin, which cannot form semiquinone, would clarify whether or not the enzyme could transfer single electrons between the flavin molecules of the dimer. Though these techniques would be potentially useful in elucidating the mechanism of half-sites reactivity in this enzyme, there are many other ways this question could be addressed.

One of the most useful approaches for understanding the molecular basis for the half-sites reactivity in this enzyme is the use of multidimensional-NMR. Chapter 5 described some of the work which had been done in this line of investigation, but further assignment is needed to complete this project. By fully elucidating the effect of ligands on the enzyme in different states, this technique should provide a detailed understanding of how the residues interact in the enzyme to confer half-sites reactivity.

The major goal that still stands is the full assignment of the resonances of the enzyme. Though the presence of the ligand 3,5-dihydroxybenzoate helps to resolve the spectrum of the protein, a full set of 3-dimensional spectra are still needed in the presence of this ligand. The production of a ^{15}N-phenylalanine labeled protein would also aid further assignment of the residues in the protein. Upon assignment of this protein a great deal can be concluded about the motion of the proteins residues. The TROSY spectra already obtained in the presence and absence of ligands would allow identification of all

the protein residues affected by ligand binding. The addition of NOESY or TOCSY experiments would allow the determination of the NMR-structure of the protein allowing a detailed picture of the positions of all the enzymes residues in the bound and unbound forms of the enzyme. Examining the enzyme under turnover conditions, or trapped in half-oxidized or half-reduced states may give clearer indications of what causes the negative cooperativity seen in this enzyme.

References

1. Krakow, G., and Vennesland, B. “The Equilibrium Constant of the Dihydroorotic Dehydrogenase Reaction” (1961) *J. Biol. Chem., 236*:142-144

2. Scannell, M.P, Fenick, D.J., Yeh S.R., Falvey, D.E., “Model Studies of DNA Photorepair: Reduction Potentials of Thymine and Cytosine Cyclobutane Dimers Measured by Flourescence Quenching” (1997) *J. Am. Chem. Soc.,* 119:1971-1977

3. Bishop, A. C., Xu J., Johnson, R. C., Schimmel, P., de Crécy-Lagard V., “Identification of the tRNA-Dihydrouridine Synthase Family” (2002) *J. Biol. Chem*., 277:25090-25095